

# **Design of pharmaceutical tablet formulation for a low water soluble drug:**

Search for the critical concentration of starch  
based disintegrant applying percolation theory and  
F-CAD (Formulation-Computer Aided Design)

**Inauguraldissertation**

zur

Erlangung der Wuerde eines Doktors der Philosophie

vorgelegt der

Philosophisch-Naturwissenschaftlichen Fakultat

der Universitaet Basel

von

Go Kimura

aus Kyoto Japan

Kyoto, 2012

Original document stored on the publication server of the University of Basel

**edoc.unibas.ch**



This work is licensed under the Creative Commons Attribution-NonCommercial-NoDerivs 2.5

Switzerland License. To view a copy of this license, visit

<http://creativecommons.org/licenses/by-nc-nd/2.5/ch/> or send a letter to Creative Commons,

444 Castro Street, Suite 900, Mountain View, California, 94041, USA.



## Attribution-NonCommercial-NoDerivs 2.5 Switzerland (CC BY-NC-ND 2.5)

This is a human-readable summary of the Legal Code (the full license) available in the following languages: [German](#)

[Disclaimer](#)

### You are free:



to **Share** — to copy, distribute and transmit the work

### Under the following conditions:



**Attribution** — You must attribute the work in the manner specified by the author or licensor (but not in any way that suggests that they endorse you or your use of the work).



**Noncommercial** — You may not use this work for commercial purposes.



**No Derivative Works** — You may not alter, transform, or build upon this work.

### With the understanding that:

**Waiver** — Any of the above conditions can be **waived** if you get permission from the copyright holder.

**Public Domain** — Where the work or any of its elements is in the **public domain** under applicable law, that status is in no way affected by the license.

**Other Rights** — In no way are any of the following rights affected by the license:

- Your fair dealing or **fair use** rights, or other applicable copyright exceptions and limitations;
- The author's **moral** rights;
- Rights other persons may have either in the work itself or in how the work is used, such as **publicity** or privacy rights.

**Notice** — For any reuse or distribution, you must make clear to others the license terms of this work. The best way to do this is with a link to this web page.

Genehmigt von der Philosophisch-Naturwissenschaftlichen Fakultät  
auf Antrag von

Prof. Dr. H. Leuenberger

und

Prof. Dr. I. Caraballo

Basel, den 21. Februar 2012

Prof. Dr. Martin Spiess  
Dekan



*To my family*



## **Acknowledgements**

I wish to express my sincere gratitude to my supervisor, Prof. Dr. H. Leuenberger for providing me this precious study opportunity as a PhD student in his laboratory. Discussion with him about "Percolation theory" was invaluable. I would like to express my deepest appreciation to Prof. Dr. J. Huwyler for giving me the permission to continue my study. I have pleasure in my sincere thanks to Prof. Dr. I. Caraballo who accepted the co-reference.

I always appreciate the feedback offered by Dr. M. Puchkov. His inspiring thought and hospitality during my stay in Basel were unforgettable. Thank you very much for the use of F-CAD as well.

I would like to thank Dr. G. Betz and Dr. K. Chansanroj for their smile, cheer, great atmosphere during my stay in the Industrial Pharmacy Lab (IPL).

Special thanks to Dr. R. Luginbuehl and Dr. E. Krausbauer for the use of their PhD thesis. Many thanks are due to Dr. M. Lanz, Dr. M. Plitzko, Dr. J. von Orelli, Ms. S. Tanja, Mr. R. Alles and Mr. S. Winzap for their laboratory help. Thanks to Dr. J. Saito for his kindness as a Japanese friend.

I am grateful to Mr. K. Eichler. I have greatly benefited from the numerous workshops in Technology Training Center. I am also grateful to Mr. C. Kaseda for the use of dataNESIA software, and to S. T. Japan Inc. for providing the valuable NIR imaging data on my experiments.

I received the financial support from Shionogi & CO., LTD.

I would like to thank Mr. Y. Katakuse and his group member of the formulation designing department, and Mr. J. Lim who is director of pharmaceutical sciences in Shionogi Inc. for their generous understanding.

Finally I am greatly indebted to my family, Kazue, So and Yuki, for their support, encouragement and sacrifice throughout my PhD works.





“努力できることが才能である”

“Trying hard is an ability”

Cited to the book “The Hideki Matsui Story-Reaching for Your Dream”



---

**Table of contents**

1	Summary .....	1
2	Introduction .....	3
3	Theoretical Introduction .....	5
3.1	Formulation design for solid dosage forms .....	5
3.1.1	The selection of pharmaceutical dosage form .....	5
3.1.2	Definition of low water soluble drug .....	5
3.1.3	Advantages of granulation process .....	6
3.1.4	Principle of wet granulation .....	7
3.1.5	Method of wet granulation .....	8
3.1.6	Flowability of powder or granules .....	9
3.1.7	Tablet formulation design and development .....	10
3.2	Near infrared (NIR) imaging .....	15
3.2.1	Introduction of NIR and NIR imaging .....	15
3.2.2	Application of NIR imaging in tablet formulation design .....	15
3.3	Response surface methodology .....	16
3.3.1	Response Surface Methodology (RSM) and Design of Experiment (DOE) ....	16
3.3.2	dataNESIA software .....	22
3.3.3	Multivariate spline interpolation .....	23
3.4	Percolation theory .....	24
3.4.1	Principles of percolation theory .....	24
3.4.2	Application of percolation theory in pharmaceutical area .....	29
3.5	Percolation threshold of disintegration time with particle packing geometry considerations .....	30
3.5.1	Random close packed (RCP) spheres system .....	30
3.5.2	Sphere caging and non-caging concept in case of binary RCP system .....	31
3.5.3	Sphere caging and non-caging concept for binary drug/disintegrant tablet ....	32
3.5.4	Water diffusion network for binary spherical drug/disintegrant tablet .....	33
3.5.5	Calculation of critical concentration of disintegrant for spherical binary drug/disintegrant tablet .....	34
3.5.6	Critical exponent .....	35
3.5.7	Fractal nature of infinite cluster near percolation threshold .....	36
3.6	F-CAD .....	37
3.6.1	Goal of in-silico pharmaceutical formulation design .....	37
3.6.2	F-CAD capability for the pharmaceutical formulation design .....	38

## Table of contents

---

3.6.3	F-CAD software applications.....	39
3.6.4	F-CAD core algorithm .....	40
4	Objectives .....	43
5	Materials and Methods.....	45
5.1	Materials .....	45
5.2	Physical properties of starting materials .....	45
5.3	Granulation .....	51
5.4	Tableting .....	54
5.5	Granules characterization.....	57
5.5.1	SEM .....	57
5.5.2	Moisture determination.....	57
5.5.3	Size distribution and Mean diameter .....	57
5.5.4	Bulk, Tapped and Apparent density .....	58
5.5.5	Intragranular pore volume .....	59
5.5.6	MA assay .....	59
5.6	Tablet characterization .....	60
5.6.1	Hardness and tensile strength .....	60
5.6.2	Calculated Porosity .....	61
5.6.3	NIR imaging .....	61
5.6.4	Disintegration time .....	62
5.6.5	Pore size distribution, Median pore diameter and Porosity.....	62
5.7	Data Analysis .....	63
5.7.1	Data treatment for NIR imaging .....	63
5.7.2	Response surface methodology.....	63
5.7.3	Renormalization .....	64
5.7.4	Assumption of disintegration time computed by F-CAD.....	65
5.7.5	F-CAD operation .....	65
6	Results and Discussion.....	69
6.1	Physical properties of starting materials .....	69
6.2	Granules characterization.....	69
6.2.1	Influence of loading volume of MA on granule characteristics .....	69
6.2.2	SEM of granules with increasing loading volume of MA .....	73
6.2.3	Intrusion volume of mercury into granules with increasing loading volume of MA.....	74
6.3	Tablet characterization .....	76
6.3.1	Influence of loading volume of MA on compression behaviour.....	76
6.3.2	Visual inspection on tablet characteristics using NIR imaging .....	85

---

6.3.3	MA domain size with increasing loading volume of MA in tablet.....	89
6.3.4	Tablet disintegration time .....	90
6.3.5	Pore size distribution, Median pore diameter and porosity .....	92
6.4	Focus on searching the critical concentration of MS .....	93
6.5	Renormalization technique considerations .....	98
6.6	Critical concentration of MS for MA tablets.....	100
6.7	Critical volume fraction of MS for MA tablets .....	102
6.8	Critical concentration of MS for 0% v/v MA tablets .....	104
6.9	Comparison of critical volume fraction for MA tablets and Caffeine tablets.....	105
6.10	Critical exponent for disintegration behavior.....	106
6.11	Computing the disintegration time of MA tablet by F-CAD .....	109
6.11.1	Particle Arrangement and Compaction (PAC) operation .....	109
6.11.2	Comparison of experimental and F-CAD computed disintegration time of MA tablets.....	109
6.11.3	Response surfaces close to the percolation threshold of sensitive tablet properties such as the disintegration time.....	113
7	Conclusions .....	118
8	Further perspectives .....	121
9	References .....	122



## 1 Summary

The topic of this PhD work is to search the critical concentration of starch based disintegrant applying percolation theory and F-CAD (Formulation-Computer Aided Design) in order to design a pharmaceutical tablet formulation for a low water soluble drug. Critical concentration of maize starch (MS) for a ternary mefenamic acid (MA) tablet formulation with respect to a minimum disintegration time is investigated. Additionally implemented application of F-CAD to compute the disintegration time of MA tablet formulation is presented. This topic is related to push forward the idea of Quality by Design (QbD) of FDA (Food and Drug Administration) / EMEA (European Medicines Agency) / PMDA (Pharmaceuticals and Medical Devices Agency) and the exploration of the design space according to ICH (International Conference of Harmonization) Q8.

The results of this work shows that the application of percolation theory is not limited to binary tablet formulation. The critical concentration of MS described by the renormalized MS concentration,  $MS/(MS+MA)$  applying the renormalization technique is always equal 0.198 (dimensionless). Moreover the critical concentration of MS is optimized using the spline approximation with the dataNESIA software. It is leading to a minimum disintegration time at 0.206, dimensionless, renormalized, which is very close to the experimental value of 0.198. According to the percolation theory, a minimum disintegration time corresponds to the formation of a continuous water-conducting cluster through the entire tablet. The critical volume fraction of an 'infinite cluster' that water can diffuse through the entire MA tablets are calculated with taking into account for the geometrical considerations between MS and MA particles based on random close packed (RCP) spheres system. The critical volume fraction of MS is calculated by the multiplication of critical concentration of MS and the solid fraction of MA tablets; which is within the range of  $0.16 \pm 0.01$  (v/v). It is concluded that the critical volume fraction for three dimensional lattices is equal to  $0.16 \pm 0.01$  (v/v); which is useful for the calculation of the critical concentration of starch based disintegrant in order to design the pharmaceutical tablet formulation based on scientific approach proposed by ICH Q8 guidance.

In addition, the disintegration behavior in the neighborhood of the percolation threshold is explained mathematically by the basic equation of the percolation theory, yielding a critical exponent  $q$  equal to  $0.28 \pm 0.06$  (Quality of fit:  $r^2 = 0.84$ ). This value is close to the critical exponent for three dimensional lattices ( $q = 0.4$ ). Thus, it is important, within a planned experimental design to optimize the disintegrant to take into account the percolation theory. However it has to be kept in mind that the determination of the percolation threshold and critical exponent does not give an answer about the absolute value of the disintegration time. Dissolution Simulation (DS) module, which is the one of F-CAD based on cellular automata

algorithm is used to simulate the disintegration time of a MA tablet. Disintegration time of tablet is assumed as the time elapsed till the water is detected at the geometric center of the virtual tablet. Comparison of experimental disintegration time of MA tablet and computed specific time point for water to reach the geometric center of the tablet by using F-CAD software has been carried out and shown an acceptable correlation (Correlation coefficient:  $r = 0.81$ ). The detailed evaluation of the data shows that there is still a need for optimization of F-CAD for the calculation of the disintegration time in order to achieve a similar or the same performance like in the prediction of the dissolution profile of a tablet formulation. It is concluded that F-CAD software is the only software so far, which is capable of computing the disintegration time of tablets. The software has a great potential to be improved and to be not only used for the safe prediction of the dissolution profile of a tablet formulation but also for a safe prediction of the disintegration time. Thus, such a software is one of the tools for the substitution of laboratory experiments for the purpose of the design and development of new pharmaceutical solid dosage forms. The replacement of expensive laboratory experiments by in-silico experiments is an important issue to reduce development costs and to comply with the requirements of ICH Q8 exploring the design space with response surface methodology. The results of this thesis show in addition that the application of percolation theory is a must in order to detect percolation thresholds. It is important to know the response surfaces close to the percolation threshold of sensitive tablet properties such as the disintegration time to get information about the robustness of the selected formulation. In this context one has to put the question forward if the application of percolation theory should be an integral part of the guidelines of ICH Q8 exploring the formulation design space.



## 2 Introduction

For the pharmaceutical formulation design and process development, the scientific understanding of those attributes that influence their quality should be provided while taking into account for quality by design (QbD) in International Conference on Harmonization (ICH) guidance Q8 (R2) [1]. The use of scientific approaches for the understanding of quality attributes, such as statistical design of experiment (DOE), response surface methodology (RSM), optimization modeling, multivariate data analysis and chemometrics in combination with the knowledge management system is required.

Pharmaceutical formulations for solid dosage forms are complex and heterogeneous disordered particular system, i.e., multi-particulate and multi-component. Topological modeling is necessary to be taken into account for a geometrical description. Percolation theory is, in fact, one of the suitable topological modeling tools to predict and simulate the geometric phase transitions in complex system, such as a tablet formulation. Thus, percolation theory allows finding the regions where the system undergoes the geometrical phase transition. It happens at critical concentration of the components where a component percolates (percolation threshold). In terms of tablet formulation design, such regions are usually linked to external values of properties such as water uptake, disintegration time, and dissolution rate.

Nowadays, because of the advance of combinatorial chemistry and high throughput screening, the number of poorly water soluble drug candidates has increased tremendously. More than 40% of newly discovered drugs are poorly water soluble. It has to be kept in mind that up to now there is no universal science-based formulation design for low water soluble drugs. In many cases disintegration is a limiting factor on the dissolution process of tablets. Disintegrant is used to aid the disintegration of tablets. Determination of the critical concentration of disintegrant is an important parameter for a tablet formulation design, especially for low water soluble drugs. Therefore, several research groups have reported the critical concentration of disintegrant that is required to achieve the minimum disintegration time [2-7]. In our laboratory, the percolation theory has been applied to determine the critical concentration of disintegrant in binary tablets [8-12]. However the further investigation is needed to determine the critical concentration of disintegrant not only for binary tablets but also for multicomponent tablets in order to design a pharmaceutical tablet formulation based on the scientific approach.

Mefenamic acid (MA) is used as a model substance of a low water soluble drug. Fifteen types of granules and tablets are prepared at different loading volume of MA (0-74.1% v/v) in exchange of lactose (LA) (7.7-90.9% v/v) as a filler and maize starch (MS) (8.5-30.3% v/v) as a disintegrant corresponding to a truly ternary tablet formulation. In order to guarantee a

quality of a tablet formulation, however, it is not sufficient to evaluate to look only at one important characteristic such as the disintegration time, because other tablet properties need to fulfill the necessary requirements as well. In this respect, it has to be kept in mind that an optimization of disintegration time may jeopardize other important tablet properties such as the tensile strength. Thus, it is a prerequisite to study at least at the same time the weight, diameter, thickness, and hardness of a tablet. The weight, diameter, and thickness of tablets together with the measurement of apparent density of granules determine the porosity of the tablets. In order to get the more scientific understanding of the tablet characteristics, near infrared (NIR) imaging technology has been applied to visualize the components distribution on the tablet surface.

The tablet quality is not only influenced by its materials [13-19] but also by tableting process parameters [20-22] when compressed. For an optimal formulation design, it would be desirable to manufacture the tablets on an industrial rotary tableting machine. However, because of the lack of a large amount of a drug substance at the earlier formulation design and development phases, these experiments are not possible. For this reason, the Presster<sup>TM</sup> [23] equipment, which needs only a small amount of powder material, was used to simulate mechanically a rotary tableting machine.

Finding the rule for pharmaceutical tablet formulation design is necessary from the development cost and scientific approach point of view. Critical concentration of MS for a ternary MA tablet formulation with respect to a minimum disintegration time and the critical exponent of the disintegration behavior based on the percolation theory are discussed. Additionally implemented application of F-CAD to compute the disintegration time of MA tablet formulation is presented in this thesis.

### **3 Theoretical Introduction**

#### **3.1 Formulation design for solid dosage forms**

##### **3.1.1 The selection of pharmaceutical dosage form**

On the basis of the information about the target profile, clinical indication and pre-formulation study, for example solubility, water-octanol partition coefficient, pKa, and stability in solution and in solid state of the new chemical entity (NCE), the dosage form for NCEs would be selected as oral dosage forms, parenteral dosage forms, topical dosage forms and so on.

NCEs are rarely administrated alone and are almost always given as a pharmaceutical dosage forms. The oral route is the one most frequently used for drug administration and tablets are the most common pharmaceutical dosage forms today. Tablets are popular for several reasons. First the patient's point of view, tablets are convenient to handle because they are portable and easy to be administered. Second the cost of manufacturing, packaging and shipping is relatively low from manufacture's point of view. The third point is that tablet formulation enables high dose of active substances to design smaller than capsule formulation containing granules or powder as well as granules or powder themselves.

The most important is however the fourth point, that solid dosage forms such as tablets, capsules etc. show a much higher physical and chemical stability than any other dosage form especially if compared with liquid formulations.

##### **3.1.2 Definition of low water soluble drug**

Nowadays, because of the advance of combinatorial chemistry and high throughput screening, the number of poorly water soluble drug candidates has increased tremendously. More than 40% of newly discovered drugs are poorly water soluble. The solubility in gastro-intestinal fluids of a drug is an important factor affecting its bioavailability. Solid drugs administered orally for systemic activity must be dissolved in the gastro-intestinal fluids prior to their absorption site. European Pharmacopoeia (Ph. Eur.) 7.0 categorizes the solubility from the view point of milliliters of solvent required for dissolving 1 g of solute referred to a temperature between 15°C and 25°C. If 1 g of solid drug requires more than 10,000 mL, this drug is classed as practically insoluble (Table 1) [24].

Table 1 European Pharmacopoeia (Ph. Eur.) 7.0 descriptive terms of solubility [24]

Descriptive Term	Approximate volume of solvent in milliliters per gram of solute		
Very soluble	less than	1	
Freely soluble	From	1	to 10
Soluble	From	10	to 30
Sparingly soluble	From	30	to 100
Slightly soluble	From	100	to 1,000
Very slightly soluble	From	1,000	to 10,000
Practically insoluble	more than		10,000

On the other hand, the solubility for a classification in the Biopharmaceutics Classification System (BCS) is defined by FDA in 2000 (Table 2) [25]. Drugs are defined as highly soluble when the highest dose strength is soluble in 250 mL or less of an aqueous media over a pH-range of 1.0-7.5. Drugs are defined as highly permeable when the extent of absorption is determined to be 90% or more of an administered dose based on a mass balance determination or in comparison to an intravenous dose. According to the FDA, the permeability class can be determined by humans, animal models (e.g. rat), in-vitro permeation studies with human or animal excised tissue or the use of cultured cell models (e.g. Caco-2 cells).

Table 2 Biopharmaceutics Classification System (BCS)

Solubility / Permeability	High	Low
High	Class I	Class III
Low	Class II	Class IV

### 3.1.3 Advantages of granulation process

The formulation designing and development for low water soluble drugs aiming to improve the dissolution behavior and thus bioavailability with common approaches is desirable for the pharmaceutical industry to shorten time to market. One common approach is granulation, which has several advantages, such as improved wettability and in vitro dissolution behavior of active ingredient [26], and improved flowability and compaction properties [27] of the whole formulation.

Granulation methods can be divided into wet granulation, which is use a granulation liquid during its process, and dry granulation in which no granulation liquid is used. This dry granulation is used for the active pharmaceutical ingredients which are sensitive to water.

### 3.1.4 Principle of wet granulation

Wet granulation process is that liquid is added to the powder mixture and will be distributed and then powder is agglomerated at the certain amount of liquid [28, 29]. Formation of granules results from a process classically defined by different states of saturation of liquid-bound particles (Figure 1) [30, 31]. These wet bridges are only temporary states during wet granulation. However they are a prerequisite for the formation of solid bridges formed by adhesive in the presence of liquid or by materials that dissolve in the granulation liquid. Otherwise powder will be obtained after drying process.

- **Pendular state**

Empty space between particles is partly filled with binding liquid, which forms concave films between the particles. This state corresponds to the nucleation phase when nuclei are formed from isolated particles, which when wetted by the binding liquid form between particles by pendular linkage.

- **Funicular state**

With increasing the quantity of liquid, the liquid bridges (concave films) coalesce. However, air is still present in the empty space. Drying this phase, the nuclei formed grow via two mechanisms;

- Isolated particles adhere to a nucleus by a pendular linkage
- Two nuclei collide and form a large nucleus

At the end of this stage many small granules of ranging sizes are obtained.

- **Capillary state**

The binding liquid totally fills the empty space between the particles, which are held together by the capillary suction at the liquid-air interface at the surface of the granules. This stage corresponds to further accretion;

- The largest granules break up and recombine with small particles
- Two granules coalesce
- Small particles combine selectively
- Particles adhere to large granules

- **Droplet state**

Continued wetting of particles can result in particles are suspended in the binding liquid. This must be totally avoided to obtain granules. On the other hand, this will be important for the process of granulation by spray drying of a suspension.

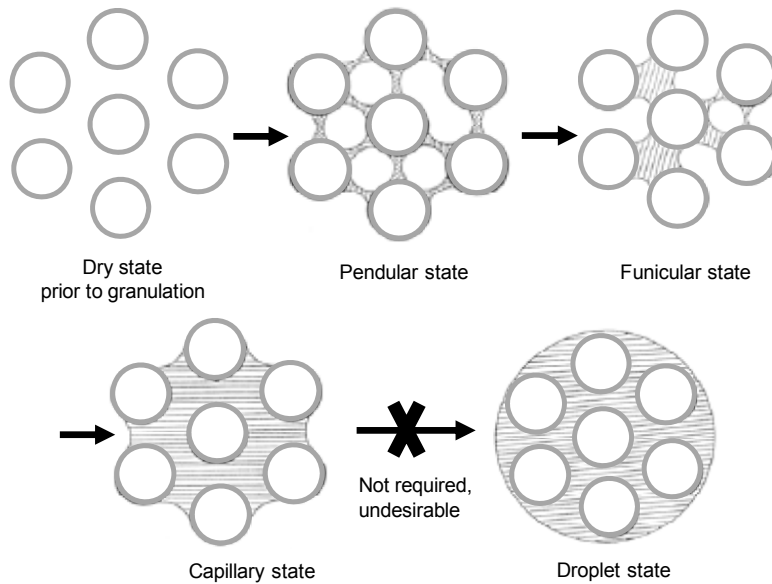


Figure 1. The difference states of saturation of liquid-bound particles.

### 3.1.5 Method of wet granulation

Wet granulation process mainly divided into using a high-speed granulation or a fluidized bed granulation. Critical factor in wet granulation is the amount of granulation liquid used to get the prerequisite size of granules. There are many reports describing how to detect the end point of wet granulation. The way to detect the end point of high-speed granulation is to measure the power consumption of impeller [32, 33, 34], to measure the granules particle size by CCD [35] camera and acoustic measurement [36]. The same approach has been investigated to measure the particle size by CCD camera [34] and acoustic signal detected by sensor as shown in Figure 2 [37] for the fluidized bed granulation.

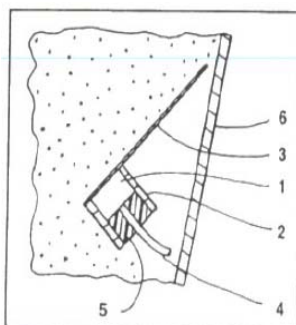


Figure 2. Sensor in fluidized bed granulator [37].

- (1) Condenser microphone, (2) Fuse, (3) Platelet, (4) Cable, (5) Potting,
- (6) Container

The advantage to use a fluidized bed granulator over high-speed granulator is that a mixing, granulation and drying are performed in one unit as well as operators are in safe side by

closed unit [38]. On the other hand, disadvantage to use a fluidized bed granulator over high-speed granulator is that there are a lot of parameter affecting granules characteristics related to apparatus, process and product [39].

This complexity leads to the problems when this process is scaled up. Leuenberger has proposed the quasi-continuous granulation process by using Glatt® Multicell™ which consists of a horizontal high-speed granulator and three fluidized bed granulator to avoid scale up problem as currently trended [40, 41].

When compared with high-speed granulation, granules manufactured by fluidized bed granulator shows superior compressibility and less granules hardness due to the porous with small bulk density [42]. It is necessary to use the fluidized bed granulator if tablet includes the component which leads to cracking and capping tendency such as mefenamic acid (MA) [43].

### 3.1.6 Flowability of powder or granules

There are many pharmaceutical manufacturing processes that require powder or granules to be moved from one location to another location. This is achieved by many kind of ways such as to use gravity force, mechanical feeding, pneumatic transfer and fluidization air. The flowability of powers or granules is a critical parameter in the production site of pharmaceutical dosage forms. In common, flowability can be evaluated by measurements of bulk density. Bulk density is a simple test developed to evaluate the flowability by comparing the poured density and tapped density of a powder or granules.

A useful empirical index is given by Carr (Equation 1) [44].

$$\text{Carr's index (\%)} = \frac{(\rho_{\text{tapped}} - \rho_{\text{bulk}})}{\rho_{\text{tapped}}} \times 100 \quad \text{Equation (1)}$$

where  $\rho_{\text{tapped}}$  is tapped density (g/cm<sup>3</sup>),  $\rho_{\text{bulk}}$ : bulk density (g/cm<sup>3</sup>).

This index can be interpreted in Table 3.

Table 3 Carr's index as an indication of powder flow

Carr's index (%)	Type of flow
5 - 15	Excellent
12 - 16	Good
18 - 21	Fair to passable
23 - 35	Poor
33 - 38	Very poor
> 40	Extremely poor

A similar index has been introduced by Hausner (Equation 2) [45].

$$\text{Hausner ratio} = \frac{\rho_{\text{tapped}}}{\rho_{\text{bulk}}} \quad \text{Equation (2)}$$

where  $\rho_{\text{tapped}}$  is tapped density ( $\text{g}/\text{cm}^3$ ),  $\rho_{\text{bulk}}$ : bulk density ( $\text{g}/\text{cm}^3$ ).

This index can be interpreted in Table 4.

Table 4 Hausner ratio as an indication of powder flow

Hausner ratio	Type of flow
< 1.25	Powder flows like granules
1.25 - 1.5	Powder is of intermediate nature
> 1.5	Powder is cohesive

### 3.1.7 Tablet formulation design and development

Tablets are the most common pharmaceutical dosage form today as described before. Pharmaceutical dosage forms compose both active pharmaceutical ingredients (API) and inactive ingredient so called excipients. The information on the compression properties of the API is extremely useful. Thus, if the API is high dose and it has plastic deformation, the chosen excipients should be brittle (e.g. lactose). If the drug is brittle or elastic, the excipients should be plastic, (e.g. microcrystalline cellulose). When the compression force is increased to the particles, deformation (particles change of form) will occur. If the deformation disappears completely (it means return to original shape) when the stress is released, it is an elastic deformation. A deformation that does not completely disappear after release of the stress is a plastic deformation. A characteristic for brittle material is the fact the plastic deformation is followed by a breaking of the materials. The deformation is dependent on the properties of the particles.

Especially a disintegrant is added to most tablet formulations and very critical to facilitate disintegrating tablet into small particles in order to increase the surface area of API when tablet is exposed to the gastrointestinal fluids. Therefore, the appropriate type and amount of disintegrant is in many cases the critical factor to determine the tablet quality, although particle size, particle shape and packing geometry of disintegrant in a tablet has to be taken into account.

The optimal selection of disintegrant is an important step, which needs a lot of laboratory experiments for the tablet formulation design based on the formulator's expertise and experience.



### 3.1.7.1 Classification of disintegrant

Main properties for a good disintegrant were pointed out [46].

- Strong hydrophilicity (to set up the continuous hydrophilic network in a tablet)
- Weak hydrosolubility
- Weak mucilaginous behavior in contact with water
- Good flowability and good compressibility

From the above mentioned point of view, disintegrants can be divided into mainly four groups: the native starches, modified starches, cross-linked polyvinylpyrrolidone, cellulose and modified cellulose [46].

- Native starches

Native starches are potato, maize and rice starches. The typical concentration range of starch in a tablet is up to 15% w/w. Starch particles can swell when it contacts with water and facilitate disintegration by particle-particle reputation.

- Modified starches

Sodium carboxymethyl starch (Primojel<sup>®</sup>, Explotab<sup>®</sup>) are developed as a high-swelling disintegrants which are included in a tablet at relatively low concentration, typically 1-5% w/w. According to the carboxymethylation and cross-linkage, the starch can be improved swelling capacity more or less up to a certain point.

Partly pregelatinized starch (StaRX 1500<sup>®</sup>) is a maize starch physically modified by heating with/without pressure in the presence of water. Flowability and compressibility is improved in comparison with starch.

- Cross-linked polyvinylpyrrolidone

Because of its high molecular weight and cross-linked structure, this polyvinylpyrrolidone is insoluble in water but it is highly hydrophilic. It can absorb more than 50% of its own weight in water. Two kinds of Cross-linked polyvinylpyrrolidone (Polyplasdone XL<sup>®</sup>, Kollidon CL<sup>®</sup>) are available on the market.

- Cellulose and Modified cellulose

Croscarmellose sodium (Ac-Di-Sol<sup>®</sup>), Carmellose calcium (ECG-505<sup>®</sup>), Carmellose (NS300<sup>®</sup>), Low-substituted hydroxypropylcellulose (L-HPC<sup>®</sup>) are representatives. Due to their origin from the pulp of woody plant, their structure is fibrous. This fibrous structure is highly hydrophilic because of the numerous hydroxyl groups that allow for fast suction of water.

### 3.1.7.2 Mechanism of tablet disintegration

Several mechanisms of disintegration are suggested, such as swelling of disintegrants, disintegrant deformation recovery, wicking water into the pore between particles, reputation to break up the particle-particle bonding in tablet and exothermic wetting reaction [47].

No simply theory was satisfactorily applied to all disintegrant process, however the four principle mechanisms are accepted as shown in Figure 3 [47]. However it is an universally fact that fast water diffusion into the tablet is necessity.

- Swelling  
Particles swell and break up the tablet from within; swelling sets up localized stresses that spread throughout the tablet.
- Deformation  
Particles swell to pre-compression size and break up the tablet.
- Wicking  
Water is pulled into pores by the disintegrant and reduces the physical bonding forces between particles.
- Repulsion  
Water is drawn into pores, and particles repulse each other because of the resulting electrical force.

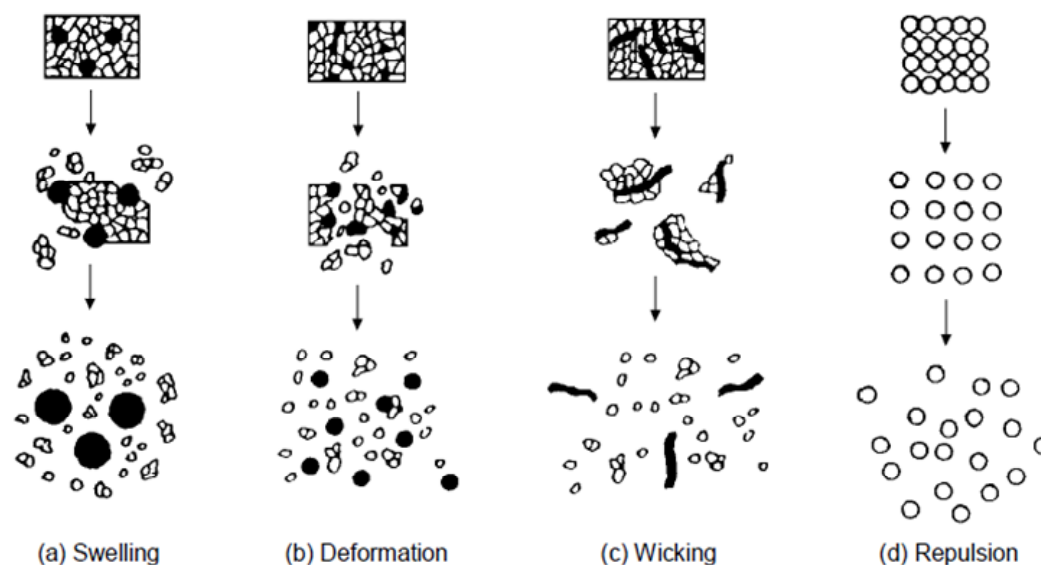


Figure 3. Mechanisms of action for tablet disintegrants.

### 3.1.7.3 Factors influencing tablet quality

The tablet quality is not only influenced by the particle size [18], particle shape [13], crystallinity [14], particle deformation properties [15-17] and its composition [19] but also by tableting conditions, such as compression force [21] and tableting speed [20, 22]. Therefore constant and robust tablet quality is still a challenge for the pharmaceutical industry.

There are two types of tablet press in common use in pharmaceutical company. One is the single station eccentric press and another is multi station rotary tablet press. There are both mainly three steps of tablet compression on a rotary press.

- Die filling

The die is filled by powder or granules when the lower punch is in the lowest position, then the lower punch is moved to its target position and excess material is scraped off. The placement of powder or granules in the die depends on its flowability, on its physical properties (size, shape, density, etc.) and on the flow conditions (hopper shape, centrifugation forces, machine vibration itself).

- Tablet formation (Pre-compression and Main-compression)

The upper punch descends and enters the die and the powder or granules are compressed until a tablet is formed. The lower punch can be stationary or move upwards in the die. After maximum applied force the upper punch leaves the powder or granules. Tanino et al. reported that pre-compression helps in removal of entrapped air and improves bonding between particles during the compaction phase [48].

- Tablet ejection and Take off

The lower punch rises and the tablet is removed by a pushing device. A lubricant plays important role to minimize the stress between tablet and punch and/or die during ejection.

Because of the lack of a large amount of API at the earlier formulation design and development phase, the experiments to use the multi station rotary tablet press are not possible. What the most difference between the multi station rotary tablet press and the single station eccentric tablet press is the dwell time during the tableting. The dwell time of the single station eccentric press is much longer as compared with the multi station rotary tablet. The difference of dwell time is the possibility to change the packing geometry related to the porosity of tablet.

#### 3.1.7.4 Introduction of Presster™

Tablet properties such as a hardness, disintegration or dissolution behavior may change when a tableting process is changed from one machine to another. In short, important parameters such as porosity, pore size and pore volume depending on compression force and compression speed [49-51] are related to the dwell time (Figure 4). As mentioned above, it would be desirable to manufacture the tablets on a rotary tableting machine for industrial use for an optimal formulation designing. However, because of the lack of a large amount of API at the earlier formulation designing and development phase, these experiments are not possible. For this reason, the MCC (Metropolitan Computing Corporation) Presster™ equipment [23], which needs only a small amount of powder material, was used to simulate mechanically a rotary tableting machine. An excellent concept of Presster™ is a linear-type rotary tableting machine replicator so that one single station tablet press (Figure 5) with

standard tooling can move with high speed by mimicking the industrial multi station rotary tablet press. Presster™ is instrumented with Linear Variable Differential Transformers (LVDT) for upper and lower punch displacement measurement. Moreover strain gauges were installed for force measurement during pre-compression and main compression, for die wall expansion measurement with instrumented die, for ejection force and for tablet take-off force.

The scale up factors Presster™ are helpful for designing a tablet formulation, but cannot completely simulate an industrial multi station rotary due to the following differences:

- Feeding protocol
- Distance between pre-compression roll and main compression roll
- Turret heating effect and Centrifugal force effect due to linear construction
- Vibration effects

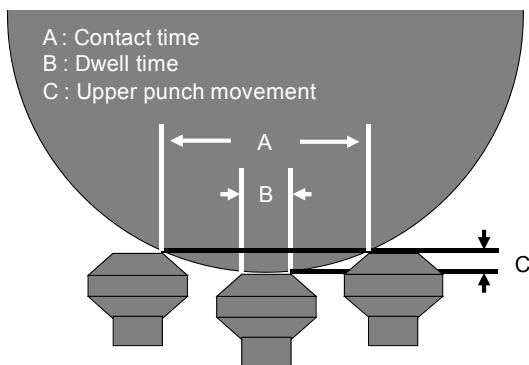


Figure 4. Schematic explanations of contact time and dwell time.

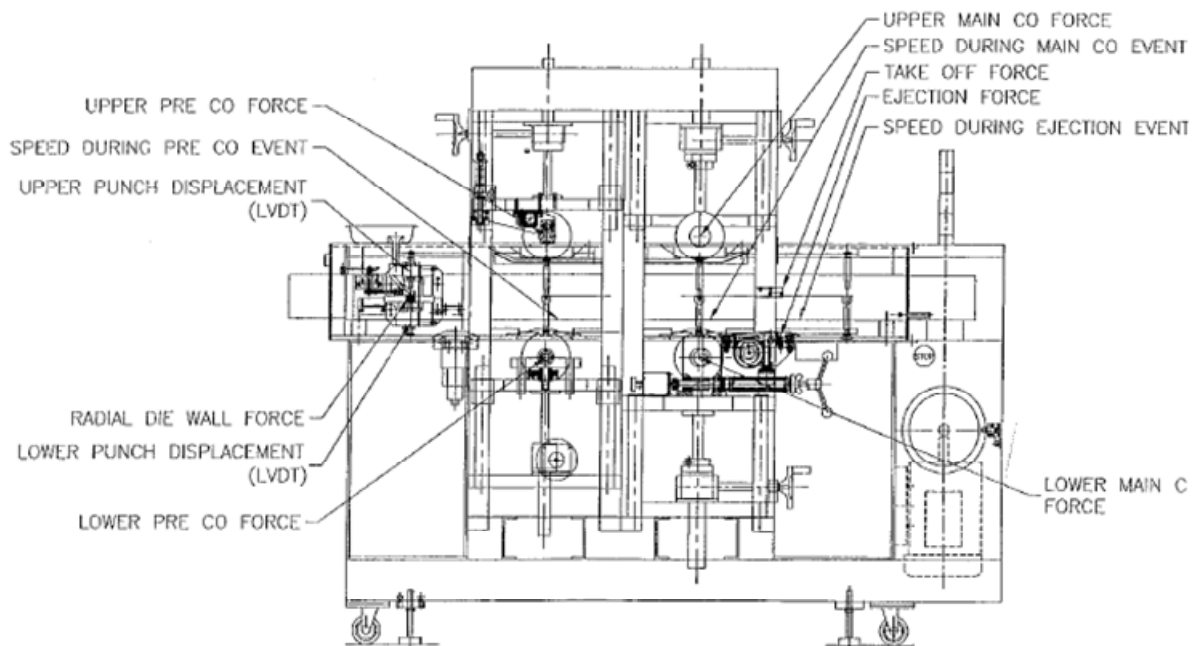


Figure 5. Schematic of Presster™.

## 3.2 Near infrared (NIR) imaging

### 3.2.1 Introduction of NIR and NIR imaging

The US Food and Drug Administration (FDA) strongly advocated that Process Analytical Technology (PAT) initiative [52] has promoted the idea of improving the quality of the pharmaceutical products by deeper understanding processes involved in drug manufacturing. The ultimate goal is to achieve quality by design of pharmaceutical dosage forms.

Spectroscopic techniques such as near infrared (NIR) are nowadays used for process control and quality assurance due to the advantage of their rapid, nondestructive analysis. NIR spectrophotometer was listed in European pharmacopoeia as a general monograph in 1997. It has a wide variety of applications for both chemical and physical analysis according to the European pharmacopoeia (Ph. Eur.), for example identification of active substances and excipients [53].

NIR spectral range extends from about 780 nm to about 2500 nm (from about 12800  $\text{cm}^{-1}$  to about 4000  $\text{cm}^{-1}$ ). NIR spectra are dominated by C-H, N-H, O-H and S-H overtone resonances and combination of fundamental vibrational modes [53]. In NIR spectroscopy, only one spectrum per sample is obtained. However the technique to acquire several thousand spectra per one measurement has developed in order to provide spatial information of a data cube which is hyperspectral NIR imaging as shown in Figure 6.

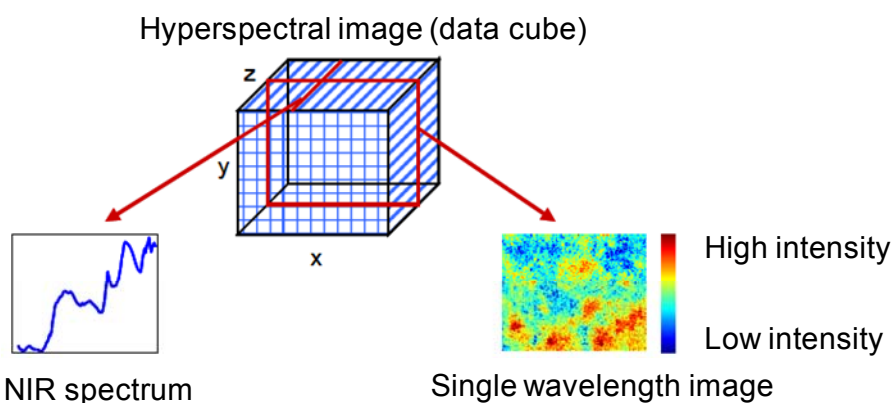


Figure 6. Diagram of hyperspectral NIR imaging [54].

### 3.2.2 Application of NIR imaging in tablet formulation design

There are various parameters established well in the modern pharmacopoeia in order to assess the tablet quality such as its appearance, weight, thickness, hardness (tensile strength), friability, moisture, assay, content uniformity, disintegration time, dissolution profiles. On the other hand, NIR imaging in pharmaceuticals has nowadays developed as an analytical tool for pharmaceutical formulation [55] insight in order to get more scientific

understanding. NIR imaging provides spatial, chemical, structural, and functional information. The increased understanding at the micro-scale such as the particle size of the APIs in the formulation and how it distributes relative to other components can improve the formulation characteristics. Several applications of NIR imaging in pharmaceuticals during formulation development have been reported. For example, it was used to show the content uniformity problems attributed to the large API agglomeration in powder blend [56], to detect the chemical composition of granules [57], it was also applied to monitor the coating thickness of tablets [58]. However a few physical characteristics related to the tablet quality have been reported. It was to assess the density or porosity in tablet when the compression force was different [59], to demonstrate the disintegrant cluster size increased with increasing the compression force in order to explain the alteration of the product dissolution [60]. In this thesis, NIR imaging technology has applied to visualize multi component distribution on the tablet surface according to the loading volume of MA in order to get the more scientific understanding of the tablet characteristics.

### **3.3 Response surface methodology**

#### **3.3.1 Response Surface Methodology (RSM) and Design of Experiment (DOE)**

Response surface methodology (RSM) is one of the useful approaches for selecting the optimum pharmaceutical formulation design on the basis of the experimental data. Leuenberger and Guitard published in 1978 from Sandoz Pharmaceutical Research Labs the article “Drug Delivery Systems for Patient Compliance” [61] with a DOE using central composite design (CCD) manufactured 27 batches, i.e. an orthogonal factorial design with five factors, which was able to show a response surface with a quadratic polynomial equation.

DOE is recommended by FDA [1, 52] as mentioned by Ajaz Hussain, at that time deputy director, who visited the laboratories of the Institute of Pharmaceutical Technology at the University of Basel in 2004 with Helen Winkle [62], the actual Director of FDA’s Office of Pharmaceutical Science of the Center for Drug Evaluation and Research (CDER). DOE should replace “Trial and Error” experiments in the Pharmaceutical R & D laboratories (Figure 7) [62]. The DOE using central composite designs (CCD) has the intrinsic property to check the response surface if a minimum or a maximum or a saddle is part of the surface (Figure 8 and 9) [61]. DOE can be also used for drug-excipient compatibility studies [63]. Thus, RSM and DOE enable to explore the behavior of a formulation by changing the concentration of the excipients, drug substance and process parameters according to today’s requirements of ICH Q8 [1, 52, 64, 65].

Such a study can be called a “sensitivity analysis” of the robustness of a formulation to be marketed. A “sensitivity analysis” is in general an integral part of an F-CAD (Formulation-Computer Aided Design, see section 3.6.2) in-silico analysis searching the most robust tablet

formulation for a specific drug dissolution profile in different buffer media (pH 1.2, pH 6.8, pH 7.2 etc.). In the present study, F-CAD was tentatively applied to give an estimate for the tablet disintegration time as the drug substance has extremely low water solubility.

## Product and Process Quality Knowledge: Science-Risk Based cGMP's

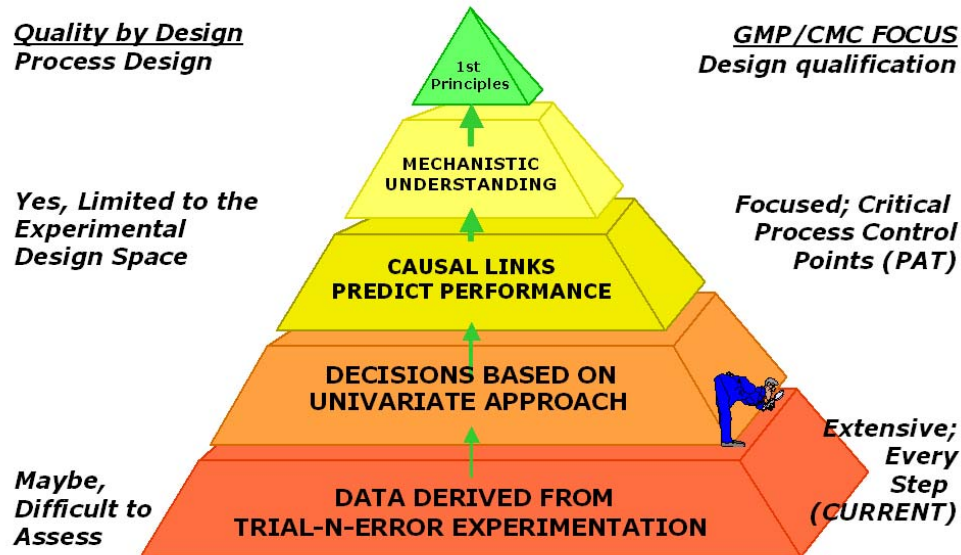


Figure 7. Knowledge pyramid (according to Dr. A. Hussain, FDA) [62]

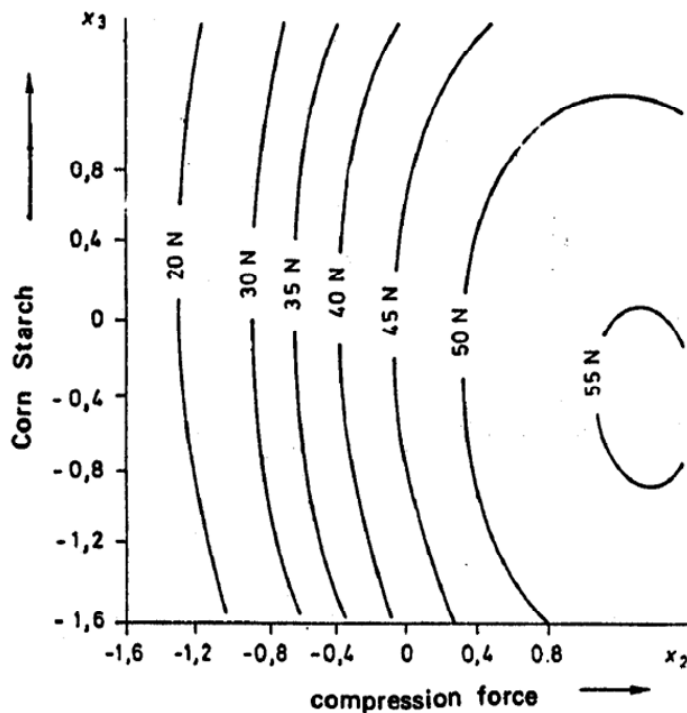
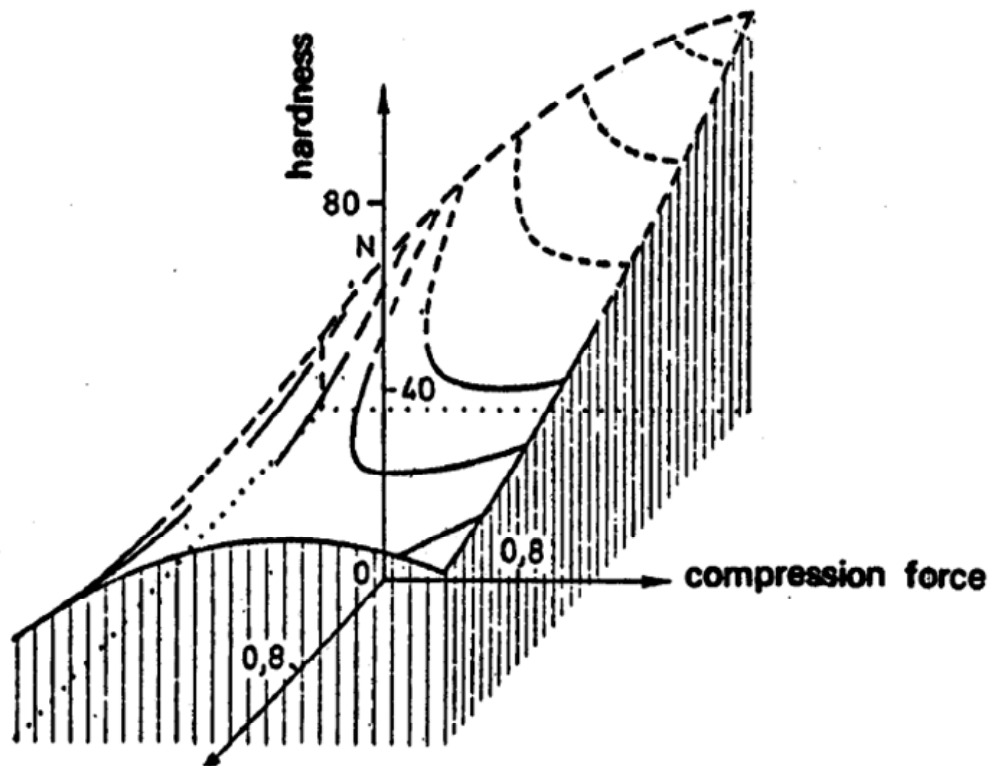


Figure 8. Hardness of a tablet as a function of compression force and concentration of corn starch [61].



### Concentration of Magnesiumstearate

Figure 9. Hardness of a tablet as a function of compression force and concentration of magnesium stearate [61].

Table 5 Three Dimensions on the Critical Path [64, 65]

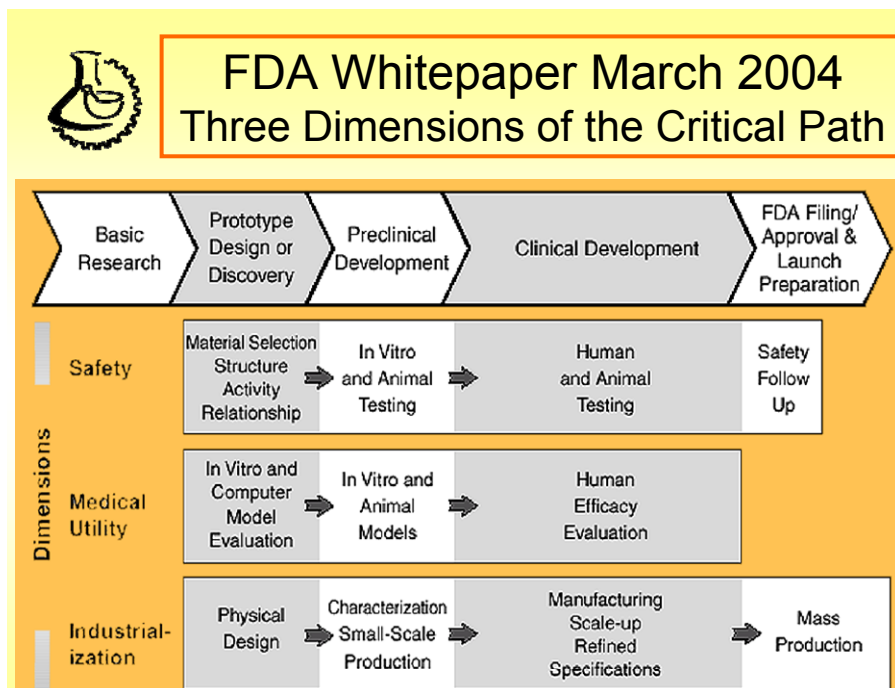
## FDA Whitepaper March 2004: Three Dimensions of the Critical Path

<b>Assessing Safety</b>	<b>Adequate safe</b> for each stage of development	<b>Preclinic:</b> Safe for early human testing. No products with safety problems. <b>Clinic:</b> Safe for commercial distribution.
<b>Demonstrating Medical Utility</b>	<b>Benefits people</b>	<b>Preclinic:</b> Appropriate design (devices) or candidate (drugs) with high probability of effectiveness <b>Clinic:</b> Effectiveness in people
<b>Industrialization</b>	Lab concept or prototype → <b>manufacturable product</b>	<ul style="list-style-type: none"> <li>• Design a <b>high-quality product</b> Phys. design/Characterization/Specifications</li> <li>• Develop <b>mass production capacity</b> Manufacturing scale-up/Quality control</li> </ul>

(C) H. Leuenberger, University of Basel
Slide 97



Table 6 Working in Three Dimensions on the Critical Path [64, 65]



The simplest  $2^n$  design with two factors A, B including the Yates scheme is described below in Table 7 and Figure 10. Table 7 and Figure 10 are part of Leuenberger's lecture in University of Basel for undergraduate students. Yates scheme of a  $2^2$  Design with A = amount of maize starch (MS, lower level -: 10 mg, upper level +: 15 mg) and B = compressional force (lower level -: 6 kN, upper level +: 8 kN). Please note that this is a "tutorial" and the Results included in Table 7 corresponding to the percentage of drug release after 1 hour. According to the Yates scheme, the effect of 2A, 2B and the interaction 2AB between the factor A and B can be quantified. This is the most important point of using factorial designs that it is possible to check for possible interactions and possible to quantify such interactions. The evaluation of the above very simple design leads to the result below:

Table 7  $2^n$  design with n = two factors A, B including the Yates scheme

Yates	A	B	AB	Results
(1)	-	-	+	82
a	+	-	-	82
b	-	+	-	78
ab	+	+	+	95
$\Sigma$	2A	2B	2AB	T/4

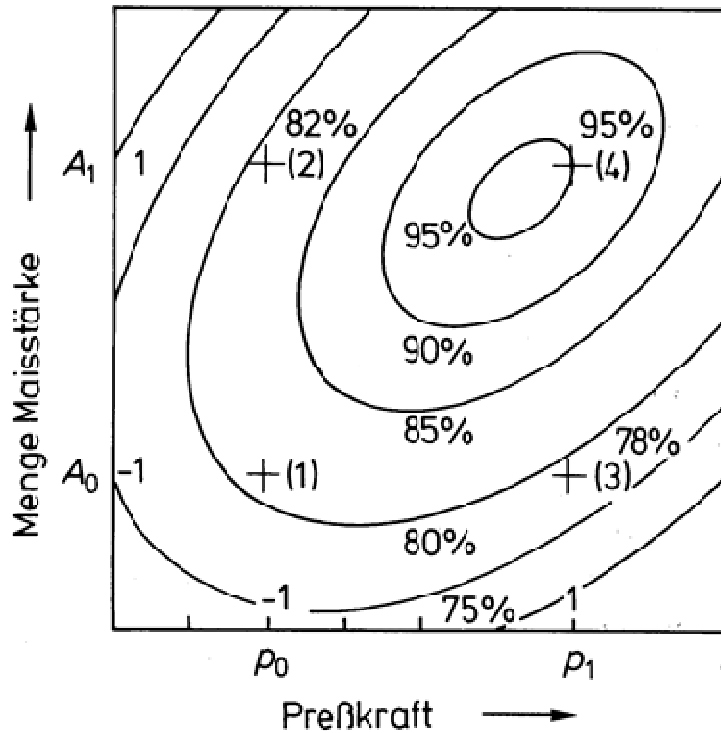


Figure 10. Graphical representation of the evaluation of the above Yates scheme with the factor A = amount of maize starch (Menge Maisstärke)  $A_0$  and  $A_1$  and the factor B (Presskraft) with the compressional force  $p_0$  and  $p_1$ .

It is possible to write down the mathematical model  $F(x_1, x_2)$  of a  $2^n$  design with  $n = 2$  factors (variable  $x_1$  corresponding to factor A, variable  $x_2$  corresponding to factor B) as follows:

$$F(x_1, x_2) = b_0 + b_1x_1 + b_2x_2 + b_{12}x_1x_2 \quad \text{Equation (3)}$$

Equation 3 is called “summarizing equation” of the  $2^2$  design with  $b_0 = T/4$ ,  $b_1 = A/2$ ,  $b_2 = B/2$  and  $b_{12} = AB/2$  (interaction term). The values of A, B and AB can be simply calculated using the Yates scheme of Table 7. Thus, e.g. the value of 2A is equal to the sum of the column of the Results taking care of the plus or minus signs in the Table 7:

$$\begin{aligned} \text{i.e. } -82\% + 82\% - 78\% + 95\% &= 17\% = 2A, & -82\% - 82\% + 78\% + 95\% &= 9\% = 2B \\ & & +82\% - 82\% - 78\% + 95\% &= 17\% = 2AB \end{aligned}$$

$$\text{i.e. } b_0 = T/4 = 84.25\%, \quad b_1 = 4.25\%, \quad b_2 = 2.25\%, \quad b_{12} = 4.25\%$$

leading to the Equation 4:

$$\begin{aligned} F(x_1, x_2), (\text{i.e. } [\%] \text{ dissolved}) &= \\ 84.25[\%] + 4.25[\%]x_1 + 2.25[\%]x_2 + 4.25[\%]x_1x_2 & \quad \text{Equation (4)} \end{aligned}$$

With the values of  $x_1$ ,  $x_2$  according to the coded values in Table 7, i.e. +1 or -1, evidently, the summarizing equation is able to reproduce the result of each experiment [(1), a, b, ab] in Table 7. Due to the fact that the  $2^n$  design is orthogonal, the value of the coefficients  $b_1$ ,  $b_2$ , and  $b_{12}$  can be compared directly. Please note that the value of  $b_{12}$ , i.e. the interaction term AB has the same magnitude, in fact identical in this case, as the effect of the factor A, which is described with the value  $b_1$ . Thus, it is important in pharmaceutical sciences that interactions can play an important role, which can be detected with DOE but can be missed by just doing a conventional experiment with changing only one factor a time and keeping constant the remaining factors. However it has to be kept in mind in Table 7 that no replicates of the experiments have been performed, i.e. the mathematical model  $F(x_1, x_2)$  is a first approximation of the reality.

The simplest central composite design (CCD) with just two factors A, B (Table 8) is called a "3 x 3" design which leads to the following nine experiments with the following factor levels; -1 (lower level), +1 (upper level), 0 (mean of the levels +1, -1) and the level  $\alpha$ , which depends whether the central composite design (CCD) is orthogonal or rotatable. In case of two factors A, B, the value of  $\alpha$  is equal to 1.414 for a rotatable and equal to 1 for an orthogonal CCD.

Table 8 Central composite design (CCD) with just two factors A, B

Experiment No.	Factor	
	A	B
1	-1	-1
2	+1	-1
3	-1	+1
4	+1	+1
5	$-\alpha$	0
6	$+\alpha$	0
7	0	$-\alpha$
8	0	$+\alpha$
9	0	0

It is also possible to write down for a CCD as a summarizing equation (Equation 5), which looks as follows for the factors A and B using the transformed variables z:

$$F(x_1, x_2) = a_0 + a_1 z_1 + a_2 z_2 + a_{12} z_{12} + a_{11} z_{11} + a_{22} z_{22} \quad \text{Equation (5)}$$

With  $z_1 = x_1 - m(x_1)$ ,  $z_2 = x_2 - m(x_2)$ ,  $z_{12} = x_1 x_2 - m(x_1 x_2)$ ,  $z_{11} = x_1^2 - m(x_1^2)$ ,  $z_{22} = x_2^2 - m(x_2^2)$ ,  $m(x)$  means mean value of  $x$ , the value of  $x$  is again coded, i.e.  $-\alpha$ ,  $-1$ ,  $0$ ,  $+1$ ,  $+\alpha$  in case of the orthogonal CCD  $\alpha$  is equal to 1. For the purpose that the coefficients  $a_0$ ,  $a_1$ ,  $a_{11}$ ,  $a_{12}$  and  $a_{22}$  are orthogonal, the mean of  $x_1^2$  and  $x_2^2$  needs to be equal to  $(4 + 2\alpha)/9 = m(x_1^2) = m(x_2^2)$  [66]. It is important to keep in mind that the summarizing equation (Equation 5) of a CCD is only able in a second approximation of the reality to yield as a response surface, which shows a minimum a saddle point or a maximum. If the grid of the lattice is too large, it is possible that a minimum surface may not be detected (see second CCD in section 6.11.3).

Please note that a formulation which contains three components such as maize starch (MS), lactose (LA) and mefenamic acid (MA) can be easily reduced to a two component system consisting of MS (disintegrant) and of the ratio LA/MA, which is the ratio of the hydrophilic filler LA and the hydrophobic drug substance MA. Thus, it is possible to construct the simplest CCD with two factors MS and LA/MA (see section 6.11.3).

For the evaluation of the CCDs in section 6.11.3, it is possible to use the software Design-Expert 7<sup>®</sup>, which is able to calculate the  $r^2$  values among others, i.e. the percentage of the data, which are explained by the mathematical model and is able to plot the corresponding response surface in three dimensions.

### 3.3.2 dataNESIA software

Conventional RSM typically uses a linear regression model and a partial least square regression (PLSR) model and a quadratic polynomial equation approximation to generate a response surface from experimental data. However the prediction of pharmaceutical responses based on the conventional RSM is often resulting in poor estimations for optimum pharmaceutical formulation design because pharmaceutical formulations for solid dosage forms are complex and heterogeneous disordered particles systems, which have non-linear characteristics [67, 68]. Artificial neural network (ANN) may be used for pharmaceutical formulation design which has non-linear characteristics; however it is laborious and time-consuming task to find the optimum modeling [68].

Yamatake & Co., LTD. and Takayama [67, 68] have developed new RSM incorporating multivariate spline interpolation (RSM-S) represented by a spline approximation (biharmonic spline or thin-plate spline) [68-70], in order to interpolate the experimental data distributed at random in a multidimensional space for the response surface generation.

### 3.3.3 Multivariate spline interpolation

Multivariate spline interpolation has been effectively used as a tool to interpolate altimeter data in the field of geophysics. The basic concept of multivariate spline interpolation involves a boundary element method which can be considered as the transformation equation of elasticity such as a thin elastic beam shown in Figure 11 as an example [67].

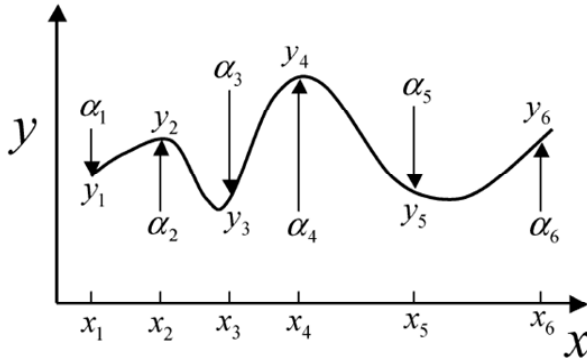


Figure 11. A function  $y$  that passes through the data points  $y_1$  located at  $x_1$  is found by applying point forces  $\alpha_1$  to a thin elastic beam [67].

The experimental data were also considered as the variations at each point, and the spline approximation gives the solution of transformation equation of elasticity to be minimized the elastic strain energy (Equation 6) [70].

$$E = \int_s (\nabla^2 f(x))^2 ds \quad \text{Equation (6)}$$

where  $\nabla^2$  is the Laplacean and  $\int_s ds$  is the integration over all ranges

Green functions were used for solving Equation 6. The biharmonic spline used in this thesis was expressed in Equation 7 [70].

$$y = \sum_{i=1}^n \alpha_i g(d_i) \quad \text{Equation (7)}$$

where  $n$  is the number of data points,  $d_i$  is the standardized Euclidian distance between  $x$  corresponding to number  $i$  data point and the optimal  $x$ ,  $g(d_i)$  is the green function whose variables are  $d_i$ .

The definition of this function is changed by the dimensions of the input variable ( $x$ ).  $\alpha_i$  is a coefficient calculated by a linear matrix operation.

### 3.4 Percolation theory

#### 3.4.1 Principles of percolation theory

Pharmaceutical formulations for solid dosage forms are complex and heterogeneous disordered particular systems. Topological modeling is necessary to be taken into an account for a geometrical description. Percolation theory is, in fact, one of the suitable topological modeling tools to predict and simulate the geometric phase transitions in complex systems, such as a tablet formulation [8]. Geometrical phase transitions are independent of physical and chemical properties of the components. In other word, the geometrical phase transitions have universally happened and this facilitates the modeling. Thus, percolation theory allows finding the regions where the system undergoes the geometrical phase transition. It happens at critical concentration of the components where a component percolates (percolation threshold,  $p_c$ ) and where the system property often shows a great change, which is called as catastrophic change in this thesis. In terms of tablet formulation design, such regions usually linked to external value of properties such as water uptake, disintegration time, and dissolution rate. It is essential to note that a percolation threshold is a volumetric (not a mass) ratio ( $v/v$ ) of the components from the view point of geometrical aspect. Percolation theory itself is an instrument of probability theory.

This introduction to percolation theory cannot be exhaustive and follows the lines given by Stauffer and Aharony. For detail understanding, it is recommended to read “Introduction to percolation theory” [71]. There is the excellent Japanese translated textbook by Odagiri [72]. Percolation theory deals with the number and properties of those clusters [71]. The underlying idea of cluster and its percolation is to see a system as composed of subunits (site) that are distributed randomly on a two dimensional lattice. In the simplest case, the lattice is square (Figure 12) and the squares are either occupied or empty. There are mainly two kinds of cluster types, site cluster and bond cluster.

- Site cluster

Some sites are occupied with a certain probability ( $p_s$ ) and some are empty with certain probability ( $1 - p_s$ ). Site clusters are defined as groups of neighboring occupied site shown as groups of circles in Figure 12.

- Bond cluster

Each sites of the lattice are occupied, and some of them are connected though line shown as circles connected by thick bars in Figure 12.

Gray colored circles represent the percolated cluster in the square lattice [73].

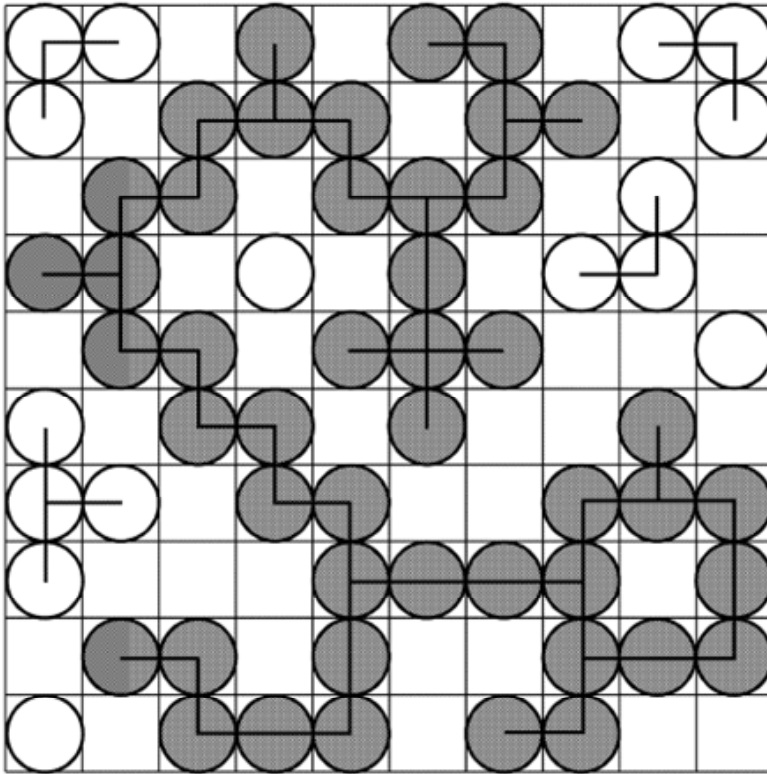


Figure 12. Groups of circles are defined as a site clusters and circles connected by thick bars are defined bond clusters. Gray colored circles represent the percolated cluster in the square lattice [73].

For the tablet formulation design, we assume that the packing geometry of particles in the tablet is more important to consider than the collision of particle each other. Thus, this thesis deals almost with site percolation.

In site percolation, the formation of clusters is a function of the occupation probability ( $p$ ) of the lattice chosen. Figure 13 and 14 show that a site percolation phenomenon with an occupation probability ( $p$ ) below and above the percolation threshold ( $p_{cs} = 0.592746$ ) in square lattice respectively [71]. The percolation threshold is defined as an occupation probability ( $p$ ) where for the first time a percolating cluster is formed. Below percolation threshold ( $p_{cs}$ ), only isolated clusters exist. However near the percolation threshold ( $p_{cs}$ ) an 'infinite cluster' is formed spanning the whole lattice from left to right and from top to bottom. This 'infinite cluster' leads to the catastrophic change in the system.

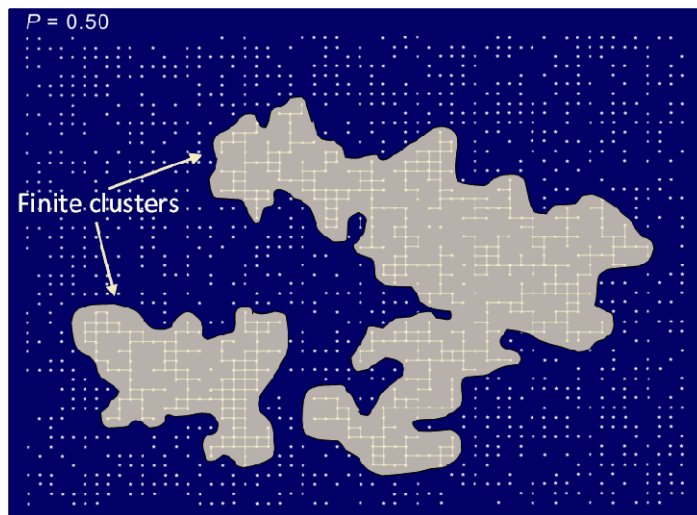


Figure 13. Square lattice (site percolation, i.e. random occupation of lattice sites) with an occupation probability ( $p$ ) below the critical concentration, i.e. percolation threshold ( $p_c$ ). No 'infinite cluster' is formed. Two finite clusters are shown [71].

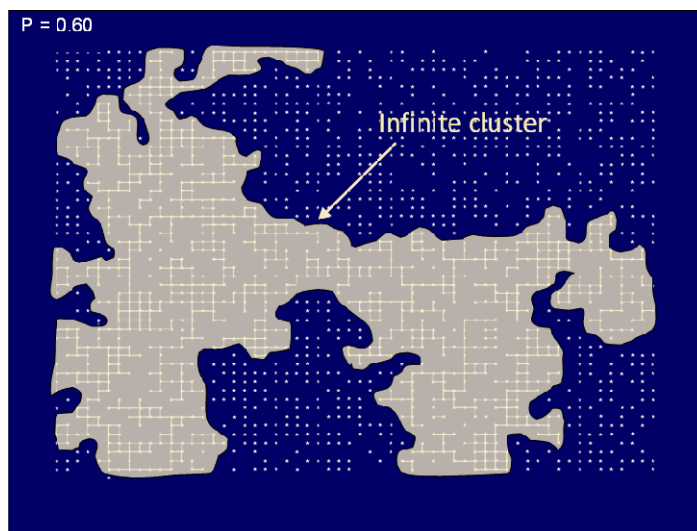


Figure 14. Square lattice (site percolation) with an occupation probability ( $p$ ) above the critical concentration, i.e. percolation threshold ( $p_{cs}$ ). An 'infinite cluster' percolates the system [71].



There are other lattices not only in two dimensions but also in three or more [71]. Examples of two dimensions (a, b) and three dimensions (c-g) lattices are shown in Figure 15.

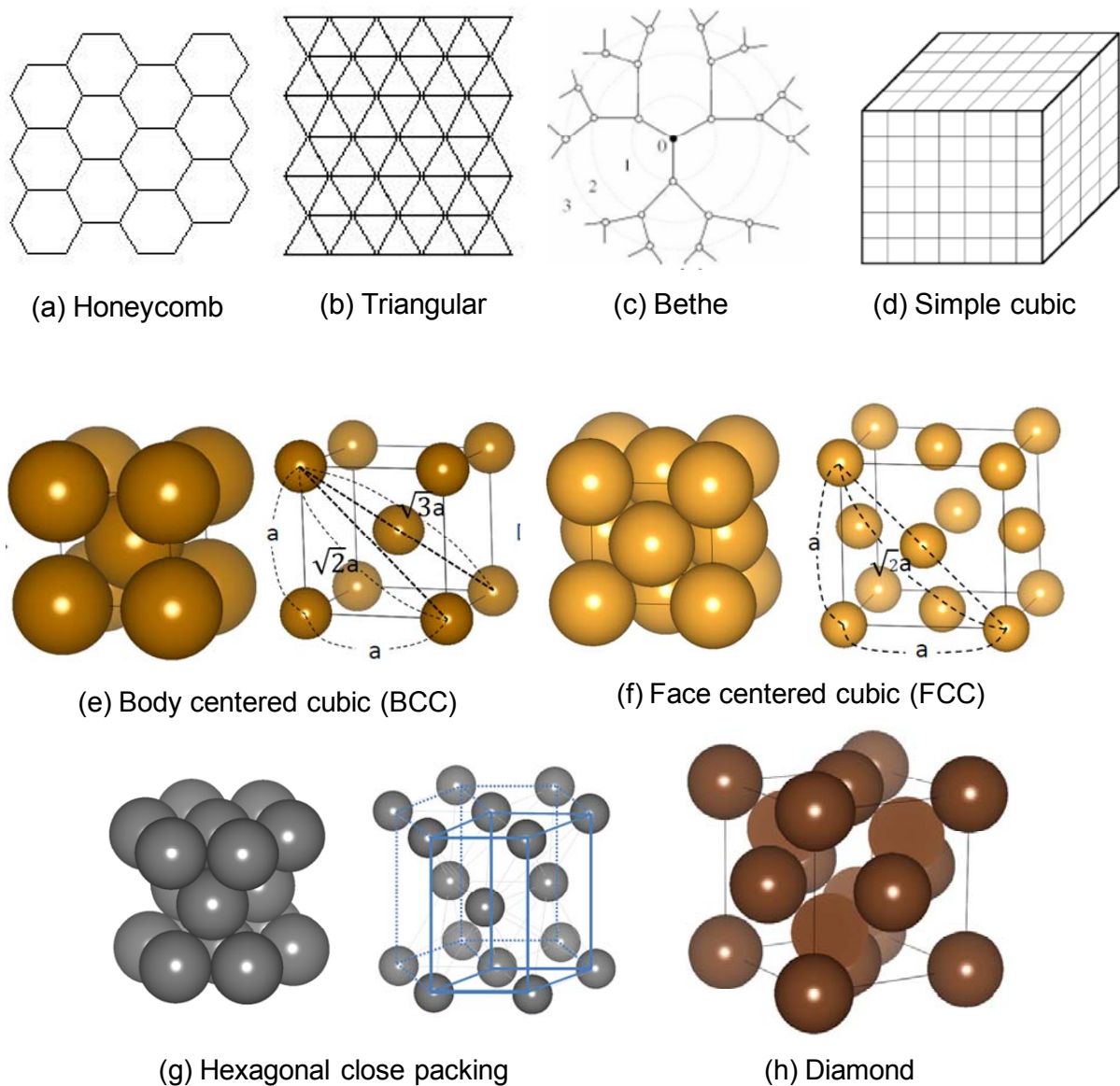


Figure15. Examples of two dimensions (a, b) and three dimensions (c-g) lattices.

- (a) Honeycomb, (b) Triangular, (c) Bethe (coordination number  $z=3$ )  
 (d) Simple cubic, (e) Body centered cubic (BCC), (f) Face centered cubic (FCC)  
 (g) Hexagonal close packing, (h) Diamond

The main postulate of percolation theory is the probability ( $p$ ) of forming an infinite cluster spanning through the infinite lattice is the Kolmogorov's zero-one law [11]. As a small isolated cluster grows, there will be a point, when for the first time it spans through the system. The percolation threshold ( $p_c$ ) is a so-called as an infinite cluster through the system. At or near the percolation threshold ( $p_c$ ), catastrophic change in the system occurs. A typical

example of catastrophic change can be seen in a particle mixture containing black particles which are electrically conductive, and white particles which are insulators and are no electrical conductivity. It is known that site percolation threshold on simple cubic lattice is 0.311608 [71]. If black/white particles system described in Figure 16 is composed to a tablet, the tablet became electrically conductive just at the percolation threshold [74, 75].

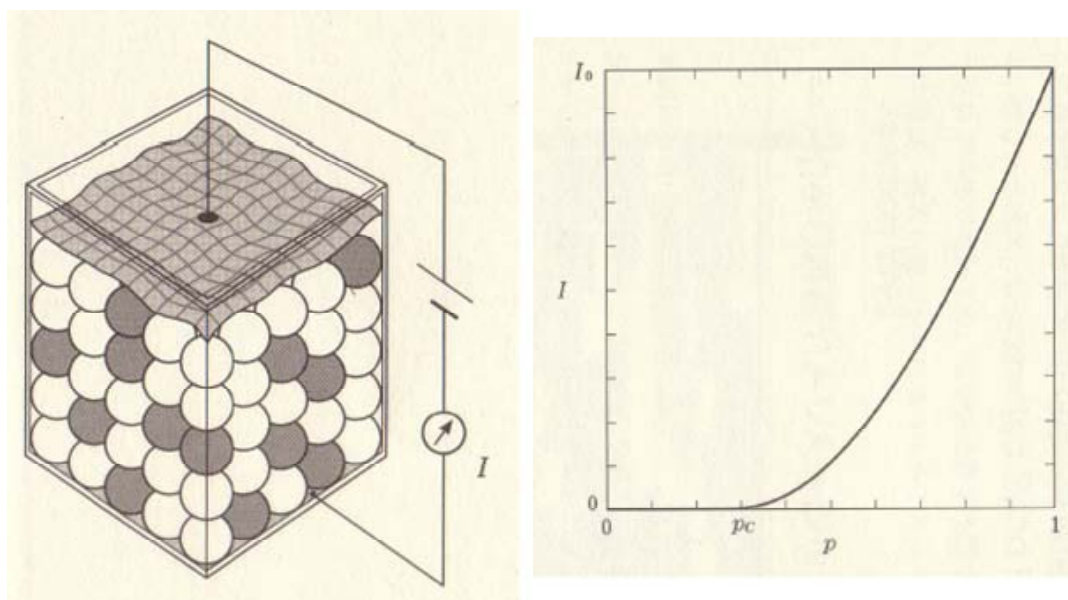


Figure 16. A typical example of catastrophic changes in the system at or near the percolation threshold ( $p_{cs} = 0.311608$ ), where  $p$  is probability of black powder,  $I$  is electrical conductivity [75].

The percolation threshold ( $p_c$ ) is a quantity for a system depending on the lattice type, the dimension of the system and on the type of percolation [71] (non-universality).

Three dimensions lattices should be considered for the designing of pharmaceutical tablets. Critical parameters on three dimensional lattices are summarized in Table 9. For three dimensional lattices face-centered cubic (FCC), body-centered cubic (BCC), simple cubic (SC), diamond and random close packed (RCP), the threshold values have been calculated [76, 77, 78, 79]. The threshold values for bond ( $p_{cb}$ ) and site ( $p_{cs}$ ) percolation are different from the different lattices.

However, the key point is that critical volume fraction ( $\phi_c$ ) is nearly constant, varying by just a few percent from three dimensions lattice to lattice. The critical volume fraction ( $\phi_c$ ) is close to 0.16 (v/v) for the three dimensions as shown in Table 9, and is close to 0.45 (v/v) for the two dimensions (universality) [77].

The relationship between  $\phi_c$  and  $p_{cs}$  is expressed in Equation 8.

$$\phi_c = f \times p_{cs} \quad \text{Equation (8)}$$

where  $f$  is the filling factor of the lattice which represents the solid fraction of the volume, and  $p_{cs}$  is site percolation threshold (= critical concentration).

Table 9 Critical parameters on three dimensional lattices

Lattice	$p_{cb}$	$p_{cs}$	Coordination Number, $z$	Filling Factor, $f$	$z p_{cb}$	$f p_{cs}$ ( $\phi_c$ )
FCC	0.119 <sup>[77]</sup>	0.198 <sup>[77]</sup>	12 <sup>[77]</sup>	0.7405 <sup>[76, 77]</sup>	1.43	0.15
BCC	0.179 <sup>[77]</sup>	0.245 <sup>[77]</sup>	8 <sup>[77]</sup>	0.6802 <sup>[76, 77]</sup>	1.43	0.17
SC	0.247 <sup>[77]</sup>	0.311 <sup>[77]</sup>	6 <sup>[77]</sup>	0.5236 <sup>[76, 77]</sup>	1.48	0.16
Diamond	0.388 <sup>[77]</sup>	0.428 <sup>[77]</sup>	4 <sup>[77]</sup>	0.3401 <sup>[76, 77]</sup>	1.55	0.15
RCP		0.27 <sup>[77]</sup>	6 <sup>[78]</sup>	0.64 <sup>[79]</sup>	1.62	0.17
Average					1.5 ± 0.1	0.16 ± 0.01

Thus, critical volume fraction ( $\phi_c = 0.16 \pm 0.01$ , v/v) can predict the site percolation threshold. Experiments were carried out to determine the conductivity threshold composed of metallic and insulating spheres for random close packed (RCP). In this context, it is important to realize, that the two components in the focus (metallic and insulating spheres) need to have different properties to show the percolation effect such as an electric conductivity or being an insulator. The critical volume fraction of metric sphere was in rough agreement with 0.16 (v/v) [80, 81, 82]. In addition, Wu and McLachlan [83] studied that critical volume fraction ( $\phi_c$ ) of graphite/boron-nitride composite was 0.15 (v/v), which was also close to 0.16 (v/v).

### 3.4.2 Application of percolation theory in pharmaceutical area

Percolation theory was introduced to design the pharmaceutical formulation by Leuenberger [8, 84] for not only solid dosage form but also liquid dosage form [85]. Caraballo et al. has applied the percolation theory to explain the influence of main formulation factors on drug release from hydroxypropyl methylcellulose (HPMC) matrix system [86].

The percolation threshold of the water uptake [9, 10, 12], disintegration time [9-12] and intrinsic dissolution rate [9, 10] of binary tablets has been investigated in our laboratory. In case of disintegration time, the critical concentration of disintegrant for which the disintegration time reaches a minimum was observed. Remarkably, the critical volume fraction of continuous water conducting cluster as the value of 16 (% v/v) was concluded to show the critical concentration of disintegrant in the random close packed (RCP) spherical

binary tablets [11, 12]. In order to design a pharmaceutical tablet formulation, the critical concentration of disintegrant should be determined not only for binary tablets but also for multicomponent tablets. Caraballo and Leuenberger et al. reported that the existence of a 'combined percolation threshold' of sum of all the hydrophilic substance was at ca. 35% v/v in the ternary controlled release matrix system containing KCl, polyvinylpyrrolidone cross-linked (PVP-CL) and Eudragit RS-PM [87]. No one, however, has reported experimentally the location of critical concentration of disintegrant for a ternary immediate release pharmaceutical tablet formulation.

### **3.5 Percolation threshold of disintegration time with particle packing geometry considerations**

Disintegration process of tablet in case of non-fibrous disintegrant, e.g. maize starch (MS) is under the following conditions;

- A disintegrant with swelling properties is present in the tablet.
- The disintegrant itself is able to conduct water.
- There is porous structure in the tablet which can conduct water by wicking.

Further theoretical postulates are based on the following assumptions regarding to the particle packing geometry;

- Pharmaceutical tablet is a random close packed (RCP) spheres system.
- Drug and disintegrant particles are assumed to be spherical.
- Particle size distributions are narrow but can be different for each component.
- There is no significant deformation of drug particle within the compact.

#### **3.5.1 Random close packed (RCP) spheres system**

Particles in a pharmaceutical tablet are arranged in a disordered close packing. It is assumed that spherical compacted particles can be placed at random and are in close contact with their direct neighbors. Such a system is named random close packed (RCP) spheres system. Macro observations of spheres in RCP reveals that the most stable, probable and smallest local packing of spheres are hexagonal close packing or simple cubic close packing highlighted by red in Figure 17.

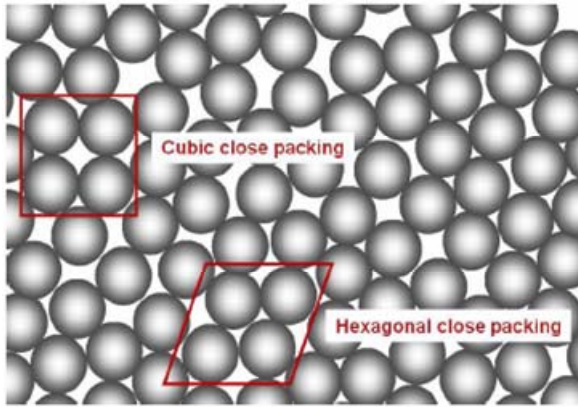


Figure 17. Two dimensional view of a RCP spheres system with example (circle in red) of the two smallest and most probable local packing: hexagonal close packing or simple cubic close packing [12].

It has to be pointed out that a RCP system can be composed of different size. A few local hexagonal close packing or simple cubic close packing can still be identified in a tablet.

### 3.5.2 Sphere caging and non-caging concept in case of binary RCP system

When RCP system is the binary system composed of small and bigger spheres, it is easier to understand the concept of the sphere caging and non-caging concept [11, 12]. If the size difference between two spheres is large enough, small sphere (red) can be caged by bigger spheres (black) in a hexagonal close packing (Figure 18 (a)-1 or (a)-2). If a small sphere (red) is too large for being caged but is still below the critical caging size, this sphere (red) can be caged by bigger spheres (black) as a part of body centered cubic (BCC) (Figure 18 (b)). Above this critical caging size, caging by black spares in simple cubic (SC) is not possible any more (Figure 18 (c)-1). The caging sphere (black) will be apart and caged sphere (red) will be closer each other (Figure 18 (c)-2).

Thus sphere caging in RCP system can be distinguished as two classes. If the small spheres can be caged by bigger sphere in hexagonal close packing or simple cubic close packing, it is defined as case I. If not, it is defined as case II.

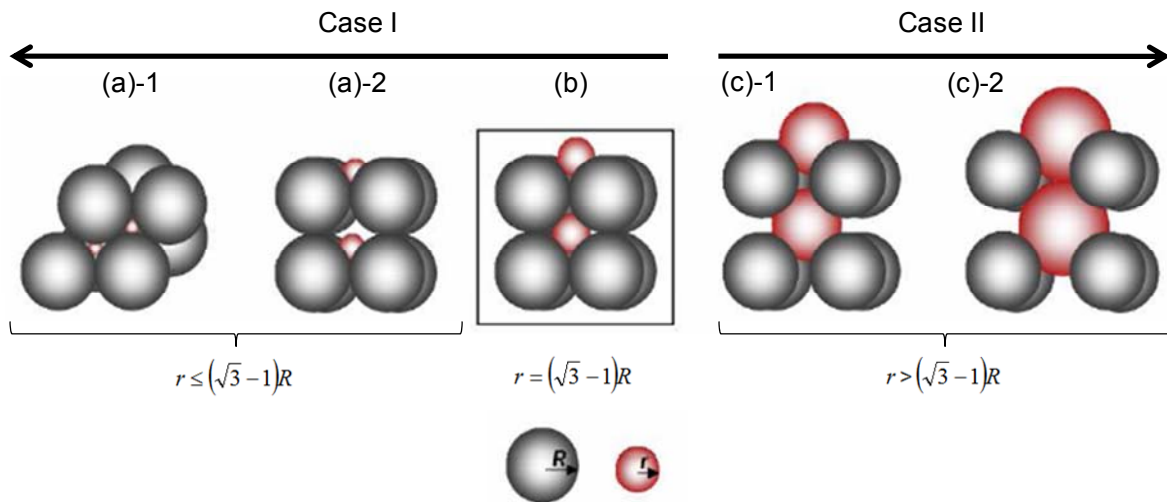


Figure 18. Sphere caging and non-caging for RCP system [12].

The radius  $r$  of the small sphere (red) that can be caged by four other bigger spheres (black) of radius  $R$  in simple cubic (SC) can be calculated by Equation 9.

$$r = (\sqrt{3} - 1)R \quad \text{Equation (9)}$$

According to Equation 9, if the  $r/R$  ratio is less or equal to 0.732 it is defined as case I. If not, it is defined as case II.

### 3.5.3 Sphere caging and non-caging concept for binary drug/disintegrant tablet

When tablet is the binary system composed of spherical drug and disintegrant particles, it is easier to understand how to apply previous concept of the sphere caging and non-caging for binary RCP system into the pharmaceutical area. The case I and II described previously are applied to the caging of disintegrant particles by drug particles. If a disintegrant particles can be caged by drug particles as a part of body centered cubic (BCC) or simple cubic (SC), it is classified as case I. If a disintegrant particles is too large for being caged by drug particles as a part of body centered cubic (BCC), it is classified as case II. Thus, the drug particles will be apart and disintegrant particles will be closer each other, and it is possible to create an infinite cluster through a tablet depending on its probability. If  $r$  is the mean particle radius of disintegrant and  $R$  is the mean particle radius of drugs, particle caging in a tablet in case of binary system of spherical drug/disintegrant is classified by Equation 10 and 11.

$$\text{Case I: } r \leq (\sqrt{3} - 1)R \quad \text{Equation (10)}$$

$$\text{Case II: } r > (\sqrt{3} - 1)R \quad \text{Equation (11)}$$

### 3.5.4 Water diffusion network for binary spherical drug/disintegrant tablet

When tablet is the binary system composed of spherical drug and disintegrant particles, it is easier to understand how the water can diffuse into the previous concept of sphere caging and non-caging in binary RCP system. Because it is important to consider and classify the water diffusion networks in a tablet according to the percolation theory. According to the percolation theory, a minimum disintegration time corresponds to the formation of a continuous water-conducting cluster through the entire tablet. The water can diffuse between drug particles by wicking (porous network) and through disintegrant particles (solid network).

In case I (left in Figure 19), the network created by disintegrant particles consists of the porous network between drug particles caging disintegrant particles and disintegrant solid network.

In case II (right in Figure 19), porosity and disintegrant represent two independent networks for the water diffusion. However the porous network is assumed to be occupied by swelling of big disintegrant particle.

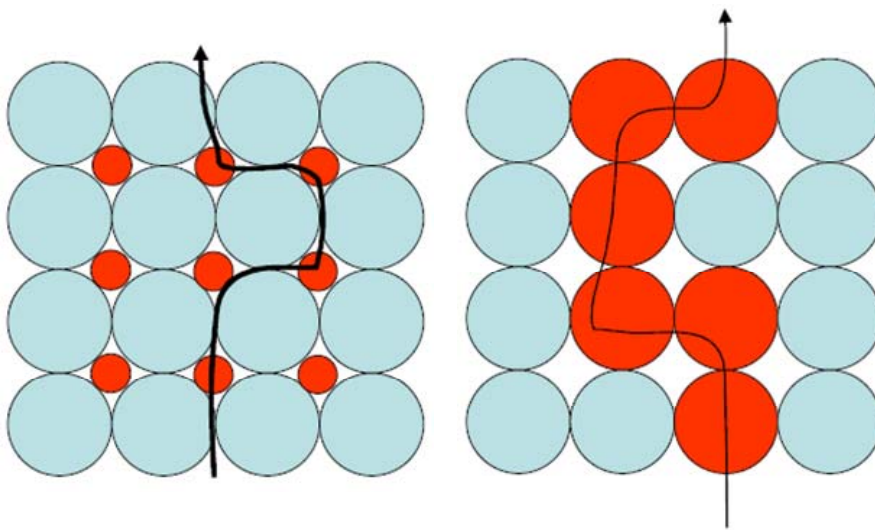


Figure 19. Left: Water diffusion porous networks in case I, Right: Water diffusion solid networks in case II.



### 3.5.5 Calculation of critical concentration of disintegrant for spherical binary drug/disintegrant tablet

As shown in Table 9, critical volume fraction ( $\phi_c$ ) of an 'infinite cluster' for random close packing (RCP) spheres system is equal to  $0.16 \pm 0.01$  (v/v). This value can be used for the calculation of the critical concentration of spherical disintegrant in order to achieve the minimum disintegration time of tablet.

When tablet is the binary spherical drug and disintegrant particles system, it is easier to understand how to calculate the critical concentration of spherical disintegrant based on the sphere caging and non-caging concept.

In the case I, the critical volume fraction of continuous water-conducting cluster involves both critical volume fraction of disintegrant and critical volume fraction of pore. If it is assumed that the porosity is constituted only by the pore between drug particles and pore is spherical, the critical concentration of the disintegrant (v/v) can be calculated by Equation 12.

$$\begin{aligned}\phi_c &= \phi_{c,dis} + \phi_{c,pore} = X_{dis}(1 - \varepsilon) + \varepsilon(1 - \varepsilon) \\ X_{dis} &= \left( \frac{\phi_c}{1 - \varepsilon} \right) - \varepsilon\end{aligned}\quad \text{Equation (12)}$$

where  $X_{dis}$  is the critical concentration of disintegrant in powder mixture (v/v),  $\phi_c$  is the critical volume fraction of an 'infinite cluster'  $0.16 \pm 0.01$  (v/v),  $\phi_{c,dis}$  is the critical volume fraction of disintegrant (v/v),  $\phi_{c,pore}$  is the critical volume fraction of pore (v/v) and  $\varepsilon$  is the tablet porosity (v/v).

In case II, porosity and disintegrant represent two independent networks for the water diffusion. However the porous network is assumed to be occupied by swelling of big disintegrant particles. The water diffusion through disintegrant particles is only taken into account. Critical concentration of the disintegrant (v/v) can be calculated by Equation 13.

$$\begin{aligned}\phi_c &= \phi_{c,dis} = X_{dis}(1 - \varepsilon) \\ X_{dis} &= \frac{\phi_{c,dis}}{1 - \varepsilon}\end{aligned}\quad \text{Equation (13)}$$

where  $X_{dis}$  is the critical concentration of disintegrant in powder mixture (v/v),  $\phi_c$  is the critical volume fraction of an 'infinite cluster'  $0.16 \pm 0.01$  (v/v),  $\phi_{c,dis}$  is the critical volume fraction of disintegrant (v/v) and  $\varepsilon$  is the tablet porosity (v/v).



Equation 14 represents a generalized model to determine the critical concentration of spherical disintegrant for drug/disintegrant RCP sphere system.

$$X_{dis} = \left( \frac{\phi_c}{1-\varepsilon} \right) - \varepsilon; \quad \text{if } \frac{r}{R} \leq \sqrt{3}-1 \quad (\text{Case I})$$

$$\frac{\phi_c}{1-\varepsilon} \quad \text{if } \frac{r}{R} > \sqrt{3}-1 \quad (\text{Case II})$$

Equation (14)

where  $X_{dis}$  is the critical concentration of disintegrant in powder mixture (v/v),  $\phi_c$  is  $0.16 \pm 0.01$  (v/v) and  $\varepsilon$  is the tablet porosity (v/v).

### 3.5.6 Critical exponent

Various system properties ( $X$ ) related to the cluster is decided by the occupation probability ( $p$ ) of cluster in the system. System property related to the occupation probability ( $p$ ) of cluster can be described by the fundamental power law of percolation theory [74, 84] in Equation 15.

$$X = S(p - p_c)^q$$

Equation (15)

where  $X$  is a system's property,  $S$  is a proportionally constant (= scaling factor),  $p$  is an occupation probability,  $p_c$  is a critical concentration (= percolation threshold),  $q$  is a critical exponent, close to the percolation threshold. Please note that the difference ( $p - p_c$ ) in Equation 15 is considered as an absolute value, i. e. there are no negative value.

It is important to know that the critical exponent only depends on the dimension of the system but neither on lattice type nor on percolation type (universality). For example, the strength of the infinite cluster for probability  $p$  above the percolation threshold can be described by Equation 16, the mean cluster size below the percolation threshold can be described by Equation 17. System properties ( $X$ ) and the corresponding critical exponents for two dimensions ( $d = 2$ ) and three dimensions ( $d = 3$ ) are summarized in Table 10.

For this reason there are two approaches to predict the region of catastrophic change in complex system by Equation 15 either to find the percolation threshold or to find the critical exponents of the system.

Table 10 System properties X and the corresponding critical exponents for d = 2 and d = 3 [71, 73]

System property (X)	Equation	Exponent	Critical exponent	
			d = 2	d = 3
Strength of infinite cluster	$ p-p_c ^\beta$ (16)	$\beta$	5/36	0.4
Mean finite cluster size	$ p-p_c ^{-\gamma}$ (17)	$\gamma$	43/18	1.8
Correlation length	$ p-p_c ^{-\nu}$ (18)	$\nu$	4/3	0.9
Cluster number density	$ p-p_c ^{2-\alpha}$ (19)	$\alpha$	-2/3	-0.6

### 3.5.7 Fractal nature of infinite cluster near percolation threshold

Figure 20 and 21 show an infinite cluster at the percolation threshold in two dimensions [74, 88] and three dimensions [89, 90] respectively. The infinite cluster at the percolation threshold exhibits a self-similar structure, which is a prerequisite to define a fractal dimension. The fractal nature of a system is related to a certain scale length, which corresponds to the correlation length  $\xi$  [74]. The fractal geometry introduced by Mandelbrot [91] was applied to quantify the complexity of internal pore structure in a matrix type controlled release system [92, 93].

The cluster mass  $M_\xi$  in the volume  $\xi^d$  is proportional to  $\xi^{d_f}$  by definition with  $d_f$  the fractal dimension. A lattice of linear size L contain  $(L/\xi)^d$  such volumes. Thus the total mass  $M_\infty$  of such a lattice is proportional to  $\xi^{d_f} (L/\xi)^d$ . The strength (P) of the infinite cluster is proportional to  $M_\infty/L^d$ . Thus the following relationship holds (Equation 20) [74];

$$P \propto \frac{M_\infty}{L^d} \propto \xi^{d_f-d} \propto (p-p_c)^{\nu(d-d_f)} \tag{Equation (20)}$$

The critical exponent of the strength (P) of the infinite cluster is equal to  $\beta$ . Thus the fractal dimension of the infinite cluster  $d_f$  can be calculated as follows for d = 2 and d = 3 (Equation 21):

$$d_f = d - \beta / \nu \tag{Equation (21)}$$

where  $\beta$  and  $\nu$  are indicated in Table 10, which are universal.

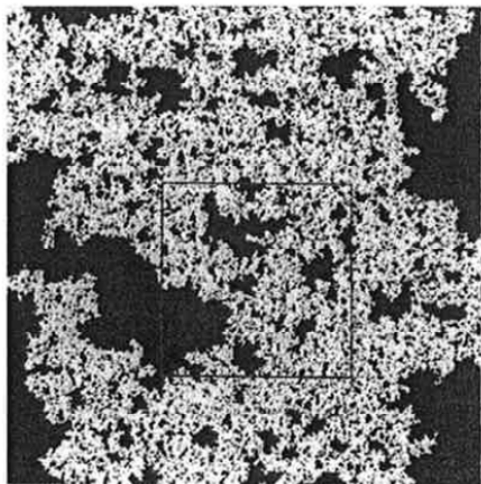


Figure 20. The infinite cluster at the percolation threshold exhibits a self-similar structure, i.e. has a fractal dimension  $d_f = d - (\beta/\nu) = 91/48$  for  $d=2$  [74, 88].

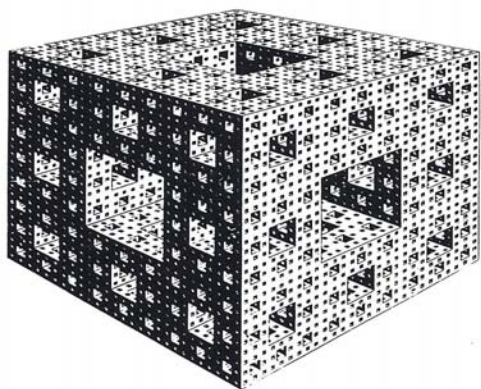


Figure 21. An idealized three dimensional network of a pore system (Menger sponge) with the fractal dimension of  $d = 2.72$  [89, 90].

## 3.6 F-CAD

### 3.6.1 Goal of in-silico pharmaceutical formulation design

The guideline published by the FDA (2004) [52] concerning the PAT-initiative presents a framework with two components:

- Set of scientific principles and tools supporting innovation.
- Strategy for regulatory implementation that will accommodate innovation.

The goal of FDA's PAT initiative is to achieve scientifically based decisions, i.e. to design the quality of the product and not to "test-in" the quality by eliminating the bad items at the end of the production creating waste of time and money [62]. The PAT-initiative is however a recommendation to the pharmaceutical industry and not a compulsory regulation. In this sense, FDA promotes as well the use of better manufacturing toolkit, in particular IT tools as below; "Scientists involved in reviewing medical devices at FDA report an urgent need for

predictive software to model the human effects of design changes for rapidly evolving devices. We believe that such software may be attainable with a concentrated effort, by assembling currently available data and identifying existing data gaps” in the "Challenge and Opportunity on the Critical Path to New Medical Products, FDA" [65]. For this software high performance computer system is necessary. But today, high performance computer systems that incorporate advanced hardware and software are commercially available, allowing scientists to simulate the formulation design, process development and its scale-up. The application of in-silico design and testing of solid dosage form is an innovative tool for fulfilling the requirements of PAT and the Quality by Design Initiative of FDA [94].

### 3.6.2 F-CAD capability for the pharmaceutical formulation design

F-CAD developed by CINCAP GmbH [95] is a first principle approach using as software based on Cellular Automata (see section 3.6.4) in three dimensional mapping of the diffusion equation in order to predict the dissolution profile of the drug substance and is capable of detecting percolation thresholds [94] in complex formulations. Thus, F-CAD is based on physical laws and has among others the following capabilities [94, 96]:

- Interpret experimentally measured data by providing the underlying physical models.
- Propose laboratory experiments that may confirm unexpected theoretical predictions.
- Cut down substantially the cost of laboratory work, based on a trial and error approach by giving valuable feedback to the experimentalists, which laboratory tests should be done for validation purposes.
- In case of complex pharmaceutical formulations: F-CAD is able to establish intellectual property rights by providing results for drug delivery systems that have not yet been tested experimentally.

Last but not least in the framework of perspectives [97]:

- Replace in future laboratory experiments in case that the accuracy of numerical computations based on a first principle approach is better than that of experiments, which is of special relevance in case of biological, pharmaceutical and medical experiments, where the variability is intrinsically high [98].

### 3.6.3 F-CAD software applications

F-CAD software has three main parts: tablet geometry designer (TGD), process simulation (PS), and 3-D rendering, analysis and playback (RAP) module [99]. Tablet geometry designer (TGD) is specially focused on the pharmaceutical tablet design [100].

- Disintegrant Optimization (DO)

This module calculates the critical concentration of disintegrant for a tablet formulation based on the percolation theory. The percolation threshold of the disintegration time is strongly dependent on the physical properties of the components. Thus it can be estimated on the basis of geometrics and physical consideration only.

Required information for calculation is;

- Volume of tablet
- Weight of tablet
- Mean particle size of the components
- True densities of the components

- Dissolution Simulation (DS)

Cellular automata algorithm is used to simulate tablet dissolution. Tablet to dissolve in-silico must be previously designed by Tablet Designer (TD) module and Particle Arrangement and Compaction (PAC) module. The release profile of the API is calculated for each time point in accordance to initial setting value of individual component.

- Tablet Designer (TD)

This module serves to design tablet pattern and to transform it into a discrete 3D virtual tablet. The shape of a tablet is not limited to classical ovals or circles but also complex geometry.

- Particle Arrangement and Compaction (PAC)

The arrangement of particles and their location in a tablet can be designed by this module. Growth algorithm is used to correspond to design the different size of particles.

### 3.6.4 F-CAD core algorithm

F-CAD is mainly based on percolation theory and special core algorithm cellular automata (CA) which is a sophisticated algorithm taken from nature phenomenon for the particulate formulation design. This is the reason why F-CAD cannot be compared to existing "Expert Systems" or "Artificial Neural Networks" [101, 102].

#### 3.6.4.1 Cellular Automata

Cellular automata were first introduced by Von Neuman and Ulam in 1940s. They had been looking for simple mathematical models describing phenomena in nature [103]. A cellular automaton (CA) is one of the topological optimization techniques [104], which can be applied in percolation theory. The underlying idea of cellular automata is to see a system as composed of subunits (square cell) that are discrete regularly on a lattice. In other words, a cellular automaton is a discrete model consisting of a regular domain of cells on a lattice. This scheme is very close to the concepts used in percolation theory. Each cell is characterized by a certain state, which typically consists of a finite domain. The system of cells evolves, in discrete time step, like simple automata which only know a simple recipe to compute their new state. New state of a cell at time  $t$  is a function of the states of a finite domain composed of target cell and its neighborhood at time  $t-1$  according to the locale rules which depends only on the state of the cell and of the state of neighboring cell. The success of the application of CA in deferent domains is mostly related to its ability to take into account of the local interaction between spatial target cell and its neighborhood.

Thus CA is considered to be suitable tool to calculate the percolation threshold in case of difficulty to calculate the percolation threshold by using percolation equation which can show the entire system's characteristic or behavior.

#### 3.6.4.2 Simplest examples of cellular automata application

An attempt to use the cellular automata for designing the pharmaceutical formulation was conducted by CINCAP GmbH in 2007. Solid particle and liquid or porosity is represented of the individual cell controlled by certain rule which guides its state changes. For example, the solid particle cell is gradually changing its state after taking the liquid or porosity during the disintegration of tablet. The rate at which the solid particle takes liquid or porosity is governed by its solubility or volumetric change (swelling) rate constant which is unique for every API as well as for new excipient and to be determined through a calibration routine. It is important to note that the calibration routines for F-CAD are not necessary to be repeated every time the system used before [100].

Now, one of the simplest one-dimensional cellular automata (CA) rule is introduced in order to understand CA and its application, which is a preferred procedure in nature. Elementary cellular automata have two possible states for each cell labeled 0 (white) and 1 (black) (Upper Figure 22). New state of a cell at time  $t$  will be formed depending on the states of a finite domain composed of target cell and its neighborhood at time  $t-1$ . Thus there are  $2 \times 2 \times 2 = 8$  possible states for the target cell as well as its neighborhood. The rule defining the cellular automaton must specify the resulting state for each of these possibilities. Wolfram [103] proposed the rule of cellular automata. Below show graphically the rule 30 and 16 updates of the system. The "00011110" is written 30 in binary. This is the reason why it is called rule 30. A picture of a seashell pattern (Lower Figure 22) resembles the system following the rule 30. Many other examples of similarity between CA based model and nature behavior were exciting [100]. It is suggested that CA based models are capable of imitating the behavior of nature system properties such as dissolution of tablet [100].

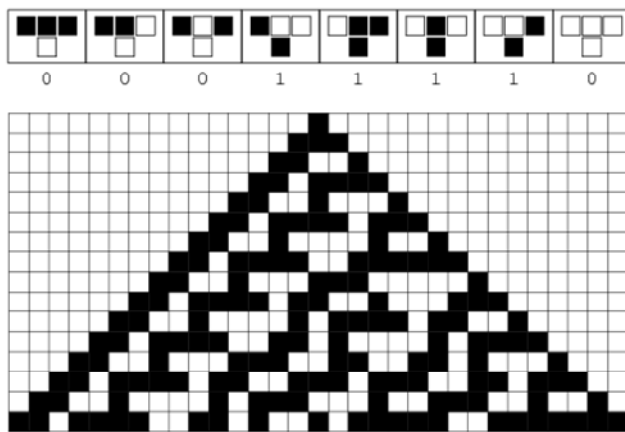


Figure 22. Upper: pattern of one dimensional cellular automata generated with rule 30 [103], Lower: natural pattern of a dangerous sea snail.

### 3.6.4.3 Application of cellular automata in pharmaceutical area

Cellular automata (CA) has been used for the sustained drug release modeling from bioerodible polymer system by its surface erosion [105, 106], from non-erodible polymeric system [107], polymer membrane system [107] and from swelling polymer system which polymer absorbs water and creates the hydrogel layer [108]. In these models, each square cell is ruled to be updated two dimensionally.

The handicap of two dimensional CA is considered that it is only able to show the percolation threshold for a two dimensional system. Kier et al. investigated a CA model for the dynamic two dimensional system (square lattice). In his report, the percolation threshold spanning the cluster entire system was observed at the range of 0.512 to 0.661 [109]. This was close to the site percolation threshold of square lattice, 0.592746, not for the three dimensional system. On the other hand, each cubic cell in F-CAD is ruled to be updated for three dimensional systems. F-CAD has more advantages to simulate the percolation threshold or dissolution profile such as a three dimensional tablet. However the rule of CA to simulate the drug release from three dimensional systems in F-CAD has not been disclosed yet.



## 4 Objectives

The objective of this PhD work is to search the critical concentration of starch based disintegrant applying percolation theory and F-CAD (Formulation-Computer Aided Design) in order to design a pharmaceutical tablet formulation for a low water-soluble drug. For the pharmaceutical formulation design and process development, the use of scientific approaches for the understanding of quality attributes in combination with the knowledge management system are required for the purpose of quality by design (QbD) based on ICH Q8.

Critical concentration of maize starch (MS) for a ternary mefenamic acid (MA) tablet formulation with respect to a minimum disintegration time is investigated. The critical volume fraction ( $\phi_c$ ) for three dimensions investigated is equal to  $0.16 \pm 0.01$  (v/v); which was demonstrated to predict the conductivity threshold in the area of the material sciences. In our laboratory, the critical volume fraction ( $\phi_c$ ) for three dimensions ( $0.16 \pm 0.01$ , v/v) has been investigated to calculate the critical concentration of non-fibrous disintegrant, StaRX1500<sup>®</sup> for the binary mixture of caffeine or paracetamol/StaRX1500<sup>®</sup> tablet [11, 12]. However the further investigation is needed to determine the critical concentration of non-fibrous disintegrant for not only binary tablets but also for pharmaceutical tablet formulation. No one, however, has reported experimentally the location of critical concentration of disintegrant for a ternary immediate release pharmaceutical tablet formulation. Percolation theory can lead to the percolation threshold and critical exponent of disintegrate behavior but it does not give an answer about the absolute value of the disintegration time. Thus, the Dissolution Simulation (DS) module which is part of F-CAD being based on a cellular automata (CA) approach is implemented to simulate the disintegration time of MA tablet. F-CAD is able to calculate, applying CA with the number  $n$  of updates,  $t_i$  necessary till water is detected at the geometric center of the virtual tablet. Thus, it is possible to define a time  $t$ , i.e. the “time elapsed” till water molecules have reached the center of the tablet. In a very first approximation, the value of the calculated “time elapsed” can be considered as an estimate of the real disintegration time. However, it has to be kept in mind that “time unit” for the updating event has to be defined in an arbitrary, but reasonable way. In an earlier study (see PhD thesis of Krausbauer [12] and Figure 9 of the paper in SWISS PHARMA [96]), a reasonable guess was made for the updating “time unit” resulted in the fact that the real disintegration time occurred after the water is detected at the geometrical center of the virtual tablet. It is evident that there may be a link between the “time elapsed” to reach the geometrical center of the tablet and the disintegration process, which may be different for non-fibrous starch type disintegrants and for other types of disintegrants such as the “superdisintegrant” Ac-Di-Sol<sup>®</sup>.

Comparison of experimental disintegration time and computed specific time point for water to reach the geometric center of the tablet by using F-CAD software is useful to show the capability of F-CAD for a tablet formulation design in order to save money by replacing laboratory experiments. Thus, classical trial and error experiments can be avoided and only a fraction of laboratory experiments need to be made for the validation of the best in-silico formulations.

## 5 Materials and Methods

### 5.1 Materials

Mefenamic acid (2-[(2,3-Dimethylphenyl)amino]benzoic acid, Figure 23), hereinafter MA, was purchased from Fluka Chemie GmbH, Lot No. 023K0927 (Buchs, Switzerland). Lactose monohydrate (LA) (Lot No. 083451, USP/EP; Pharma 200/15, Alpavit, Lauben/Allgaeu, Germany) and maize starch (MS) (Lot No. 41951073, USP/EP; Maisita 21.000-50, Agrana, Gmuend, Austria) were used in the formulation of the ternary system with hydroxypropyl cellulose (HPC SL) (Lot No. NCH-0911, EP/JP; HPC SL, Nippon soda, Tokyo, Japan) as a binder for the wet granulation process. Magnesium stearate (Mg-St) (Lot No. K2 41155, Actelion Pharma Schweiz AG, Allschwil, Switzerland) was used as a lubricant for tableting.

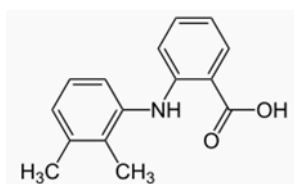


Figure 23. Chemical formula of mefenamic acid (MA)

### 5.2 Physical properties of starting materials

The physical properties of the above mentioned materials are compiled in Table 11. MA, LA, MS and Mg-St was used as API, filler, disintegrant and lubricant respectively. The shape of MA (Figure 24), LA (Figure 25), MS (Figure 26) and Mg-St (Figure 27) were examined by the Scanning Electron Microscope (SEM) using JSM-5310LV (JEOL, Tokyo, Japan, Figure 28) under the conditions described below;

- Vacuum pressure : 27 Pa (Low vacuum condition)
- Accelerated voltage : 15 kV
- Current load : 104  $\mu$ A

Table 11 Physical properties of the starting materials

	Mean diameter ( $\mu$ m)	True density (g/cm <sup>3</sup> )	SSA, (m <sup>2</sup> /g)
MA	6.57	1.264	1.87
LA	39.4	1.556	0.33
MS	25.0	1.537	0.31
Mg-St	4.15	1.088	20.2

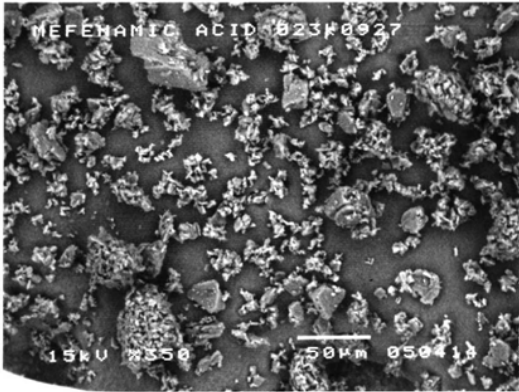


Figure 24. SEM of mefenamic acid (MA).

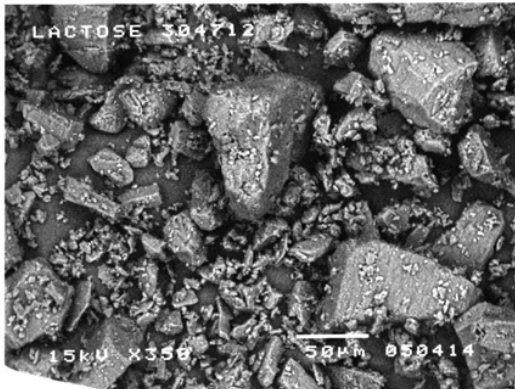


Figure 25. SEM of lactose monohydrate (LA).

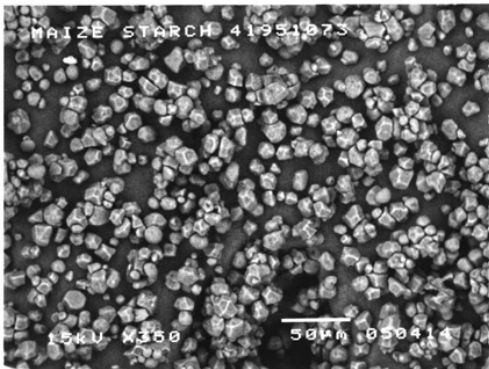


Figure 26. SEM of maize starch (MS).

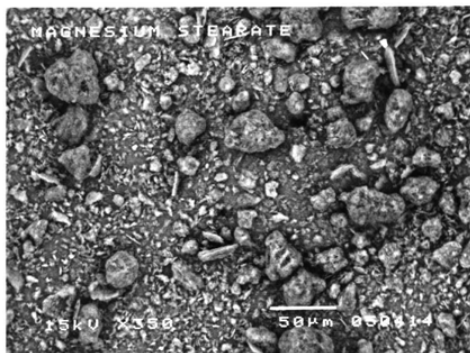


Figure 27. SEM of magnesium stearate (Mg-St).



Figure 28. Scanning Electron Microscope (JSM-5310LV, JEOL, Tokyo, Japan).

The mean diameter by volume of starting material was determined with a laser diffractometer (HEROS & LODOS, Sympatec, Clausthal-Zellerfeld, Germany, Figure 29) at 500 mm focal length. The dispersing pressure was 0.2 MPa and the injector suction was 0.01 MPa. The particle size distribution of MA, LA and MS are shown in Figure 30, 31 and 32 respectively. The true density was measured by a helium pycnometer (AccuPyc 1330, Micromeritics, Norcross, GA, USA, Figure 33) at room temperature. The cell and expansion volume were 12.0563 cm<sup>3</sup> and 8.4153 cm<sup>3</sup>, respectively. The equilibration rate was 0.01 psig/min, i.e. 68.91 Pa/min. The specific surface area (SSA) was determined by nitrogen adsorption method using an automatic surface area analyzer (Gemini 2360, Micromeritics, Norcross, GA, USA, Figure 34). For this purpose, MA, LA, MS and Mg-St MA was dried for 1 hour at 100 °C, LA for 1 hour at 80 °C, MS for 28 hours under vacuum at room temperature (MS) and Mg-St for 2 hours at 40 °C, respectively. The measurements were performed using a 6-point Brunauer-Emmett-Teller (BET) mode with nitrogen gas and a relative pressure range between 0.05 and 0.30. Data were calculated according to BET methods [110].

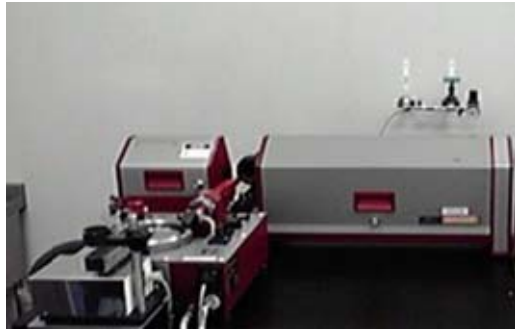


Figure 29. Laser diffractometer (HEROS & LODOS, Sympatec, Clausthal-Zellerfeld, Germany).

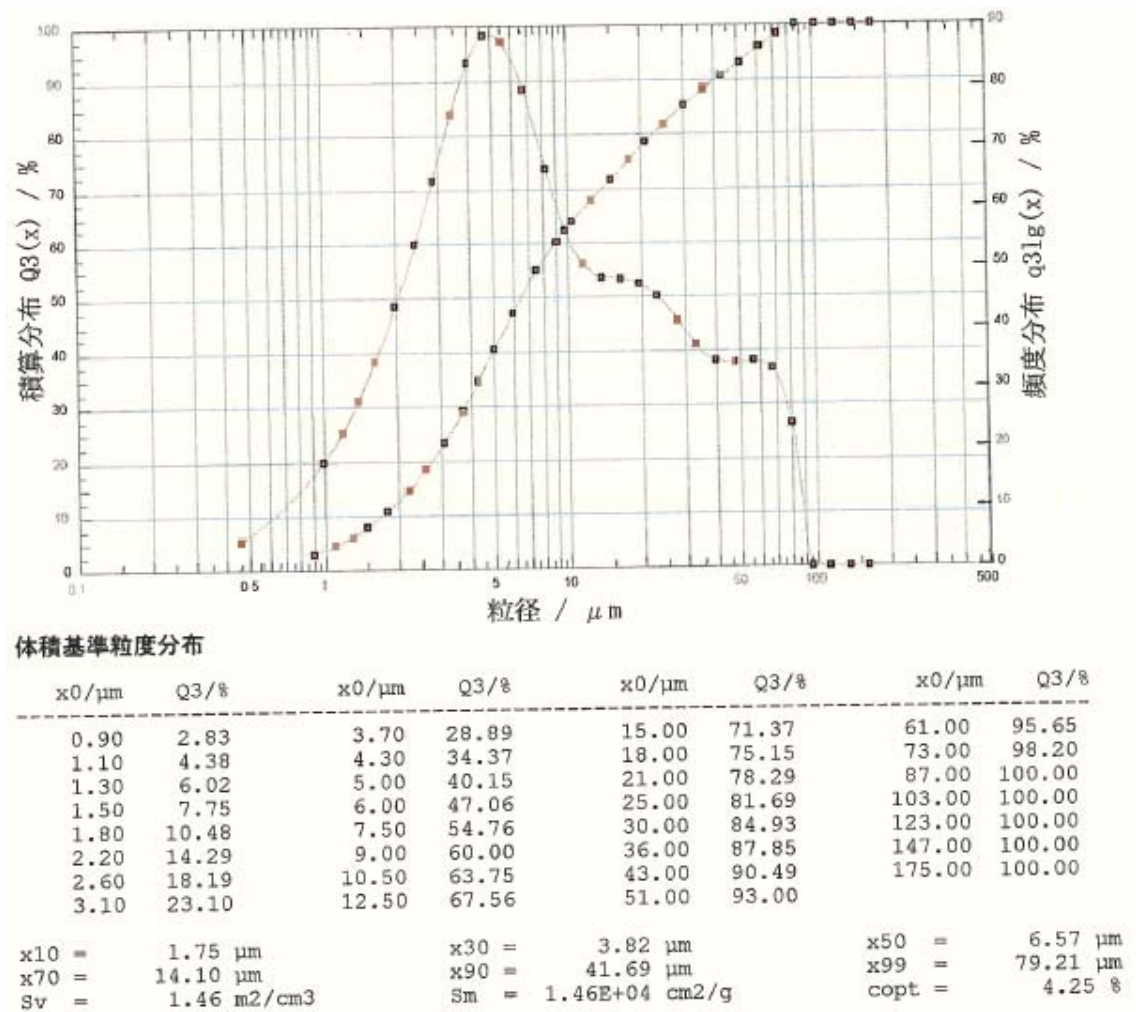


Figure 30. MA particle size distribution.

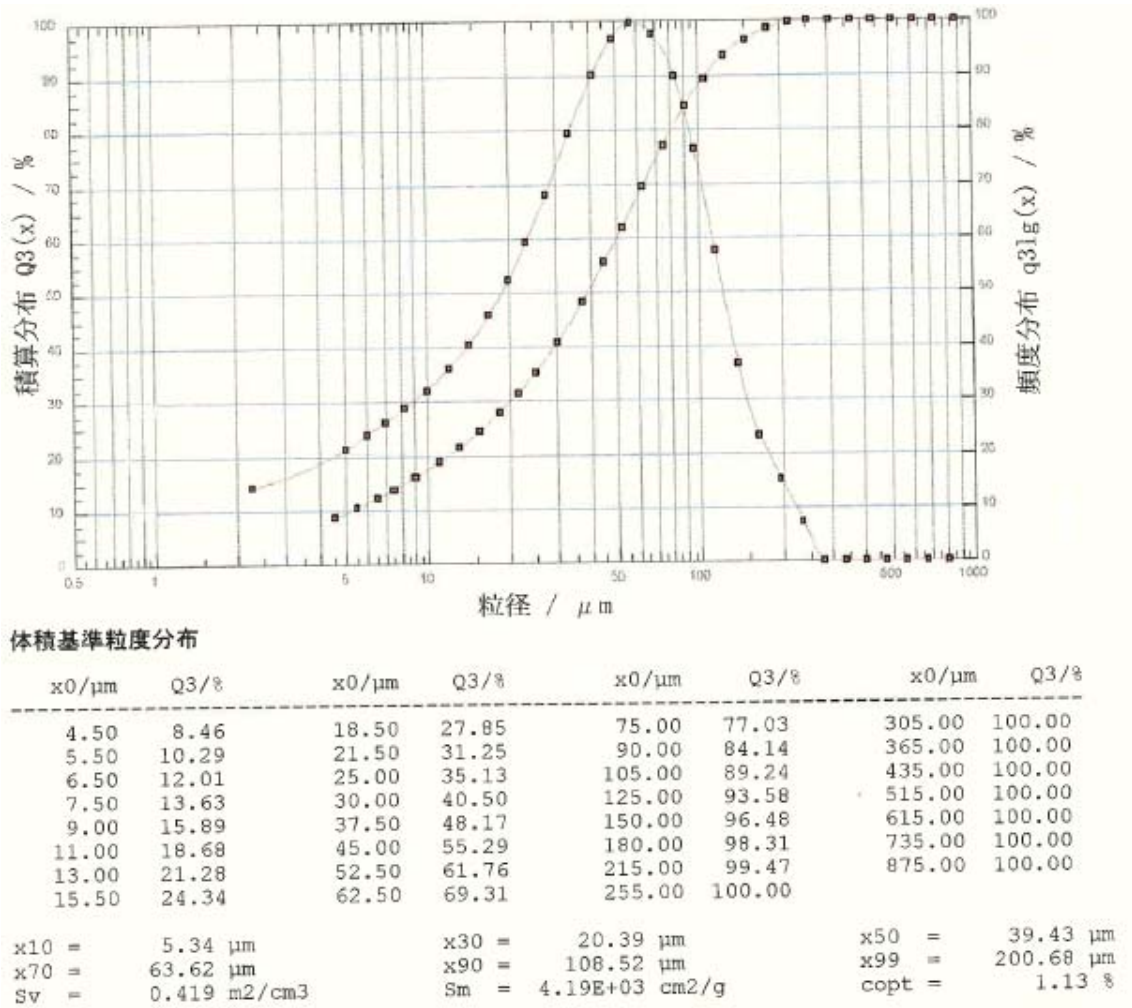


Figure 31. LA particle size distribution.



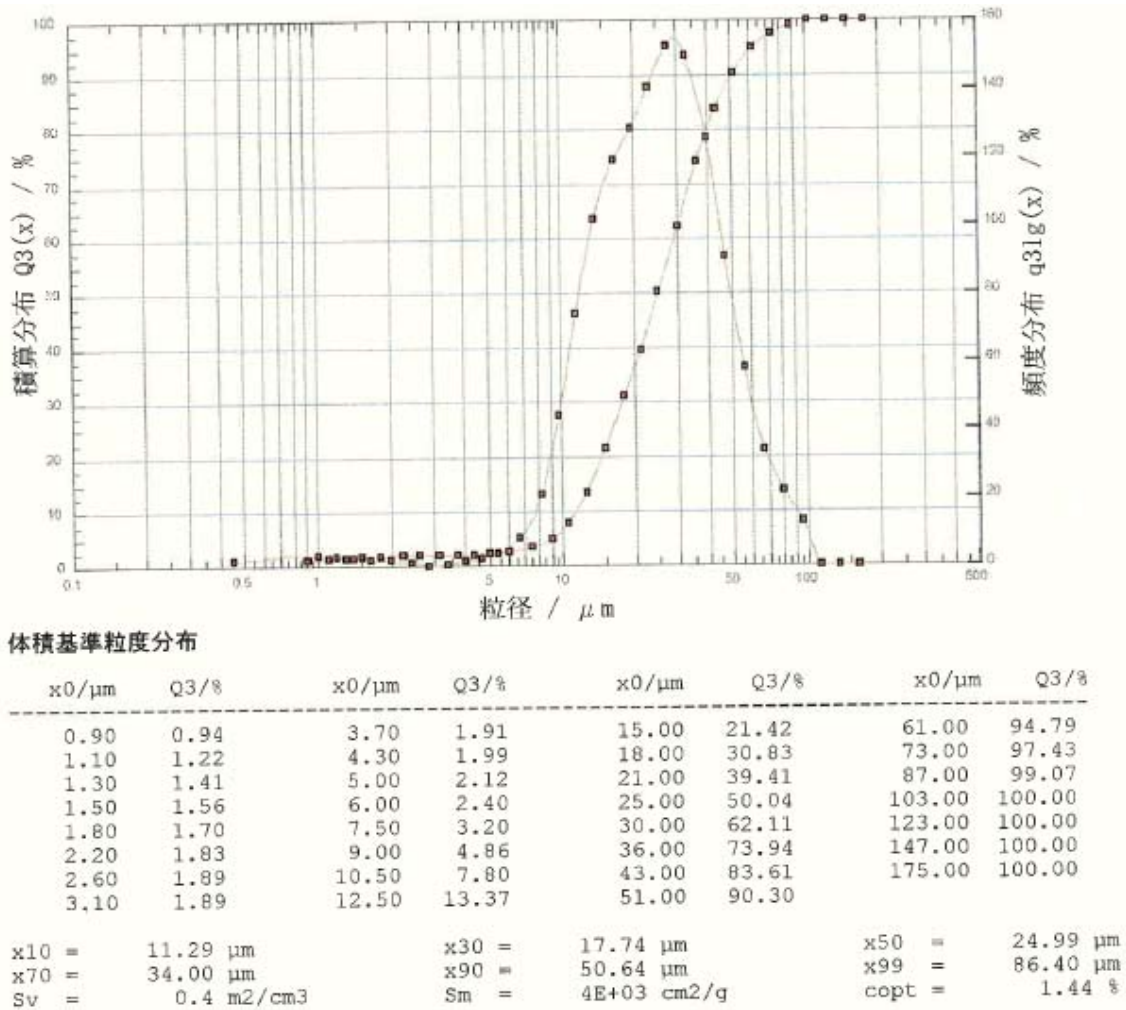


Figure 32. MS particle size distribution.



Figure 33. Pycnometer (AccuPyc 1330, Micromeritics, Norcross, GA, USA).





Figure 34. Automatic surface area analyzer (Gemini 2360, Micromeritics, Norcross, GA, USA).

### 5.3 Granulation

Granulation was performed with 125 g batch per batch by fluidized bed granulator Mini-Glatt (Glatt, Binzen, Germany, Figure 35). The starting compositions and quantity per batch for the granulation are shown in Table 12 and 13 respectively. The compositions are indicated by both % w/w, and % v/v. The composition of MA was increased by 10% w/w in exchange of LA/MS (7/3) as excipients from Granule A to H. The composition of MS was kept at 15% w/w, 21% w/w and 9% w/w from Granule I to K, L to M and N to O respectively.

The HPC SL solution of 6% w/v was top-sprayed as a granulating binder. The content of HPC SL in the final granulate was kept at 3.5% (w/w) for all batches. The spraying rate of HPC SL solution was kept at 6.4-10.6 g/min (Sci-Q pump, 323U/D, Watson-Marlow Bredel Pumps, Falmouth, UK); the atomizing air pressure was kept at 0.04 MPa for all batches. The inlet air temperature was varied within 70-80 °C; the fluidization air pressure was varied within the range of 0.012-0.03 MPa. During the granulation, the product temperature and relative humidity in the powder bed were monitored using a hygrometer (HMI41/HMP42, VAISALA, Helsinki, Finland). Temperature and relative humidity (R.H.) were in the range of 22.6-33.3 °C and 46.3-85.7% R.H., respectively. Granulation time was kept within the range of 753-1133 seconds. Drying was stopped when the product relative humidity (R.H.) was below 5.0%.



Figure 35. Fluidized bed granulator Mini-Glatt (Glatt, Binzen, Germany).

Table 12 Starting compositions for wet granulation

	Composition (%)					
	MA		LA		MS	
	(w/w)	(v/v)	(w/w)	(v/v)	(w/w)	(v/v)
A	0	0	70	69.7	30	30.3
B	10	12.0	63	61.4	27	26.6
C	20	23.5	56	53.4	24	23.1
D	30	34.5	49	45.7	21	19.8
E	40	45.0	42	38.4	18	16.6
F	50	55.1	35	31.3	15	13.6
G	60	64.8	28	24.6	12	10.6
H	70	74.1	21	18.1	9	7.8
I	0	0	85	84.8	15	15.2
J	30	34.5	55	51.3	15	14.2
K	70	74.1	15	12.9	15	13.0
L	0	0	79	78.8	21	21.2
M	70	74.0	9	7.7	21	18.3
N	0	0	91	90.9	9	9.1
O	30	34.5	61	57.0	9	8.5

Table 13 Quantity per batch for granulation

	Quantity per batch (g)														
	A	B	C	D	E	F	G	H	I	J	K	L	M	N	O
MA	0	12.5	25.0	37.5	50.0	62.5	75.0	87.5	0	37.5	87.5	0	87.5	0	37.5
LA	87.5	78.75	70.0	61.25	52.5	43.75	35.0	26.25	106.25	68.75	18.75	98.75	11.25	113.75	76.25
MS	37.5	33.75	30.0	26.25	22.5	18.75	15.0	11.25	18.75	18.75	18.75	26.25	26.25	11.25	11.25
Subtotal	125.0	125.0	125.0	125.0	120.5	125.0	125.0	125.0	125.0	125.0	125.0	125.0	125.0	125.0	125.0
HPC SL	4.38	4.38	4.38	4.38	4.38	4.38	4.38	4.38	4.38	4.38	4.38	4.38	4.38	4.38	4.38
Total	129.4	129.4	129.4	129.4	129.4	129.4	129.4	129.4	129.4	129.4	129.4	129.4	129.4	129.4	129.4

## 5.4 Tableting

For this study the resulting granules were fractionated in order to remove the fines (< 90 µm) and the fraction above 500 µm. Thus ensembles of the particles with the size between 90 µm and 500 µm were used for compression. They were mixed with 0.5% w/w of Mg-St in a Turbula mixer (Type T2A, Willy A. Bachofen, Basel, Switzerland, Figure 36) for 2 minutes and then compressed to a 416 mg (± 1.0%) tablets as described in Table 14. The mixtures were compressed to tablets by using a compaction simulator (Presster™, Metropolitan Computing Corporation, East Hanover, NJ, Figure 37), mechanically simulating a high-speed industrial rotary tableting press, Korsch PH 336 at the turret speed of 35 rpm corresponding to the output capacity of 75,600 tablets per hour. The diameter of pre-compression roll and compression roll was identical with those of Korsch PH 336, which are 110 mm and 300 mm, respectively. The ejection angle was set to 7.6 °. Tablets were compressed at approximately 7.0 kN (6.6-7.4 kN), 5.0 kN (4.7-5.3 kN) and 3.0 kN (2.7-3.3 kN) with the dwell time of 16.9 ms using 10 mm flat-faced standard IPT B-tooling. Pre-compression force was kept between 0.6-1.7 kN. The dwell time (ms) was calculated by Equation 22 [23].

$$Dwell\ time = \frac{L \cdot NS \cdot 3,600,000}{\pi \cdot PCD \cdot OC} \quad \text{Equation (22)}$$

where L is the diameter of the flat portion of the punch head (12.7 mm in the case of IPT, Industrial Pharmaceutical Technology, standard B tooling), NS is the number of stations , PCD is the pitch circle diameter of the turret and OC is the output capacity in tablets per hour.



Figure 36. Turbula mixer (Type T2A, Willy A. Bachofen, Basel, Switzerland).



Figure 37. Compaction simulator (Presster™, Metropolitan Computing Corporation, East Hanover, NJ)



## 5.5 Granules characterization

### 5.5.1 SEM

The shape of granule A, D, F and H were examined by the Scanning Electron Microscope (SEM) using JSM-5310LV (JEOL, Tokyo, Japan) under the conditions described below;

- Vacuum pressure : 27 Pa (Low vacuum condition)
- Accelerated voltage : 15 kV
- Current load : 104  $\mu$ A

### 5.5.2 Moisture determination

Loss on drying of 1.5 g samples was measured at 80 °C for one hour using an infrared drying unit (LP 16, Mettler, Greifensee, Switzerland, Figure 38).



Figure 38. Infrared drying unit (LP 16, Mettler, Greifensee, Switzerland).

### 5.5.3 Size distribution and Mean diameter

The size distribution of granule was evaluated by sieve analysis method using the 710, 500, 355, 250, 180, 125, and 90  $\mu$ m ISO-norm sieves. The sieves were vibrated at 50 Hz for 5 min by using a sieve shaker (Vibro, Retsch, Haan, Germany, Figure 39). The sieve load was 25.0 g. The fraction remaining on each sieve was determined by weighing. The mean diameter was calculated as 50% in diameter by plotting the cumulative percentage oversize against sieve size on log-probability graph.



Figure 39. Sieve shaker (Vibro, Retsch, Haan, Germany).

### 5.5.4 Bulk, Tapped and Apparent density

Bulk and tapped density was calculated as the ratio of the weight to the volume of granules poured into a glass cylinder without or with tapping using a Jolting volumeter (J. Engelsmann, Ludwigshafen/Rhein, Germany, Figure 40) at a tapping rate of 247 taps per minute for one minute. Apparent density of the granules (90-500  $\mu\text{m}$ ) was measured using a pycnometer (AccuPyc 1330, Micromeritics, Norcross, GA, USA) with helium gas at room temperature. The cell and expansion volume were 12.0563  $\text{cm}^3$  and 8.4153  $\text{cm}^3$ , respectively. The equilibration rate was 0.01 psig/min, i.e. 68.91 Pa/min.

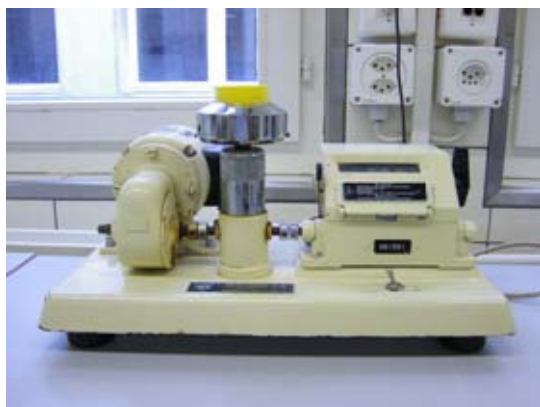


Figure 40. Jolting volumeter (J. Engelsmann, Ludwigshafen/Rhein, Germany).



### 5.5.5 Intragranular pore volume

Intrusion volume of mercury into the particle size fraction of granules (90-500  $\mu\text{m}$ ) was determined using a mercury porosimeter (Poresizer 9320, Micromeritics, Norcross, GA, Figure 41) at different pressure ranging from 1.5 to 30,000 psia, i.e. from 10.34 kPa to 206.73 MPa, corresponding to the pore diameters between 120  $\mu\text{m}$  and 6 nm. Equilibration time was 10 seconds at each pressure. The pore diameter corresponding to the intrusion volume of mercury under a certain pressure was calculated by Equation 23 using mercury porosimetry [111].

$$D = K_{\text{washburn}} \frac{-4\gamma \cos \theta}{P} \quad \text{Equation (23)}$$

where  $D$  is the pore diameter ( $\mu\text{m}$ ),  $K_{\text{washburn}}$  is the washburn constant,  $\gamma$  is the surface tension of mercury ( $485 \times 10^{-5} \text{ N/cm}$ ),  $\theta$  is the contact angle ( $130^\circ$ ) and  $P$  (psia) is the pressure.

The pore diameter less than 14  $\mu\text{m}$  is assumed to be an intragranular pore open to the surface [112].



Figure 41. Mercury porosimeter (Poresizer 9320, Micromeritics, Norcross, GA).

### 5.5.6 MA assay

414 mg of the particle size fraction of granules (90-500  $\mu\text{m}$ ) was accurately weighed in a volumetric flask. 30.0 mL of distilled water was added and shaken at the speed of 150 cycles per minute (cpm) in a water bath at  $37^\circ\text{C}$  for 30 min. 0.1 N NaOH was added accurately until 100.0 mL and filtered (HLC-DISK 13, 0.45  $\mu\text{m}$ , Kanto Chemical, Tokyo, Japan). The filtrate was diluted to the range of 8-20  $\mu\text{g/mL}$  as MA concentration with 0.1 N NaOH and measured by UV spectrophotometer (DU<sup>®</sup> 530, Beckman Coulter, Fullerton, CA, Figure 42) at 285 nm.



Figure 42. UV spectrophotometer (DU<sup>®</sup> 530, Beckman Coulter, Fullerton, CA).

## 5.6 Tablet characterization

### 5.6.1 Hardness and tensile strength

The hardness of six tablets was measured with a tablet tester (8M, Dr. Schleuniger Pharmatron, Solothurn, Switzerland, Figure 43). The tensile strength of each tablet was calculated by Equation 24 [113].

$$TS = \frac{2 \cdot H}{\pi \cdot D \cdot T} \quad \text{Equation (24)}$$

where TS is the tensile strength (N/cm<sup>2</sup>), H is the hardness (N), D is the diameter (cm) and T is the thickness (cm) of a tablet, respectively. The diameters and thicknesses of the tablets were measured with a digital caliper (Figure 44).

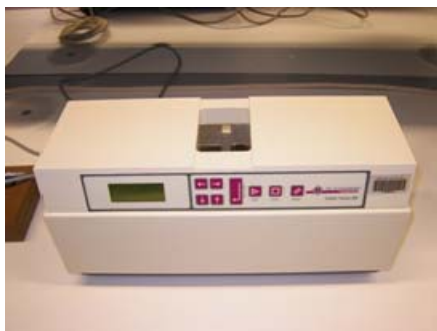


Figure 43. Tablet tester (8M, Dr. Schleuniger Pharmatron, Solothurn, Switzerland).



Figure 44. Digital caliper.

### 5.6.2 Calculated Porosity

The porosity of the tablets was calculated according to Equation 25 [112].

$$\varepsilon = 1 - \left( \frac{M}{V} \cdot \frac{1}{\rho} \right) \cdot 100 \quad \text{Equation (25)}$$

where  $\varepsilon$  is the porosity (% v/v) of a tablet,  $M$  is the tablet weight (g),  $V$  is the tablet volume ( $\text{cm}^3$ ) and  $\rho$  is the apparent density of granules ( $\text{g}/\text{cm}^3$ ) used for tableting.

### 5.6.3 NIR imaging

One faces of each tablet were imaged by chemical imaging system (Sapphire, Malvern Instruments Ltd., UK, Figure 45). The instrument consists of a liquid crystal tunable filter (LCTF) for wavelength selection, and cooled indium antimony (InSb) focal plane array (FPA) detector with  $256 \times 320$  pixels. The system includes an appropriate optics to preferentially capture diffusely reflected light from each specimen, while minimizing background specular reflection off polished mounting plate. Four tungsten source lamps illuminate the imaging target field. The NIR imaging data of the diffuse reflection spectra were collected 10 nm intervals in the 1200-2400 nm regions with 32 co-added scans at each wavelength point. The spatial resolution of NIR imaging data in this experiment was  $40 \mu\text{m}/\text{pixel}$ , so the field of view was  $10.2 \times 12.8$  mm. The size of domain of each component which was defined as a group of each component were measured based on the pixel size.

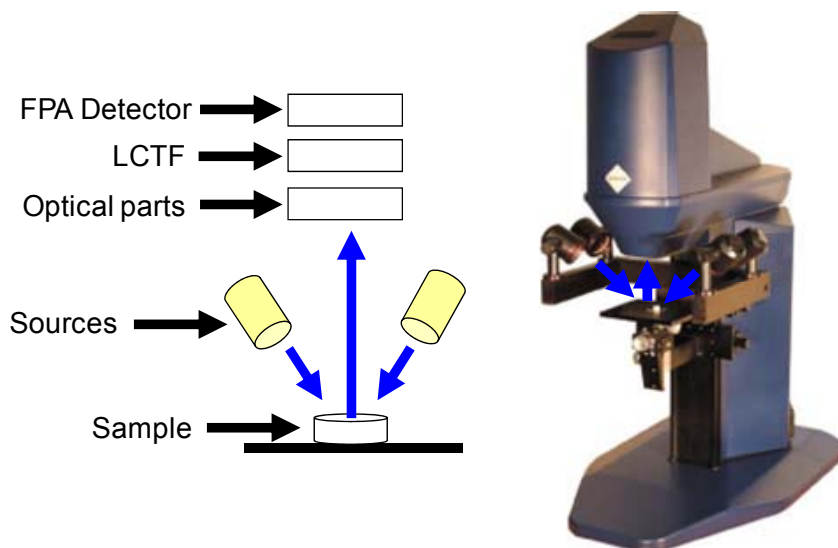


Figure 45. Chemical imaging system (Sapphire, Malvern Instruments Ltd., UK) [55].

#### 5.6.4 Disintegration time

The disintegration time of the triplets of the tablets was measured by using the SOTAX disintegration testing equipment (DT 2, Sotax, Allschwil/Basel, Switzerland, Figure 46) without disk. The medium consisting of 750 mL distilled water was kept at  $37 \pm 0.5$  °C. The frequency of the basket-rack movement was kept at 30 cycles per minute.



Figure 46. Disintegration testing equipment (DT 2, Sotax, Allschwil/Basel, Switzerland).

#### 5.6.5 Pore size distribution, Median pore diameter and Porosity

The pore diameter of tablet corresponding to the intrusion volume of mercury under a certain pressure was calculated by Equation 23 using a mercury porosimeter. The median pore diameter by volume was defined as the pore diameter at which 50% of the mercury volume intruded up to 30,000 psia ( $V_{Hg,30,000psia}$ ) [114]. The compact volume of tablet and

porosity (%) were measured by Equation 26 and Equation 27 respectively [111]. Tablets before and after using a mercury porosimeter are pictured in Figure 47.

$$V_{SAMPLE} = V_{CELL} - V_{Hg,25\text{ psia}} \quad \text{Equation (26)}$$

$$Porosity = \left\{ 1 - \left( \frac{V_{SAMPLE} - V_{Hg,30,000\text{ psia}}}{V_{SAMPLE}} \right) \right\} \cdot 100 \quad \text{Equation (27)}$$

where  $V_{SAMPLE}$  is the sample volume (mL),  $V_{CELL}$  is the sample cell volume (mL),  $V_{Hg,25\text{psia}}$  is the mercury volume (mL) intruded up to 25 psia, i.e. 172.28 kPa.



Figure 47. Tablet before and after using a mercury porosimeter.

## 5.7 Data Analysis

### 5.7.1 Data treatment for NIR imaging

Data were treated using chemical imaging software (ISys, Malvern Instruments Ltd., UK). That enables the simultaneous manipulation of 81,920 pixels from a single field of view. For imaging analyses, the second derivative spectra calculated from the original data before proceeding with further analyses were used. The concentration of the each component in tablet was estimated by using the partial least square regression (PLSR) technique. No concentration standards are required for this experiment, as the spectra of starting materials were taken for reference.

### 5.7.2 Response surface methodology

The response surface of the disintegration time of tablet as a function of MA volume (% v/v) and maize starch volume (% v/v), was established by dataNESIA software (Yamatake, Fujisawa, Japan). Given method is based on the spline approximation incorporating the multivariate interpolation.

### 5.7.3 Renormalization

The current study is focused as ternary formulation: MA, LA, MS in order to establish the connectivity to the binary systems, the following renormalization leading to a dimension reduction was applied (Equation 28):

$$X'_{MS} = \frac{X_{MS}}{X_{MS} + X_{MA}} \quad \text{Equation (28)}$$

where  $X'_{MS}$  is a volumetric part of maize starch recalculated for a binary system,  $X_{MS}$ ,  $X_{MA}$  are volumetric parts of maize starch and mefenamic acid, respectively.

The renormalization is mainly a technique to map three dimensional data down to two dimensions. This dimension reduction is only possible and allowed due to the dominating effect of MA in the tablet for concentrations of MA  $\gg$  23.5 % (v/v), i.e. for concentrations, that exceed the percolation threshold of MA ( $p_{cMA}$ ). Thus, in practice it is important and prerequisite to look only at formulations with a high dose of MA, i.e. with an MA load larger than 20% (w/w). It has to be noted that proposed renormalization is independent on the nature of a third component in the mixture. However, there are limitations. Thus, the renormalization procedure should be applied with caution.

Depending on the situation, a renormalization process is not an absolute necessity as the comparison between Figure 57 and 61 is documenting. Both figures show clearly the behavior of the disintegration time of tablets compressed at 7 kN and the existence of the percolation threshold. In case of Figure 57 as a function of the content of MA and in case of Figure 61 as a function of the renormalized concentration of MS/(MS+MA). Instead of the renormalization process mentioned above, an elegant solution for a reduction of one factor is to introduce a ratio for one of the factors. Thus, in the case of three components MS, LA and MA the reduction is as follows: factor A = MS and factor B= LA/MA. It is evident that the second and the third component should not have a similar function as the disintegrant, which is studied, i.e. the third as well as the second component should not show a swellability or showing a function in competition with the excipient studied.

It has to be kept in mind that renormalization is possible if number of particles of third component is significantly less than of the particles of the other components in the mixture. In the present case this is guaranteed by high load of MA above the percolation threshold. Another limitation is that the particles of the third component should preferably have a non-fibrous structure, i.e. should look in an ideal case like a sphere. In addition, it should be kept in mind that the majority of pharmaceutical formulations, which consist in reality of more than two components can be reduced to two component systems in a really straight-forward way.

It is often absolutely correct to do the following abstraction from a complex tablet formulation consisting of one single drug substance and e.g. seven other excipients. For the scientific formulator, it will be important, at which volume fraction the drug substance will percolate. Thus, it will be important to know the particle size distribution of the drug substance and the particle size distribution of all other excipients involved. In other words, the scientific formulator has reduced the complex, multi-component system to a simple binary system. The same procedure can be applied for any other component in the system such as the disintegrant. The system becomes more complicated if two different disintegrants are involved in a complex formulation.

#### 5.7.4 Assumption of disintegration time computed by F-CAD

Disintegrant Optimization (DO) module of F-CAD currently is used to calculate the critical concentration of disintegrant in a tablet for a minimum disintegration time based on the percolation theory. F-CAD cannot calculate the disintegration time because the mechanical destructive force in disintegration testing [115] and/or the experimental method used in the laboratory for example, with disk or without disk is not able to be taken into account.

In this PhD work, Dissolution Simulation (DS) module, which is the one of F-CAD are used to simulate the disintegration time of a MA tablet compressed at 7 kN which is assumed that the time elapsed till water is detected at the geometric center of the virtual tablet.

#### 5.7.5 F-CAD operation

There are mainly three F-CAD operations [100] are required to compute the specific time the water is detected at the geometric center of the virtual tablet.

- Three dimensional design of MA tablet in order to create the wall constraint by Tablet Designer (TD) module.
- Packing the components of MA tablet into the hollow tablet by Particle Arrangement and Compaction (PAC) module.
- Compute the specific time elapsed until the water is detected at the geometric center of the virtual tablet by Dissolution Simulation (DS) module.

### 5.7.5.1 Tablet Designer (TD) operation

Figure 48 shows the wall appearance of Tablet F (flat-face) compressed at 7 kN created by TD module. Inputted parameters for Tablet F compressed at 7 kN are described as a sample followings;

- Number of Handles: 32
- Smooth point: 5
- Smooth (mm): 0
- Circle, Radius (mm): 4.985
- Flat portion, height (mm): 4.47
- Elliptic Cap Radi. (mm): 4.985

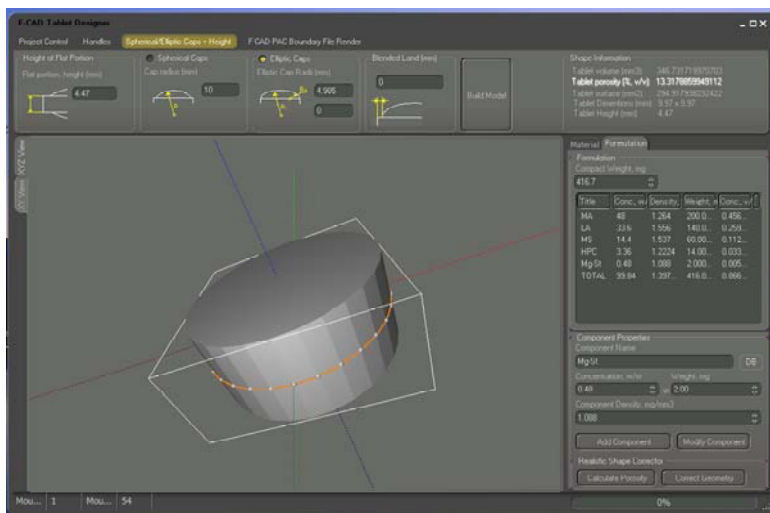


Figure 48. Wall appearance of Tablet F compressed at 7 kN created by TD module of F-CAD with permission from CINCAP GmbH.

### 5.7.5.2 Particle Arrangement and Compaction (PAC) operation

The second stage of F-CAD operation is an arrangement of MA granules and St-Mg and their location in a tablet created by TD module. Before that, tablet created by TD module has to be discretized in order to put the prerequisite number of three dimensional cells into it. In this study, the number of three dimensional cell inside of the tablet was 104 which size was 96.15  $\mu\text{m}$ /cube side.

In order to simulate that granules are arranged into tablet, the 'Swiss cheese' procedure developed by CINCAP GmbH was applied [100] because it is assumed that granulated particle should be grown until a specified or sized size at limited location in a tablet as competed with direct compressive tablet from powder mixture.



Figure 49 shows the top view of Tablet F (flat-face) compressed at 7 kN created by PAC module. The order the each component was arranged is described below;

- i. Grow LA
- ii. Grow MS
- iii. Distri. MA
- iv. Distri. HPC SL
- v. Distri Mg-St
- vi. Remove LA and Grow LA ('Swiss cheese' procedure)
- vii. Remove MA and MS
- viii. Distri. MA and MS

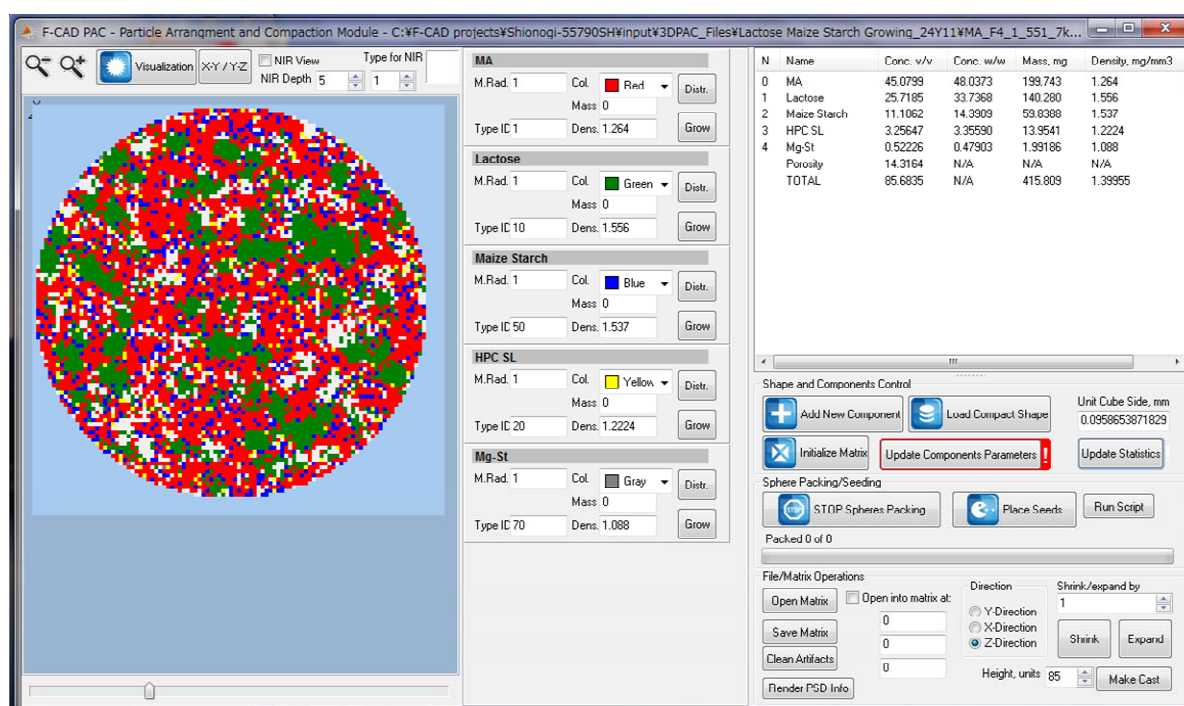


Figure 49. The top view of Tablet F (flat-face) compressed at 7 kN created by PAC module of F-CAD with permission from CINCAP GmbH.

Red: MA, Green: LA, Blue: MS, Yellow: HPC SL and Gray: Mg-St.

### 5.7.5.3 Dissolution Simulation (DS) operation

DS module can compute the specific time elapsed until the water is detected at the geometric center of the virtual tablet in accordance to setting value of individual component regarding to the water-solubility, swellability and hydrophilicity of pores defined in Table 15 as a surrogate as “Pore water solubility”. However, it is not currently possible to compute this specific time in case there is no API in the tablet created by PAC modules. From a principal point of view, it would be possible to calculate with F-CAD the dissolution profile of lactose (LA) as a hydrophilic and well soluble ingredient (filler) and to determine the specific time till the water molecules have reached the geometrical center of the tablet. However, in this PhD work the dissolution profile of lactose was not calculated.

Table 15 Setting value of individual component

Components (F-CAD classification)		Setting values	
		Water-solubility	Swellability
MA	(API)	27,000	0
LA	(Non-swelling, soluble fillers)	65	0
MS	(Spherical disintegrant, swelling)	500	5
HPC SL	(Non-swelling, soluble binders)	690	5
Mg-St	(Hydrophobic ingredient)	65,000	0
Porosity	(Pore)	5	0

## 6 Results and Discussion

### 6.1 Physical properties of starting materials

MA, is a nonsteroidal anti-inflammatory agent classified as Class II on the basis of the biopharmaceutical classification system [25, 116] because of its poor solubility over the pH range 1.2 to 7.5 (Solubility: 0.2  $\mu\text{g/mL}$  (pH 1.2), 0.029 mg/mL (JP 2, pH 6.8), 0.12 mg/mL (pH 7.5)) [117, 118] and high permeability in Caco-2 cell model (Permeability coefficient =  $17.9 \pm 0.4 \times 10^{-6}$  cm/sec) [118].

The mean diameter of MA, LA and MS was 6.57, 39.4, and 25.0  $\mu\text{m}$ , respectively. MA was agglomerated by fine powder. The shape of each component was almost spherical, not fibrous according to their SEM pictures. The true density of MA was determined to be 1.26  $\text{g/cm}^3$  which was much lower than that of LA and MS. Specific surface area (SSA) of MA was found to be 1.87  $\text{m}^2/\text{g}$ , which was much higher than that of LA and MS.

### 6.2 Granules characterization

#### 6.2.1 Influence of loading volume of MA on granule characteristics

The characteristics of granules with increasing loading volume of MA in exchange of lactose/maize starch (7/3) [42] as excipients from Granule A to H are given in Table 16a. During the granulation process it was important to adopt the relatively low fluidized air pressure in order to avoid adherence of starting materials to the upper part of the fluidized bed granulator. MA is well known to be difficult to handle in fluidized bed granulation and tableting processes due to the tendency to stick to surfaces [119]. Special attention was paid to keep the bed expansion constant during the whole granulation process. The apparent density of granules was decreasing with increasing loading volume of MA, although the mean diameter, bulk and tapped density was independent thereof. In terms of granules flowability, the flowability was no issue on the basis of Carr's index and Hausner ratio regardless of the loading volume of MA.

The MA content of Granule B-C, D-E and F-H were determined to be 85-87%, 91-94% and 97-98% in comparison with the theoretical content, respectively. The decrease of MA content determined to be 85-94% for the loading volume from 12.0-45.0% v/v can be explained by the attachment of MA particles to the inner surface of the fluidized bed granulator. This was attributed to the tendency of MA to stick to any type of surface. The decrease of MA content with the loading volume from 55.1-74.1% v/v can be explained that a small fraction, i.e. 2-3%, of MA powder can pass through the filter unit which has a pore size of 10  $\mu\text{m}$ . It should be kept in mind that MA due to electrostatic effects easily forms agglomerates with a diameter

larger than 10  $\mu\text{m}$ . The loading volume of MA has to be taken into account for the manufacturing process of fluidized bed granulation.

Table 16a Characteristics of Granule A to H

Granule (Loading volume of MA, % v/v) / Particle Size distribution (%)	A (0)	B (12.0)	C (23.5)	D (34.5)	E (45.0)	F (55.1)	G (64.8)	H (74.1)
710 $\mu\text{m}$ on	0.6	0.04	0	0.04	0.04	0	0.2	0
500 $\mu\text{m}$ on	0.2	0.5	0.4	0.2	0.5	0.04	0.3	0.2
355 $\mu\text{m}$ on	4.8	10.7	5.9	4.3	6.4	2.0	12.0	5.0
250 $\mu\text{m}$ on	27.0	45.5	42.1	31.2	40.7	25.7	39.9	34.7
180 $\mu\text{m}$ on	40.8	29.4	31.6	39.0	30.2	39.0	22.3	29.4
125 $\mu\text{m}$ on	15.5	9.0	13.1	15.9	14.8	20.2	14.8	16.7
90 $\mu\text{m}$ on	6.1	2.4	5.5	5.8	4.4	8.5	5.9	8.0
90 $\mu\text{m}$ pass	5.0	2.4	1.2	3.7	3.0	4.6	4.6	6.0
Mean diameter ( $\mu\text{m}$ )	223	267	250	230	247	212	253	228
Powder moisture before granulation (%)	2.32	2.13	2.78	2.32	2.68	2.50	1.37	0.79
Granules moisture after drying (%)	1.89	1.99	3.20	2.49	2.04	1.61	1.39	1.08
Yield (%)	97.0	95.0	94.6	91.5	93.8	93.9	90.4	92.1
Bulk density ( $\text{g}/\text{cm}^3$ )	0.387	0.329	0.320	0.308	0.335	0.315	0.358	0.342
Tapped density ( $\text{g}/\text{cm}^3$ )	0.426	0.373	0.363	0.354	0.382	0.363	0.413	0.392
Hausner ratio	1.1	1.1	1.1	1.1	1.1	1.2	1.2	1.2
Carr Index (%)	9.1	11.8	11.8	12.9	12.1	13.2	13.2	12.6
Yield (500-90 $\mu\text{m}$ , %)	91.4	92.2	93.0	87.9	90.5	89.6	85.7	86.4
Apparent density ( $\text{g}/\text{cm}^3$ )	1.558	1.534	1.502	1.475	1.446	1.419	1.389	1.365
Assay (%)	0	84.6	86.9	91.2	93.7	97.8	97.0	97.9

Table 16b Characteristics of Granule I to O

Granule (Loading volume of MA, % v/v)	I (0)	J (34.5)	K (74.1)	L (0)	M(74.0)	N (0)	O (34.5)
<i>/ Particle size distribution (%)</i>							
710 $\mu\text{m}$ on	0	0	0	0	0	0	0
500 $\mu\text{m}$ on	0.5	0.2	0	0.4	0.1	0.8	0.2
355 $\mu\text{m}$ on	9.8	3.2	0.6	10.2	0.6	13.2	3.8
250 $\mu\text{m}$ on	44.8	32.0	20.9	43.9	14.5	48.4	32.3
180 $\mu\text{m}$ on	28.2	36.8	41.4	30.0	36.0	27.8	38.0
125 $\mu\text{m}$ on	9.4	13.6	21.0	10.7	27.3	7.7	17.3
90 $\mu\text{m}$ on	3.3	8.2	7.2	3.0	13.4	1.8	5.4
90 $\mu\text{m}$ pass	4.0	6.0	8.9	2.0	8.0	0.4	3.1
Mean diameter ( $\mu\text{m}$ )	261	223	199	263	184	281	230
Powder moisture before granulation (%)	1.23	2.50	1.59	2.49	1.57	1.80	1.22
Granules moisture after drying (%)	1.32	0.80	0.69	1.78	1.93	1.48	0.89
Yield (%)	91.8	93.4	88.1	95.6	89.6	99.1	95.2
Bulk density ( $\text{g}/\text{cm}^3$ )	0.381	0.317	0.314	0.312	0.327	0.329	0.314
Tapped density ( $\text{g}/\text{cm}^3$ )	0.436	0.365	0.365	0.361	0.385	0.377	0.370
Hausner ratio	1.1	1.2	1.2	1.2	1.2	1.1	1.2
Carr Index (%)	12.6	13.2	14.0	13.6	15.1	12.7	15.1
Yield (500-90 $\mu\text{m}$ , %)	87.6	87.6	80.2	93.3	82.3	98.0	92.1
Apparent density ( $\text{g}/\text{cm}^3$ )	1.571	1.468	1.355	1.556	1.349	1.561	1.472

### 6.2.2 SEM of granules with increasing loading volume of MA

The SEM of MA granules A, D, F and H corresponding to 0%, 34.5%, 55.1% and 74.1% v/v of MA magnified x 100 and x 350 are given in Figure 50a, 50b, 50c and 50d respectively. The LA and MS particles were clearly observed in Granule A. MA particles were granulated with nuclei of LA and MS particles in Granule D, F and H. In Granule H, however, almost LA and MS particles were covered by MA particle. The dissolution rate of MA from granules covered by MA such as Granule H is assumed to be slow.

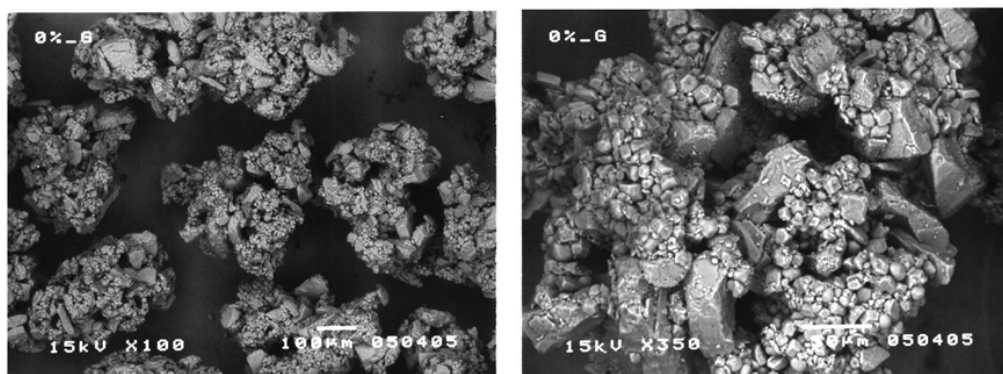


Figure 50a. Left: Granule A (x 100) composed of 0% v/v MA. Right: Granule A (x 350) composed of 0% v/v MA.

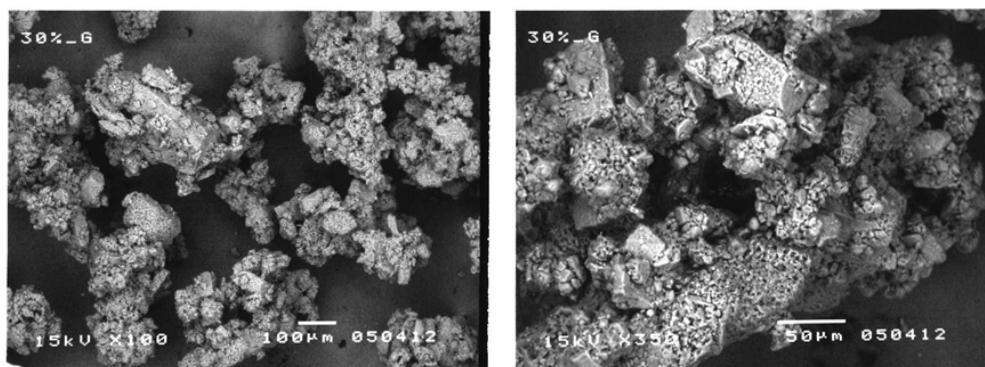


Figure 50b. Left: Granule D (x 100) composed of 34.5% v/v MA. Right: Granule D (x 350) composed of 34.5% v/v MA.

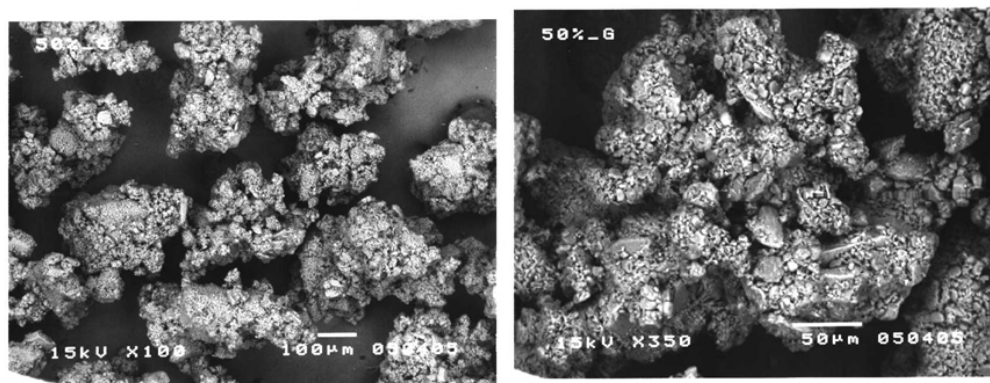


Figure 50c. Left: Granule F (x 100) composed on 55.1% v/v MA. Right: Granule F (x 350) composed on 55.1% v/v MA.

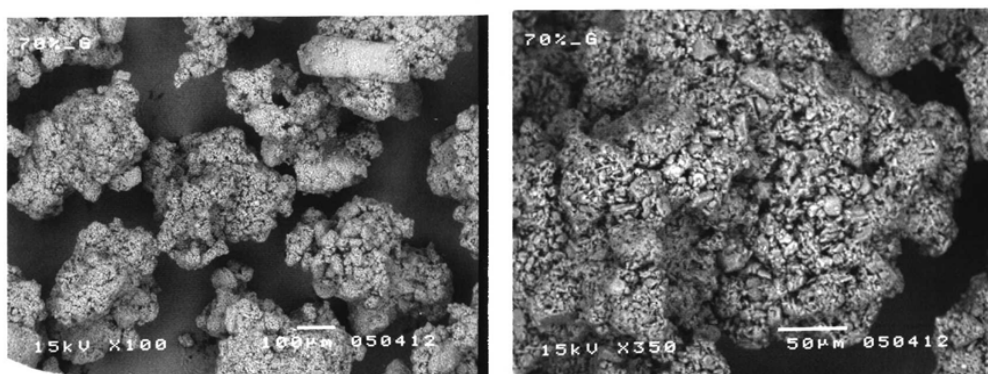


Figure 50d. Left: Granule H (x 100) composed on 74.1% v/v MA. Right: Granule H (x 350) composed on 74.1% v/v MA.

### 6.2.3 Intrusion volume of mercury into granules with increasing loading volume of MA

Intrusion volume of mercury into the granules prepared with increasing loading volume of MA showed that the volume of intragranular pore which is assumed to be lower than 14  $\mu\text{m}$  in diameter [112] was increasing with increasing loading volume of MA. It is assumed that MA particles attached each other by only the effect of binder, which is HPC SL in this study, without dissolving each other in the granules. The relationship between intragranular pore volume and apparent density of granules are shown in Table 17 and Figure 51. With increasing loading volume of MA, intragranular pore volume was increasing and apparent density of granules was decreasing, although mean diameter, bulk and tapped density of granules was independent thereof (Table 16a). This was attributed to the true density of MA powder determined to be 1.26  $\text{g}/\text{cm}^3$  (Table 11), which was much lower than that of LA and MS in the granules.



Table 17 Intrusion volume of mercury into granules with increasing loading volume of MA

Granule (Loading volume of MA, % v/v)	Apparent density (g/cm <sup>3</sup> )	Intrusion volume (mL/g)		
		Total	> 14 μm	< 14 μm
A (0)	1.558	1.921	1.729	0.193
B (12.0)	1.534	2.112	1.837	0.275
C (23.5)	1.502	2.308	2.014	0.294
D (34.5)	1.475	2.485	2.213	0.272
E (45.0)	1.446	2.189	1.849	0.340
F (55.1)	1.419	2.427	2.038	0.388
G (64.8)	1.389	2.114	1.704	0.411
H (74.1)	1.365	2.170	1.781	0.389

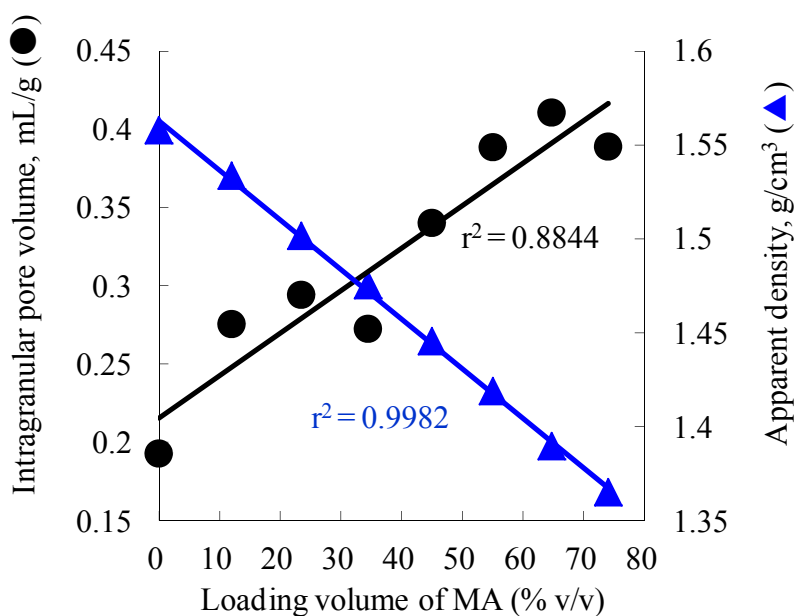


Figure 51. Relationship between intragranular pore volume (●) and apparent density (▲) of granules.

### 6.3 Tablet characterization

#### 6.3.1 Influence of loading volume of MA on compression behaviour

The characteristics of the tablets compressed at 7.0 kN from granules with increasing loading volume of MA in exchange of LA/MS (7/3) as excipients from Tablet A to H are given in Table 18a. The tensile force of Tablet A, B-E and F-H were 103, 128-134 and 142-143 N/cm<sup>2</sup> respectively (Figure 52). Tensile strength of MA tablet can be divided into two groups either Tablet B-E or F-H depending on the loading volume of MA. This was related to the following considerations;

- Porosity of MA tablet gradually decreased (Table 18a).
- MA particles in a tablet increased, which particle size was smaller than that of LA and MS (Table 11).
- MA particles in a tablet increased due to the brittle behavior of MA during compression [119].
- Increasing intragranular porosity of granules was observed because the fragmentation of lactose granules with a high intragranular porosity before compaction was leading to smaller intergranular pores in the tablet [120, 121].

Linear increasing of thickness of tablets was also observed with increasing loading volume of MA (Figure 52). It was increasing with decreasing of apparent density of granules compressed into tablet as shown in Table 19 and Figure 53. It can be concluded that thickness of tablet is completely decided by the apparent density of granules used for compression.

The ejection force of tablets which is the friction between the die wall and the tablet surface resulting from compression process increased with increasing loading volume of MA (Figure 54). This was also attributed to the tendency of MA to stick to any type of surface [119]. The ejection force of tablet has to be taken into account for the manufacturing process of tableting although there was no capping of tablet tendency in this experiment due to the granules manufactured by fluidized bed granulator with spraying the HPC SL binder solution [43].

Table 18a Characteristics of Tablet A to H compressed at 7 kN

Tablet (Loading volume of MA, % v/v)	Weight (mg)	Diameter (mm)	Thickness (mm)	Tensile strength (N/cm <sup>2</sup> )	Cal. Porosity (%)	Ejection force (N)
A (0)	417.7 ± 0.82 (n=6)	10.0 ± 0.00 (n=6)	4.30 ± 0.01 (n=6)	103 ± 3.20 (n=6)	20.6 ± 0.32 (n=6)	109 ± 11.4 (n=26)
B (12.0)	416.5 ± 1.10 (n=6)	10.0 ± 0.01 (n=6)	4.24 ± 0.01 (n=6)	128 ± 4.64 (n=6)	18.2 ± 0.21 (n=6)	231 ± 8.57 (n=19)
C (23.5)	415.6 ± 1.07 (n=7)	9.96 ± 0.01 (n=7)	4.28 ± 0.01 (n=7)	133 ± 3.60 (n=7)	17.0 ± 0.28 (n=7)	357 ± 18.1 (n=20)
D (34.5)	417.5 ± 1.32 (n=7)	9.96 ± 0.01 (n=7)	4.35 ± 0.01 (n=7)	132 ± 3.89 (n=7)	16.6 ± 0.28 (n=7)	505 ± 18.6 (n=19)
E (45.0)	416.5 ± 0.73 (n=6)	9.97 ± 0.01 (n=6)	4.41 ± 0.01 (n=6)	134 ± 3.35 (n=6)	16.2 ± 0.20 (n=6)	593 ± 12.2 (n=18)
F (55.1)	416.7 ± 1.40 (n=6)	9.97 ± 0.01 (n=6)	4.47 ± 0.01 (n=6)	143 ± 7.14 (n=6)	15.8 ± 0.24 (n=6)	703 ± 22.5 (n=18)
G (64.8)	417.7 ± 0.55 (n=6)	9.97 ± 0.00 (n=6)	4.56 ± 0.00 (n=6)	142 ± 4.76 (n=6)	15.5 ± 0.14 (n=6)	697 ± 27.9 (n=18)
H (74.1)	416.9 ± 1.72 (n=6)	10.0 ± 0.01 (n=6)	4.65 ± 0.01 (n=6)	143 ± 3.52 (n=6)	16.4 ± 0.37 (n=6)	802 ± 19.6 (n=18)

Table 18b Characteristics of Tablet I to O compressed at 7 kN

Tablet (Loading volume of MA, % v/v)	Weight (mg)	Diameter (mm)	Thickness (mm)	Tensile strength (N/cm <sup>2</sup> )	Cal. Porosity (%)	Ejection force (N)
I (0)	416.6 ± 0.43 (n=6)	10.0 ± 0.00 (n=6)	4.26 ± 0.01 (n=6)	97.6 ± 2.71 (n=6)	20.6 ± 0.16 (n=6)	209 ± 11.0 (n=24)
J (34.5)	415.0 ± 0.62 (n=6)	10.0 ± 0.00 (n=6)	4.34 ± 0.02 (n=6)	135 ± 2.10 (n=6)	17.0 ± 0.26 (n=6)	583 ± 12.9 (n=24)
K (74.1)	414.6 ± 1.02 (n=6)	10.0 ± 0.00 (n=6)	4.66 ± 0.02 (n=6)	129 ± 1.95 (n=6)	16.3 ± 0.32 (n=6)	989 ± 18.9 (n=25)
L (0)	417.5 ± 0.31 (n=6)	9.99 ± 0.01 (n=6)	4.27 ± 0.01 (n=6)	118 ± 1.96 (n=6)	19.7 ± 0.15 (n=6)	188 ± 18.6 (n=14)
M (74.0)	416.6 ± 0.75 (n=6)	9.99 ± 0.00 (n=6)	4.70 ± 0.01 (n=6)	131 ± 2.17 (n=6)	16.2 ± 0.11 (n=6)	1094 ± 38.4 (n=17)
N (0)	417.2 ± 0.48 (n=6)	9.99 ± 0.00 (n=6)	4.28 ± 0.02 (n=6)	125 ± 4.07 (n=6)	20.4 ± 0.47 (n=6)	323 ± 8.59 (n=16)
O (34.5)	417.2 ± 0.62 (n=6)	10.0 ± 0.01 (n=6)	4.38 ± 0.01 (n=6)	133 ± 4.58 (n=6)	17.4 ± 0.29 (n=6)	729 ± 17.8 (n=22)

Table 18c Characteristics of Tablet A to H compressed at 5 kN

Tablet (Loading volume of MA, % v/v)	Weight (mg)	Diameter (mm)	Thickness (mm)	Tensile strength (N/cm <sup>2</sup> )	Cal. Porosity (%)	Ejection force (N)
A (0)	416.1 ± 0.31 (n=3)	9.94 ± 0.01 (n=3)	4.62 ± 0.01 (n=3)	58.3 ± 0.16 (n=3)	25.4 ± 0.22 (n=3)	183 ± 6.46 (n=18)
B (12.0)	415.6 ± 0.95 (n=3)	9.93 ± 0.01 (n=3)	4.62 ± 0.01 (n=3)	67.5 ± 2.14 (n=3)	24.3 ± 0.28 (n=3)	265 ± 8.24 (n=18)
C (23.5)	415.4 ± 0.75 (n=3)	9.93 ± 0.01 (n=3)	4.64 ± 0.01 (n=3)	70.1 ± 2.12 (n=3)	23.0 ± 0.14 (n=3)	342 ± 7.21 (n=18)
D (34.5)	416.4 ± 0.06 (n=3)	9.92 ± 0.01 (n=3)	4.66 ± 0.02 (n=3)	80.4 ± 1.77 (n=3)	21.6 ± 0.16 (n=3)	423 ± 7.14 (n=18)
E (45.0)	415.1 ± 0.83 (n=3)	9.93 ± 0.00 (n=3)	4.71 ± 0.01 (n=3)	79.0 ± 1.28 (n=3)	21.2 ± 0.07 (n=3)	495 ± 9.85 (n=18)
F (55.1)	416.1 ± 0.60 (n=3)	9.93 ± 0.01 (n=3)	4.77 ± 0.01 (n=3)	88.4 ± 0.86 (n=3)	20.5 ± 0.20 (n=3)	633 ± 16.5 (n=18)
G (64.8)	416.4 ± 0.12 (n=3)	9.94 ± 0.01 (n=3)	4.86 ± 0.01 (n=3)	84.8 ± 1.36 (n=3)	20.5 ± 0.22 (n=3)	701 ± 13.8 (n=18)
H (74.1)	417.2 ± 0.76 (n=3)	9.93 ± 0.00 (n=3)	4.95 ± 0.01 (n=3)	92.5 ± 0.53 (n=3)	20.2 ± 0.05 (n=3)	865 ± 13.3 (n=18)

Table 18d Characteristics of Tablet I to O compressed at 5 kN

Tablet (Loading volume of MA, % v/v)	Weight (mg)	Diameter (mm)	Thickness (mm)	Tensile strength (N/cm <sup>2</sup> )	Cal. Porosity (%)	Ejection force (N)
I (0)	416.5 ± 0.64 (n=3)	9.99 ± 0.00 (n=3)	4.48 ± 0.02 (n=3)	70.2 ± 1.87 (n=3)	24.5 ± 0.36 (n=3)	190 ± 12.1 (n=20)
J (34.5)	416.0 ± 0.76 (n=3)	9.99 ± 0.01 (n=3)	4.60 ± 0.00 (n=3)	91.5 ± 1.34 (n=3)	21.3 ± 0.10 (n=3)	495 ± 13.6 (n=19)
K (74.1)	415.3 ± 0.78 (n=3)	9.99 ± 0.01 (n=3)	4.96 ± 0.01 (n=3)	83.5 ± 2.70 (n=3)	21.2 ± 0.28 (n=3)	816 ± 22.8 (n=18)
L (0)	413.7 ± 0.61 (n=3)	9.99 ± 0.00 (n=3)	4.53 ± 0.01 (n=3)	69.9 ± 1.76 (n=3)	25.1 ± 0.10 (n=3)	190 ± 5.06 (n=18)
M (74.0)	414.2 ± 0.06 (n=3)	10.0 ± 0.00 (n=3)	4.94 ± 0.01 (n=3)	87.2 ± 0.70 (n=3)	20.9 ± 0.09 (n=3)	807 ± 21.8 (n=19)
N (0)	416.3 ± 0.62 (n=3)	9.98 ± 0.01 (n=3)	4.46 ± 0.02 (n=3)	87.4 ± 1.83 (n=3)	23.4 ± 0.48 (n=3)	221 ± 9.04 (n=19)
O (34.5)	415.6 ± 0.95 (n=3)	9.99 ± 0.00 (n=3)	4.58 ± 0.02 (n=3)	90.4 ± 1.33 (n=3)	21.4 ± 0.09 (n=3)	482 ± 18.5 (n=18)

Table 18e Characteristics of Tablet A to H compressed at 3 kN

Tablet (Loading volume of MA, % v/v)	Weight (mg)	Diameter (mm)	Thickness (mm)	Tensile strength (N/cm <sup>2</sup> )	Cal. Porosity (%)	Ejection force (N)
A (0)	416.2 ± 0.57 (n=3)	9.94 ± 0.01 (n=3)	5.03 ± 0.00 (n=3)	28.0 ± 0.02 (n=3)	31.6 ± 0.03 (n=3)	119 ± 4.54 (n=18)
B (12.0)	416.3 ± 0.55 (n=3)	9.93 ± 0.00 (n=3)	5.01 ± 0.01 (n=3)	36.3 ± 0.68 (n=3)	30.0 ± 0.08 (n=3)	170 ± 3.89 (n=18)
C (23.5)	415.8 ± 1.18 (n=3)	9.93 ± 0.01 (n=3)	5.00 ± 0.01 (n=3)	38.5 ± 0.06 (n=3)	28.5 ± 0.28 (n=3)	238 ± 7.33 (n=18)
D (34.5)	416.2 ± 0.62 (n=3)	9.93 ± 0.01 (n=3)	5.02 ± 0.01 (n=3)	43.5 ± 1.26 (n=3)	27.4 ± 0.11 (n=3)	292 ± 5.82 (n=18)
E (45.0)	416.8 ± 0.64 (n=3)	9.93 ± 0.00 (n=3)	5.03 ± 0.01 (n=3)	48.4 ± 1.28 (n=3)	26.0 ± 0.12 (n=3)	342 ± 17.6 (n=18)
F (55.1)	415.0 ± 0.56 (n=3)	9.92 ± 0.01 (n=3)	5.09 ± 0.02 (n=3)	52.6 ± 2.12 (n=3)	25.6 ± 0.28 (n=3)	432 ± 11.9 (n=18)
G (64.8)	416.8 ± 0.55 (n=3)	9.92 ± 0.01 (n=3)	5.21 ± 0.01 (n=3)	52.2 ± 0.83 (n=3)	25.5 ± 0.34 (n=3)	457 ± 8.79 (n=18)
H (74.1)	416.6 ± 0.61 (n=3)	9.93 ± 0.01 (n=3)	5.28 ± 0.01 (n=3)	56.9 ± 0.82 (n=3)	25.2 ± 0.11 (n=3)	580 ± 12.4 (n=18)

Table 18f Characteristics of Tablet I to O compressed at 3 kN

Tablet (Loading volume of MA, % v/v)	Weight (mg)	Diameter (mm)	Thickness (mm)	Tensile strength (N/cm <sup>2</sup> )	Cal. Porosity (%)	Ejection force (N)
I (0)	416.1 ± 0.38 (n=3)	9.99 ± 0.00 (n=3)	4.87 ± 0.01 (n=3)	34.9 ± 0.78 (n=3)	30.5 ± 0.08 (n=3)	118 ± 7.43 (n=18)
J (34.5)	416.4 ± 0.55 (n=3)	9.99 ± 0.01 (n=3)	4.99 ± 0.01 (n=3)	47.7 ± 0.85 (n=3)	27.4 ± 0.29 (n=3)	347 ± 15.0 (n=19)
K (74.1)	415.7 ± 0.36 (n=3)	10.0 ± 0.00 (n=3)	5.38 ± 0.01 (n=3)	46.2 ± 2.01 (n=3)	27.3 ± 0.10 (n=3)	540 ± 16.1 (n=18)
L (0)	415.5 ± 1.00 (n=3)	9.99 ± 0.00 (n=3)	4.93 ± 0.02 (n=3)	34.9 ± 1.30 (n=3)	30.9 ± 0.09 (n=3)	141 ± 8.26 (n=18)
M (74.0)	415.9 ± 0.71 (n=3)	10.0 ± 0.00 (n=3)	5.39 ± 0.01 (n=3)	43.3 ± 1.88 (n=3)	27.2 ± 0.26 (n=3)	551 ± 11.7 (n=19)
N (0)	417.0 ± 0.38 (n=3)	9.98 ± 0.00 (n=3)	4.88 ± 0.01 (n=3)	41.9 ± 0.09 (n=3)	30.0 ± 0.20 (n=3)	169 ± 7.62 (n=19)
O (34.5)	417.1 ± 0.40 (n=3)	9.99 ± 0.00 (n=3)	4.98 ± 0.02 (n=3)	50.4 ± 0.84 (n=3)	27.3 ± 0.25 (n=3)	300 ± 13.5 (n=18)



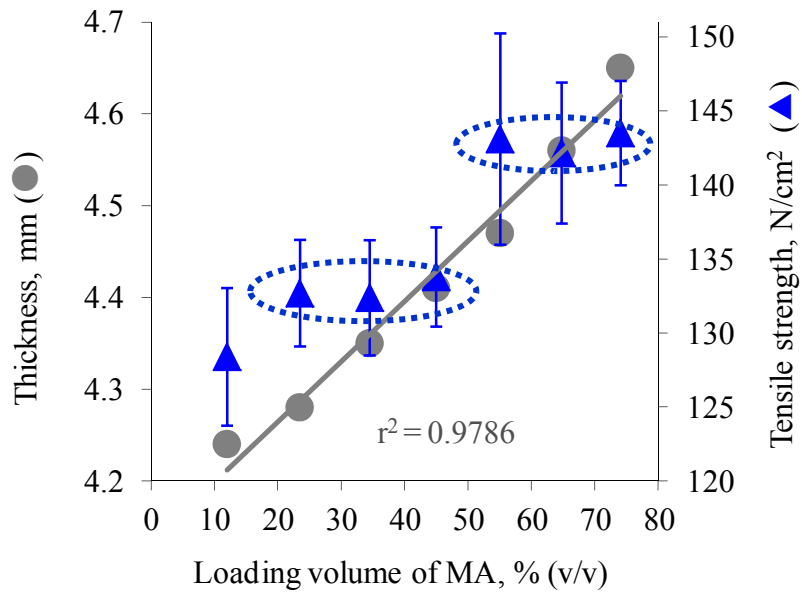


Figure 52. Thickness and tensile strength of tablets compressed at 7.0 kN from granules with increasing loading volume of MA.

Table 19 Relationship between apparent density of granules and tablet thickness compressed at 7.0 kN

Granule (Loading volume of MA, % v/v)	Apparent density (g/cm <sup>3</sup> )	Thickness (mm)	
		Average	S.D.
A (0)	1.558	4.30	0.01
B (12.0)	1.534	4.24	0.01
C (23.5)	1.502	4.28	0.01
D (34.5)	1.475	4.35	0.01
E (45.0)	1.446	4.41	0.01
F (55.1)	1.419	4.47	0.01
G (64.8)	1.389	4.56	0.004
H (74.1)	1.365	4.65	0.01

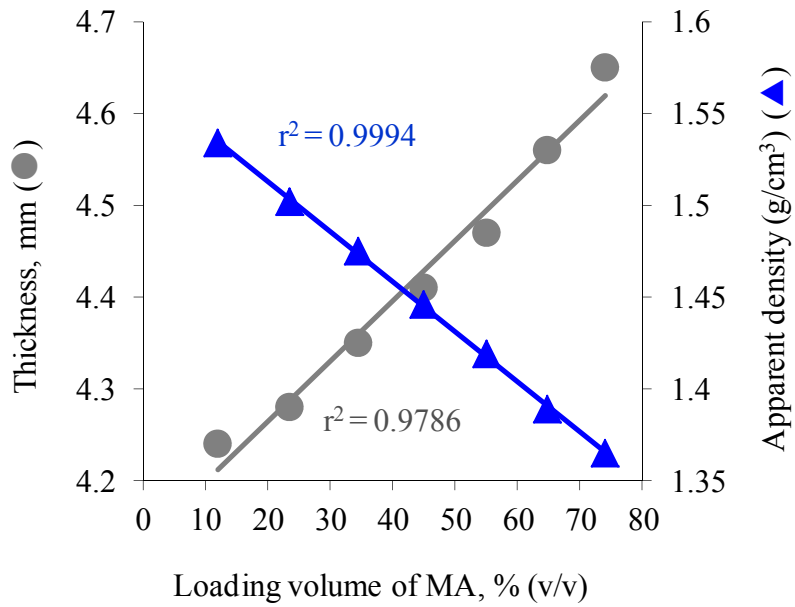


Figure 53. Relationship between apparent density of granules and tablet thickness compressed at 7.0 kN.

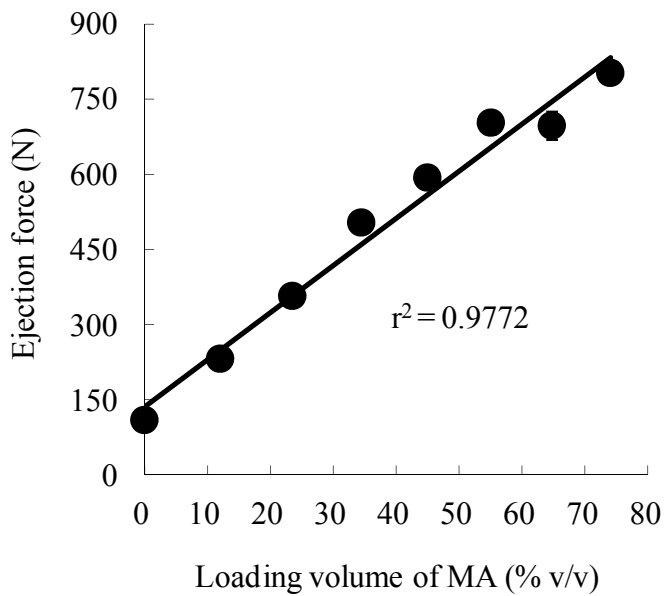


Figure 54. Relationship between loading volume of MA and ejection force of tablets compressed at 7.0 kN.

### 6.3.2 Visual inspection on tablet characteristics using NIR imaging

In order to get the more scientific understanding of the tablet characteristics, especially for tensile strength of tablet, near infrared (NIR) imaging technology has been applied to visualize their component distribution on the tablet surface compressed at 7.0 kN according to the loading volume of MA. Figure 55 shows the distribution of the predicted concentration for MA, LA, MS by partial least square regression (PLSR) technique on one surface of each tablet from A to H. The intensity spectral from a second derivative calculation was illustrated as a color. MA, LA and MS were showed by Red, Green and Blue respectively and overlaid as a Red-Green-Blue (RGB) imaging [55].

MA has been well distributed homogenously with increasing the loading volume of MA from RGB imaging visually. In Tablet H, LA and MS particles are located on the surface of tablet although LA and MS particles are covered by MA particles in the Granules H. LA and MS particles should be located in order to induce the water into tablet for the disintegration.

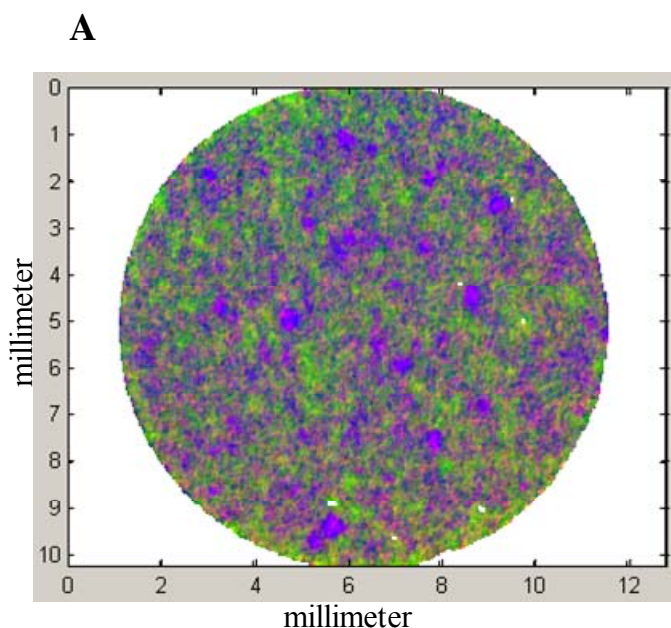


Figure 55a. RGB imaging of Tablet A (MA: 0% w/w).

**B**

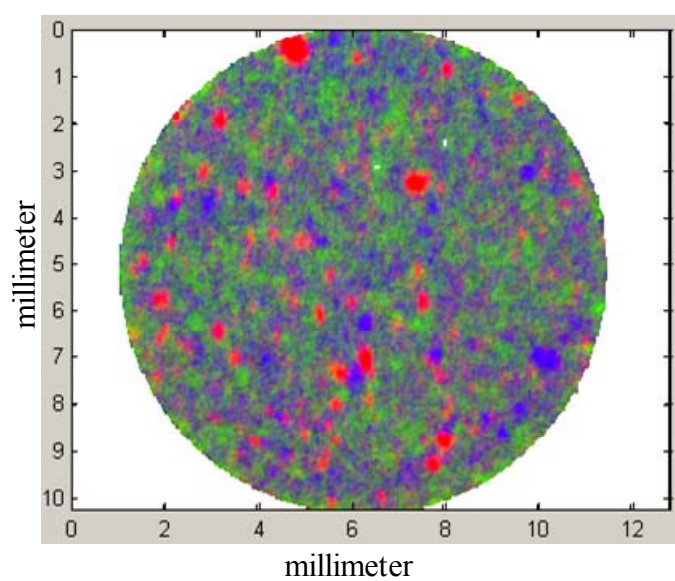


Figure 55b. RGB imaging of Tablet B (MA: 10% w/w, 12.0% v/v).

**C**

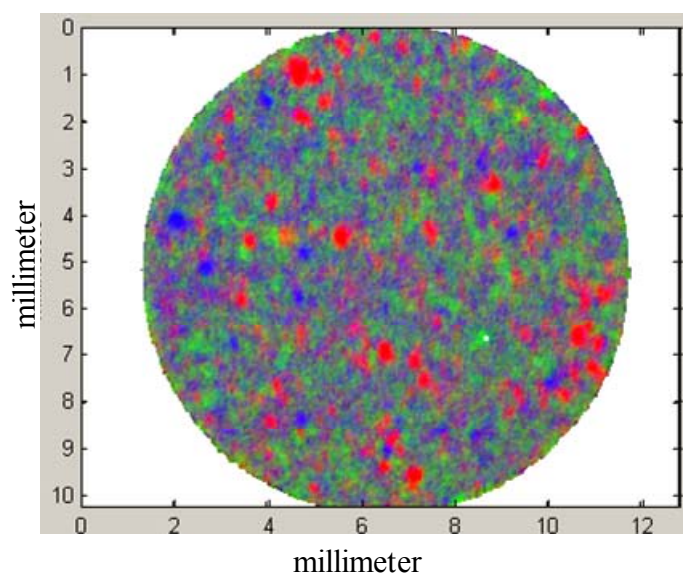


Figure 55c. RGB imaging of Tablet C (MA: 20% w/w, 23.5% v/v).

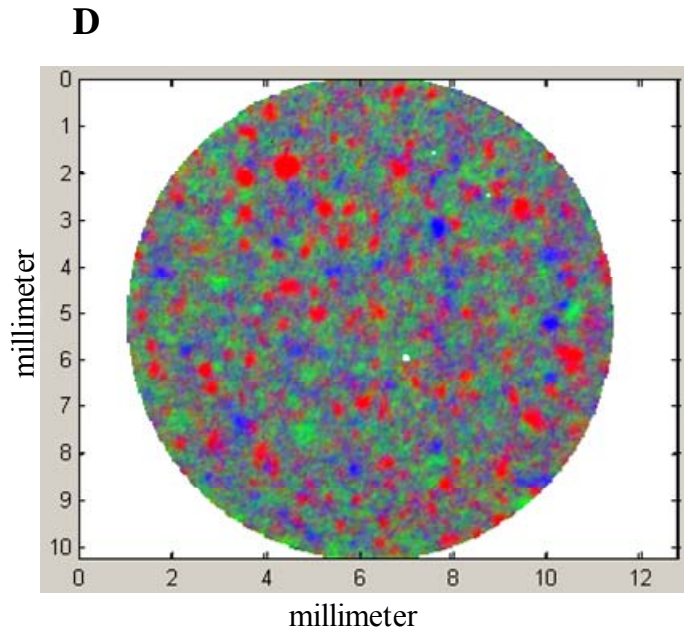


Figure 55d. RGB imaging of Tablet D (MA: 30% w/w, 34.5% v/v).

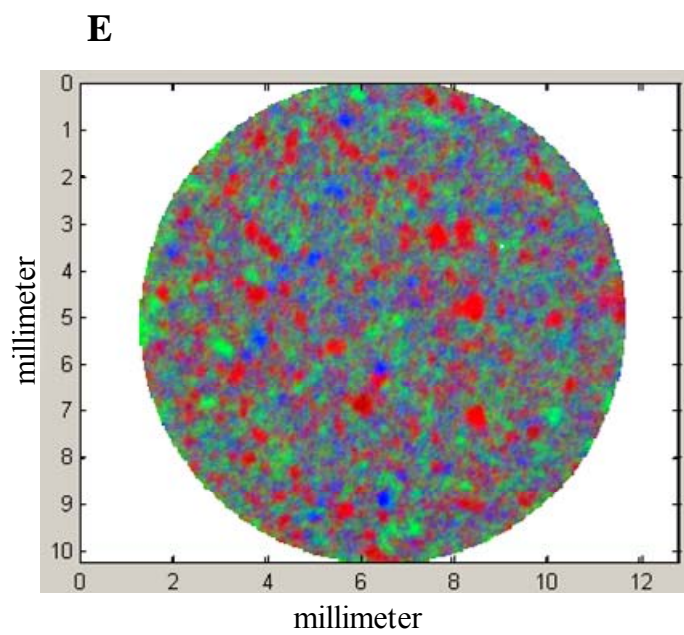


Figure 55e. RGB imaging of Tablet E (MA: 40% w/w, 45.0% v/v).

**F**

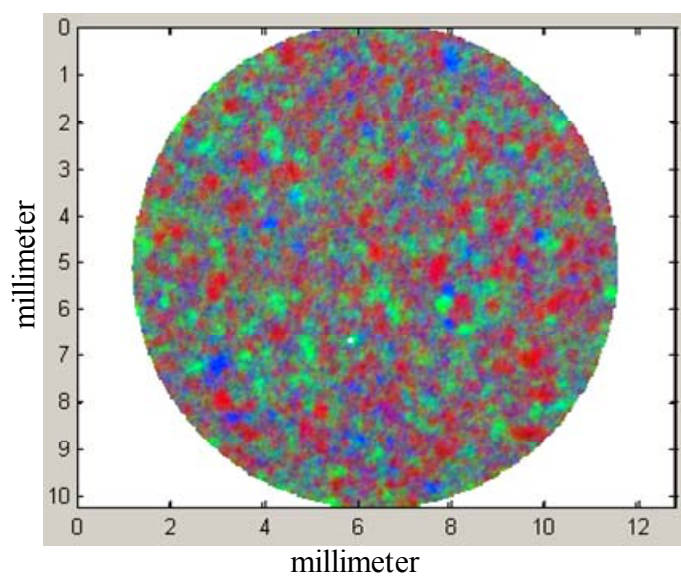


Figure 55f. RGB imaging of Tablet F (MA: 50% w/w, 55.1% v/v).

**G**

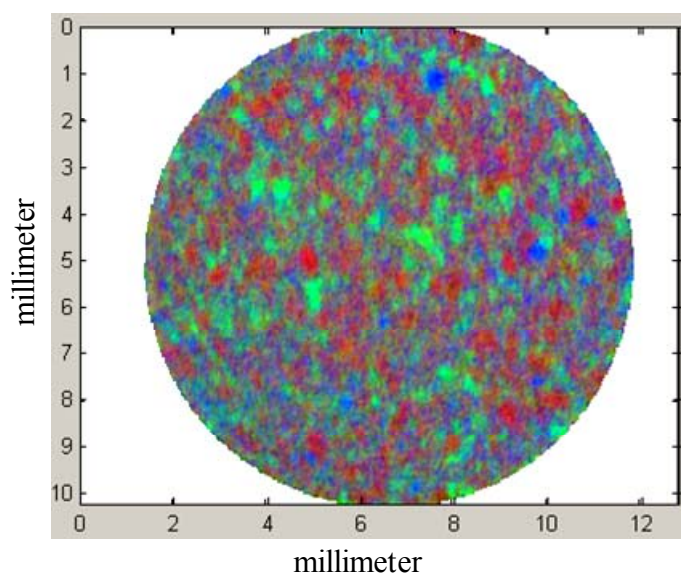


Figure 55g. RGB imaging of Tablet G (MA: 60% w/w, 64.8% v/v).



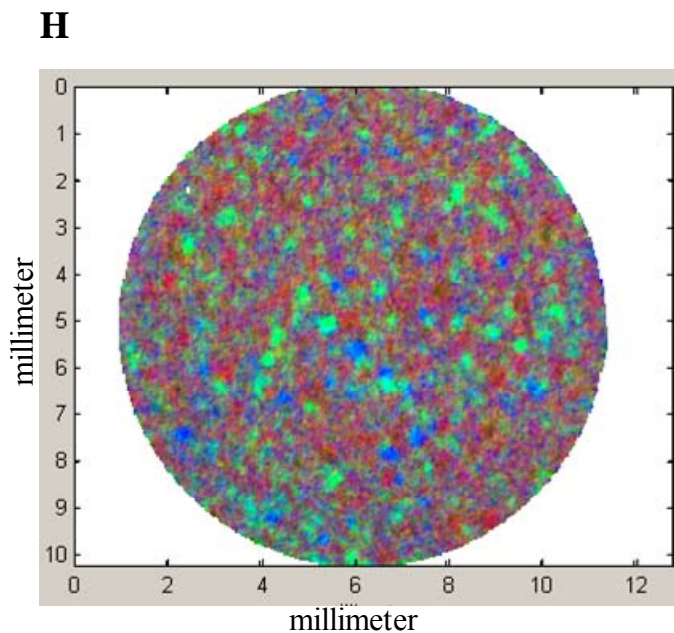


Figure 55h. RGB imaging of Tablet H (MA: 70% w/w, 74.1% v/v).

### 6.3.3 MA domain size with increasing loading volume of MA in tablet

Mean domain size of each component on the surface of tablets compressed at 7.0 kN was determined by the pixel size of NIR imaging as shown in Table 20 and Figure 56. The domain size of MA was increasing up to the 45.0% v/v (Tablet E) loading volume of MA. Then its domain size was decreasing with increasing the loading volume of MA up to the 74.1% v/v (Tablet H) although the domain size of LA and MS was kept constant. This revealed that the decreasing the domain size of MA also resulted in increasing the tensile strength of tablet due to increase the number of MA particle in tablet because the tensile strength of tablet has jumped from Tablet E to F corresponding to 45.0% v/v to 55.1% v/v of MA in Figure 52. It is concluded MA is key attribute on the tablet characteristics in terms of thickness and tensile strength as compared with LA and MS.

Table 20 Mean domain size of MA, LA and MS on the tablet surface

Tablet (Loading volume of MA, % v/v)	Mean domain size ( $\mu\text{m}$ )		
	MA	LA	MS
A (0)	—	104	94.3
B (12.0)	171	95.2	83.4
C (23.5)	193	97.1	74.0
D (34.5)	211	104	83.0
E (45.0)	211	111	85.3
F (55.1)	177	123	81.4
G (64.8)	137	138	74.8
H (74.1)	83.2	118	82.9

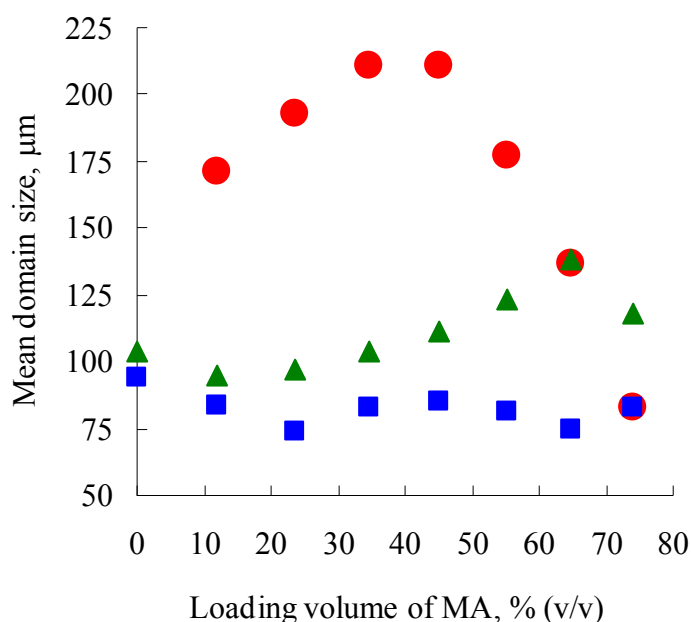


Figure 56. Mean domain size of MA (●), LA (▲) and MS (■) on the tablet surface with increasing loading volume of MA.

#### 6.3.4 Tablet disintegration time

The disintegration process is an important factor for drug dissolution, especially for drugs with low solubility in water or in gastrointestinal fluids. The disintegration time of tablets compressed at 7.0 kN was roughly constant up to 34.5% v/v (Tablet D) loading volume of MA, and then decreased to a minimum with 55.1% v/v (Tablet F) loading volume of MA and finally increased again with increasing the loading volume of MA up to 74.1% v/v (Tablet H) as shown in Table 21 and Figure 57. The decreasing volume of MS in the tablet as a disintegrant from 30.3% v/v to 13.6% v/v corresponding to the increasing loading volume of



MA from 0% v/v to 55.1% v/v is suggested to have a positive influence on the disintegration process [122].

Leuenberger et al. found the amount (% v/v) of StaRX1500<sup>®</sup> corresponded to the critical concentration, i.e. to the percolation threshold in terms of percolation theory, of StaRX1500<sup>®</sup> for binary mixture: caffeine or paracetamol - StaRX1500<sup>®</sup> [9-12]. It is important to mention here that percolation threshold of disintegrant is also found for an immediate release of a realistic pharmaceutical tablet formulation in this study.

**Table 21** Disintegration time of tablets compressed at 7.0 kN

Tablet (Loading volume of MA, % v/v)	Disintegration time (sec.) (n=3)
A (0)	550 ± 23
B (12.0)	596 ± 8
C (23.5)	616 ± 6
D (34.5)	604 ± 21
E (45.0)	428 ± 16
F (55.1)	266 ± 8
G (64.8)	453 ± 24
H (74.1)	758 ± 15

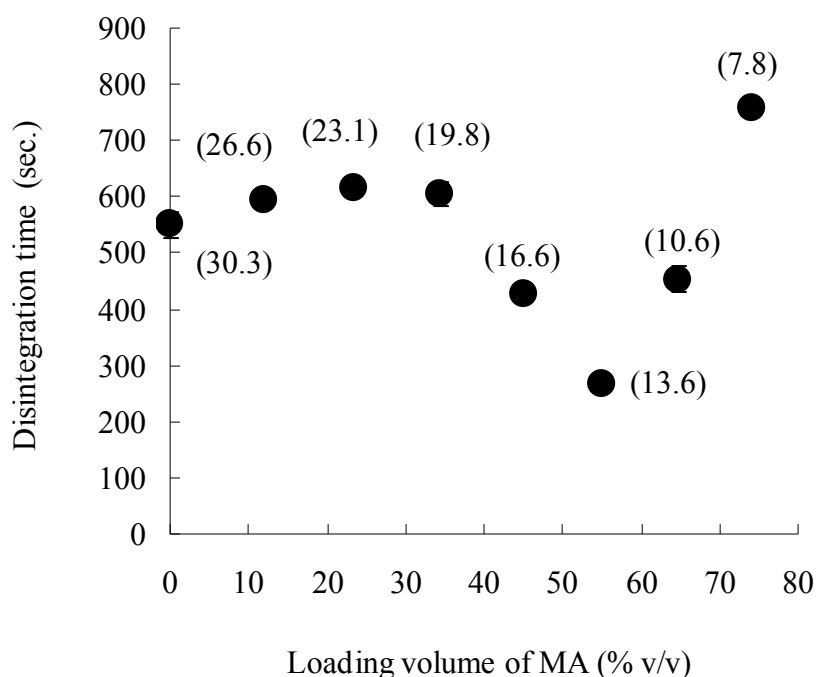


Figure 57. Disintegration time of tablets compressed at 7.0 kN with increasing loading volume of MA. The volume (% v/v) of MS in tablet is represented in brackets.

### 6.3.5 Pore size distribution, Median pore diameter and porosity

In order to consider the other factors related to the minimum disintegration time of tablet compressed at 7.0 kN, which was found with 55.1% v/v (Tablet F) loading volume of MA [122], the pore size distribution, median pore diameter by volume and porosity of tablet were investigated. The pore diameter of tablets compressed from granules prepared at different loading volumes of MA corresponding to the intrusion volume of mercury was plotted to show the pore size distribution of tablet (Figure 58). With increasing loading volume of MA, the volume of large pore of tablet was decreasing and the peak of pore size distribution was shifting towards the smaller pore diameter. The median pore diameter and porosity are shown in Table 22. The median pore diameter and porosity of tablets was gradually decreasing with increasing loading volume of MA which was same results with when porosity was calculated by Equation 25. It is suggested that the calculated porosity is enough to evaluate the tablet properties in this study. This linear trend was not observed with the results obtained by measuring the disintegration time of the tablets. It can be concluded that the pore diameter and porosity of tablet was not a significant parameter in this study to explain the minimum disintegration time which was found with 55.1% v/v (Tablet F) loading volume of MA. Further, it can be concluded that the dominant factor on disintegration for MA tablets was the swelling property of MS in the tablet. The critical concentration of disintegrant (% v/v) can exert the swelling property on the surrounding particles and induce water for more effective disintegration of the tablet.

Below and above the critical concentration of disintegrant, the disintegration time was increasing, giving a typical V-shape curve. The increase of disintegration time above the critical concentration of disintegrant was assumed so far as followings;

- There is not enough space for disintegrant particles to expand in the tablet. The excess of disintegrant particles might start retarding the swelling properties of MS each other [122].
- The continuous cluster of disintegrant particles or pores conducting water might starts to extend by forming dead-end arms from the backbone (excess of disintegrant). The increased complexity of the network retards the penetration of water within the tablet as compared with the continuous cluster at the percolation threshold [12].

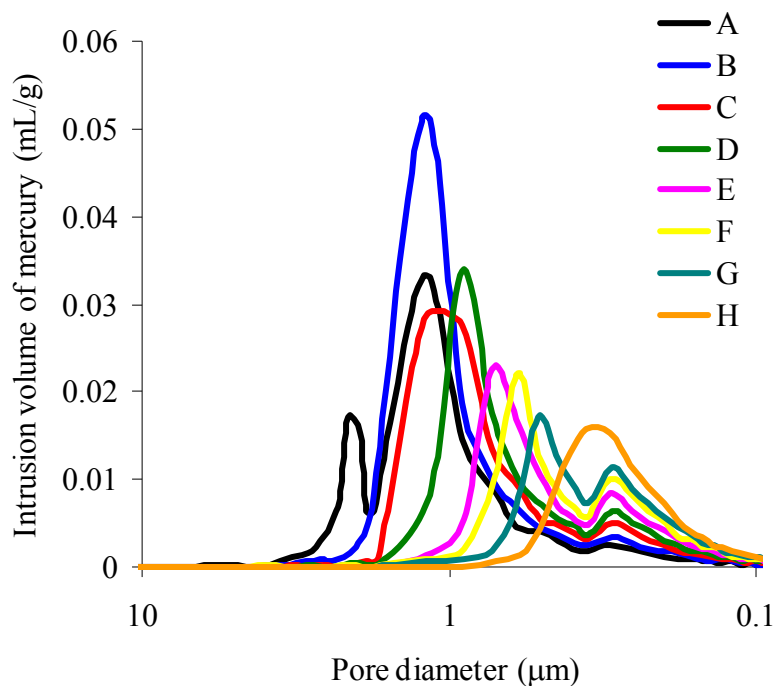


Figure 58. Pore size distribution of tablets compressed at 7.0 kN with increasing loading volume of MA.

Table 22 Median pore diameter, Porosity of tablets compressed at 7.0 kN

	Median pore diameter ( $\mu\text{m}$ ) (n=1)	Porosity (%) (n=1)	Cal. Porosity (% v/v) (n=6-7)	$\Delta$ %
A	1.365	22.3	$20.6 \pm 0.32$	1.7
B	0.893	20.4	$18.2 \pm 0.21$	2.2
C	0.620	19.6	$17.0 \pm 0.28$	2.6
D	0.483	19.4	$16.6 \pm 0.28$	2.8
E	0.341	18.6	$16.2 \pm 0.20$	2.4
F	0.307	18.5	$15.8 \pm 0.24$	2.7
G	0.255	18.1	$15.5 \pm 0.14$	2.6
H	0.232	17.9	$16.4 \pm 0.37$	1.5

#### 6.4 Focus on searching the critical concentration of MS

The minimum disintegration time ( $266 \pm 8$  sec.) of tablet compressed at 7.0 kN for MA tablet has been determined for a ternary composition of 55.1% v/v (50% w/w) MA, 31.3% v/v (35% w/w) LA and 13.6% v/v (15% w/w) MS [122]. However, it has to be kept in mind that it was not a truly ternary components system as the ratio of LA/MS (7/3) was kept constant [122]. In the following section, the ratio of LA to MS has been extended to correspond to a truly ternary components tablet formulation [123]. It also has to be kept in mind again that up

to now there is no universal science-based formulation technique for low water soluble drugs. Therefore several research groups reported about the critical concentration of disintegrant that is required to achieve the minimum disintegration time [2-6]. Determination of the critical concentration of disintegrant is an important parameter for design of a tablet formulation, especially for low water soluble drugs as mentioned above, to increase the specific surface area by an optimal and fast disintegration.

Ringard and Guyot-Hermann [7] have introduced the following equation for the calculation of the most effective disintegrant concentration by taking into account the geometrical description of the involved particles (drug or filler, disintegrant) and the change of the particle size of the disintegrant due to swelling (Equation 29).

$$M_s = 0.32 \frac{\rho_1}{\rho_2} \left\{ \left( \frac{D_1}{D_2} + 1 \right)^3 - 1 \right\} \frac{D_1}{D_{1s}} \quad \text{Equation (29)}$$

where  $M_s$  is an optimal amount of disintegrant (w/w),  $\rho_1$ ,  $\rho_2$  ( $\text{g/cm}^3$ ) are true densities of disintegrant and active substance respectively;  $D_1$ ,  $D_2$  are average diameters (Ferret's diameters) of dry disintegrant particles and active substance, respectively;  $D_{1s}$  is an average diameter of the swollen disintegrant particle.

This equation was described by assuming that the fine particles of the disintegrant form an "infinite" network and cover totally the surface of the coarser drug particles.

Krausbauer, Puchkov and Leuenberger [11, 12] have finally proposed the caging and non-caging concept (Equation 14) in order to calculate the critical concentration of non-fibrous disintegrant in a binary tablets composed of caffeine or paracetamol and partially pregelatinized maize starch, StaRX1500®.

However the further investigation is needed to determine the critical concentration of non-fibrous disintegrant not only for binary tablets but also for ternary pharmaceutical tablets. No one, however, has reported experimentally the location of critical concentration of disintegrant for a ternary immediate release pharmaceutical tablet formulation.

The holistic description is an important issue as formulations are complex systems such as pharmaceutical tablet formulation and its quality of the product depends on the variability of the manufacturing processes involved and on the variability of the physical and chemical quality of the components in the tablet. The number of compositions has increased and each composition of granules was compressed at not only 7 kN but also 5 kN and 3 kN. Thus the results of the tensile strength, porosity and disintegration time are listed in Table 23 as a physical description and documentation of the tablet quality.

Figure 59 shows the response surfaces of disintegration MA tablets compressed at 7 kN, 5 kN and 3 kN as a function of MA (% v/v) and MS (% v/v). Minimum disintegration time of

tablets compressed at 7 kN and 5 kN was found for the Tablet O, F and M corresponding to 34.5% v/v, 55.1% v/v and 74.0% v/v of MA respectively. The minimum disintegration time of MA tablets was surprisingly observed at a ratio of MS/MA = 0.25. However, a catastrophic change reading to disintegration time of MA tablets compressed at 3 kN was not strongly observed. The dominant network that the water can diffuse for the disintegration of MA tablet is considered through the disintegrant network, not through the porous network. On the other hand, the disintegration time of Tablet A, I, L and N corresponding to 0% v/v of MA was almost constant regardless of the porosity of tablet.

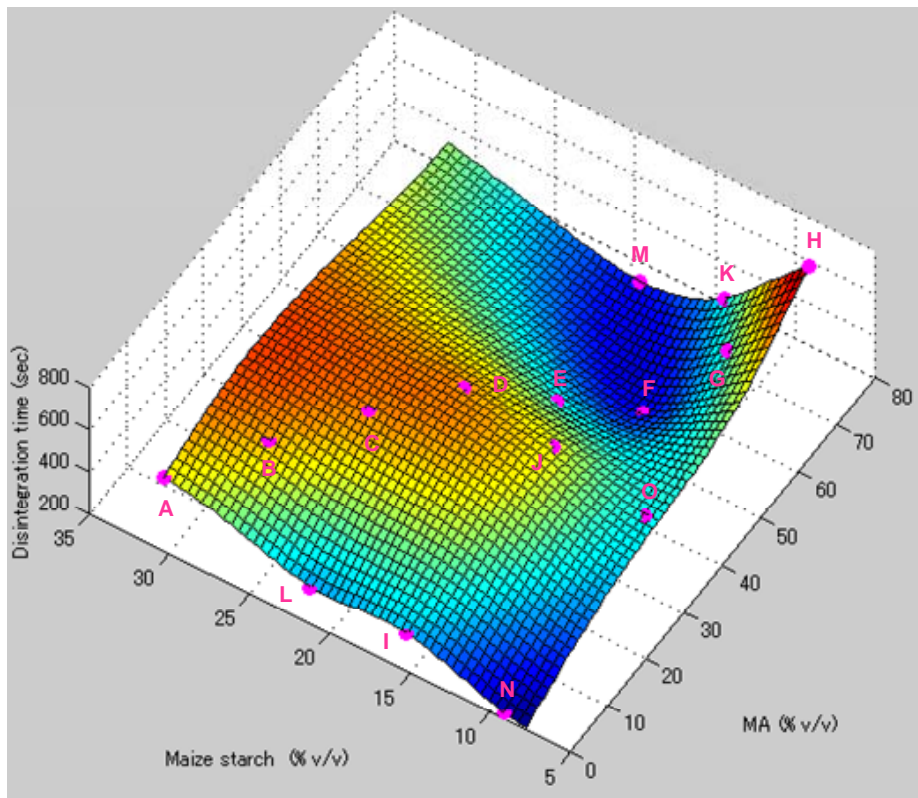


Figure 59a. Response surfaces of disintegration MA tablets compressed at 7 kN as a function of MA (% v/v) and MS (% v/v).

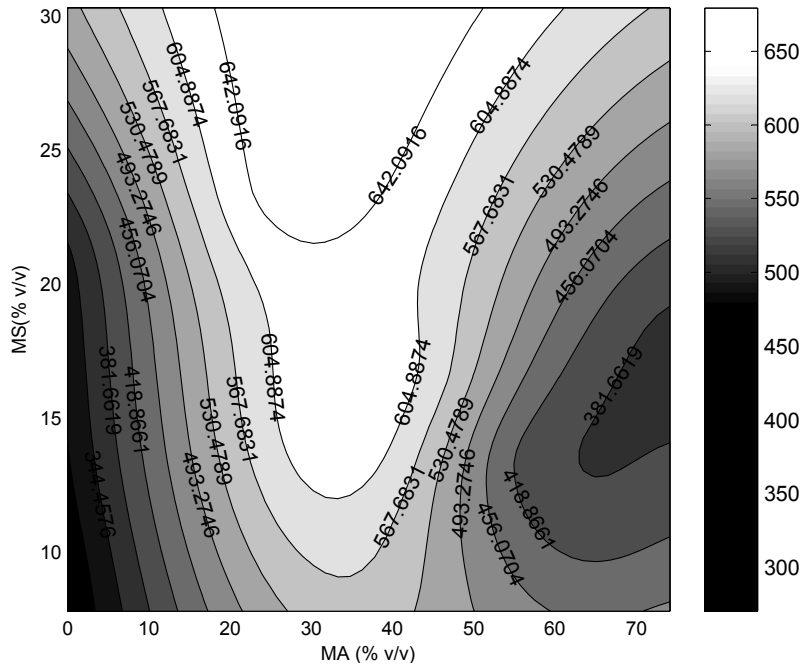


Figure 59b. Response surfaces of disintegration MA tablets compressed at 5 kN as a function of MA (% v/v) and MS (% v/v).

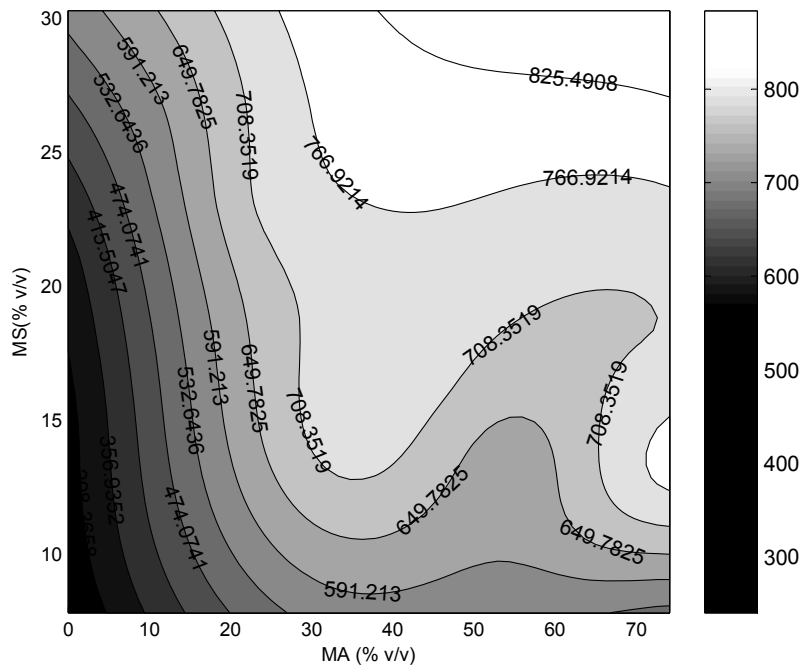


Figure 59c. Response surfaces of disintegration MA tablets compressed at 3 kN as a function of MA (% v/v) and MS (% v/v).

Table 23 Holistic investigation of characteristics of MA tablets

Composition (% v/v)			MS/MA	7 kN			5 kN			3 kN			
MA	LA	MS		Porosity (% v/v) (n=6-7)	TS (N/cm <sup>2</sup> ) (n=6-7)	TDis (sec.) (n=3)	Porosity (% v/v) (n=3)	TS (N/cm <sup>2</sup> ) (n=3)	TDis (sec.) (n=3)	Porosity (% v/v) (n=3)	TS (N/cm <sup>2</sup> ) (n=3)	TDis (sec.) (n=3)	
A	0	69.7	30.3	-	20.6 ± 0.32	103 ± 3.20	550 ± 23	25.4 ± 0.22	58.3 ± 0.16	517 ± 22	31.6 ± 0.03	28.0 ± 0.02	554 ± 28
B	12	61.4	26.6	2.217	18.2 ± 0.21	128 ± 4.64	596 ± 8	24.3 ± 0.28	67.5 ± 2.14	573 ± 23	30.0 ± 0.08	36.3 ± 0.68	593 ± 21
C	23.5	53.4	23.1	0.983	17.0 ± 0.28	133 ± 3.60	616 ± 6	23.0 ± 0.14	70.1 ± 2.12	644 ± 14	28.5 ± 0.28	38.5 ± 0.06	715 ± 71
D	34.5	45.7	19.8	0.574	16.6 ± 0.28	132 ± 3.89	604 ± 21	21.6 ± 0.16	80.4 ± 1.77	627 ± 8	27.4 ± 0.11	43.5 ± 1.26	734 ± 19
E	45.0	38.4	16.6	0.369	16.2 ± 0.20	134 ± 3.35	428 ± 16	21.2 ± 0.07	79.0 ± 1.28	589 ± 25	26.0 ± 0.12	48.4 ± 1.28	728 ± 31
F	55.1	31.3	13.6	0.247	15.8 ± 0.24	143 ± 7.14	266 ± 8	20.5 ± 0.20	88.4 ± 0.86	418 ± 11	25.6 ± 0.28	52.6 ± 2.12	619 ± 21
G	64.8	24.6	10.6	0.164	15.5 ± 0.14	142 ± 4.76	453 ± 24	20.5 ± 0.22	84.8 ± 1.36	403 ± 11	25.5 ± 0.34	52.2 ± 0.83	658 ± 25
H	74.1	18.1	7.8	0.105	16.4 ± 0.37	143 ± 3.52	758 ± 15	20.2 ± 0.05	92.5 ± 0.53	461 ± 15	25.2 ± 0.11	56.9 ± 0.82	518 ± 15
I	0	84.8	15.2	-	20.6 ± 0.16	97.6 ± 2.71	379 ± 7	24.5 ± 0.36	70.2 ± 1.87	312 ± 7	30.5 ± 0.08	34.9 ± 0.78	281 ± 14
J	34.5	51.3	14.2	0.412	17.0 ± 0.26	135 ± 2.10	535 ± 12	21.3 ± 0.10	91.5 ± 1.34	633 ± 23	27.4 ± 0.29	47.7 ± 0.85	737 ± 24
K	74.1	12.9	13.0	0.175	16.3 ± 0.32	129 ± 1.95	413 ± 8	21.2 ± 0.28	83.5 ± 2.70	392 ± 25	27.3 ± 0.10	46.2 ± 2.01	783 ± 15
L	0	78.8	21.2	-	19.7 ± 0.15	118 ± 1.96	373 ± 36	25.1 ± 0.10	69.9 ± 1.76	339 ± 11	30.9 ± 0.09	34.9 ± 1.30	339 ± 54
M	74.0	7.7	18.3	0.247	16.2 ± 0.11	131 ± 2.17	290 ± 2	20.9 ± 0.08	87.2 ± 0.70	373 ± 17	27.2 ± 0.26	43.3 ± 1.88	713 ± 25
N	0	90.9	9.1	-	20.4 ± 0.47	125 ± 4.07	232 ± 20	23.4 ± 0.48	87.4 ± 1.83	276 ± 25	30.0 ± 0.20	41.9 ± 0.09	256 ± 37
O	34.5	57.0	8.5	0.246	17.4 ± 0.29	133 ± 4.58	420 ± 9	21.4 ± 0.09	90.4 ± 1.33	561 ± 17	27.4 ± 0.25	50.4 ± 0.84	589 ± 10

## 6.5 Renormalization technique considerations

The current study is focused on ternary formulation: MA, LA, MS. In order to establish the connectivity to the binary systems, the renormalization leading to a dimension reduction was applied. The renormalization is mainly a technique to map three dimensional data down to two dimensions (Figure 60). Each volumetric percentage of MA and MS were expressed by  $MS/(MS+MA)$  as X axis. It is called as renormalized MS concentration.

Figure 61 shows a plot of disintegration time of MA formulations compressed at 7 kN, 5 kN, and 3 kN with respect to renormalized MS concentration. This dimension reduction is only possible and allowed due to the dominating effect of MA in the formulation for concentrations of  $MA \gg 23.5\%$  (v/v), i.e. for concentrations (see Figure 60), that exceed the percolation threshold of MA ( $p_{cMA}$ ). Thus, in practice it is important and prerequisite to look only at formulations with a high dose of MA, i.e. with an MA load larger than 20% (w/w). It has to be noted that proposed renormalization is independent on the nature of a third component in the mixture. However, it should be applied with limitations. Reducing of third component is possible if the amount of third component's particles is significantly less than of the particles of other components in the mixture. In the present case this is guaranteed by high load of MA. Another limitation is that third component should not have fibrous structure.

It also has to be kept in mind that the evaluation of the Equation 15 according to the percolation theory is only allowed in the vicinity of the percolation threshold [74]. The regions of an initial steep fall and a following sharp rise of a tablet disintegration time are corresponding to the interval of the  $MS/(MS+MA)$  ratio from around 0.1 till 0.3 as shown in Figure 61. This region is followed by the leveling off the disintegration time at a constant value which is not shown in following section of this PhD work [cut off at 0.3].



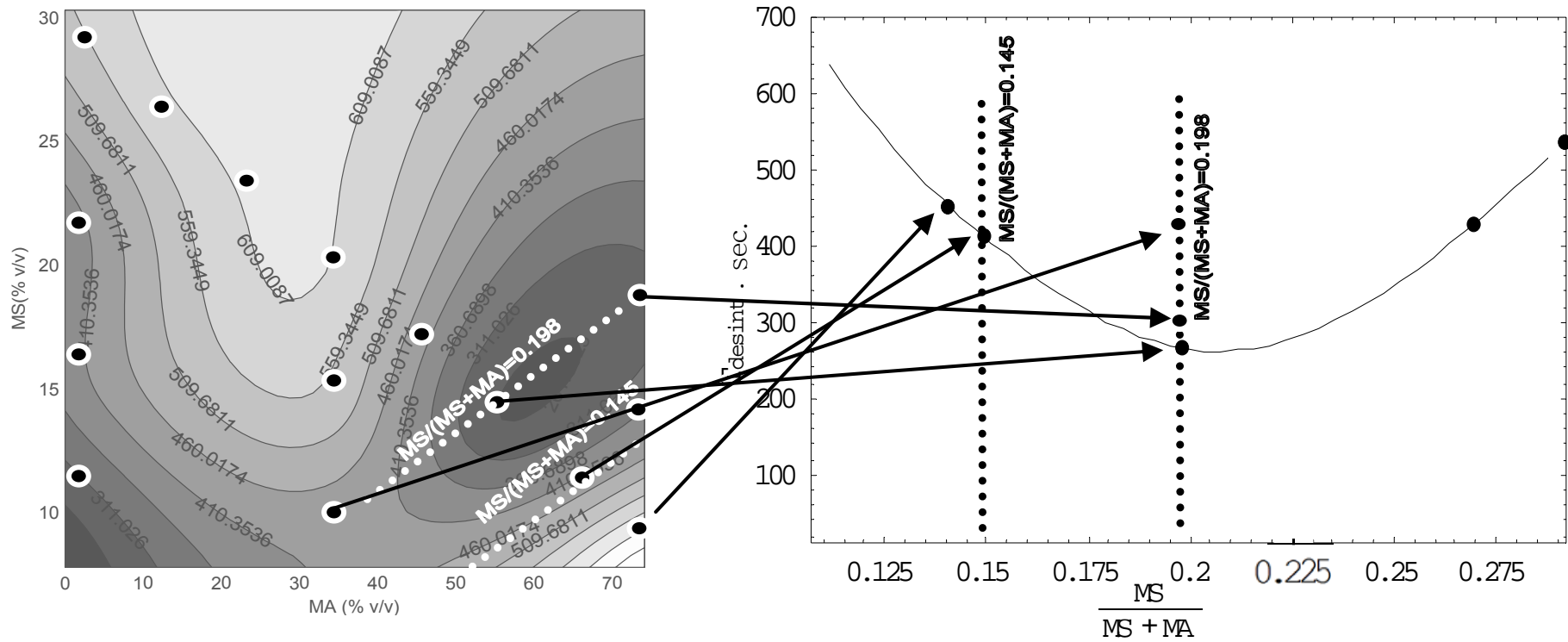


Figure 60. Mapping from three dimensional data down to two dimensions when MA concentrations  $\gg$  23.5 % (v/v) regarding to the disintegration time of MA tablets compressed at 7 kN.

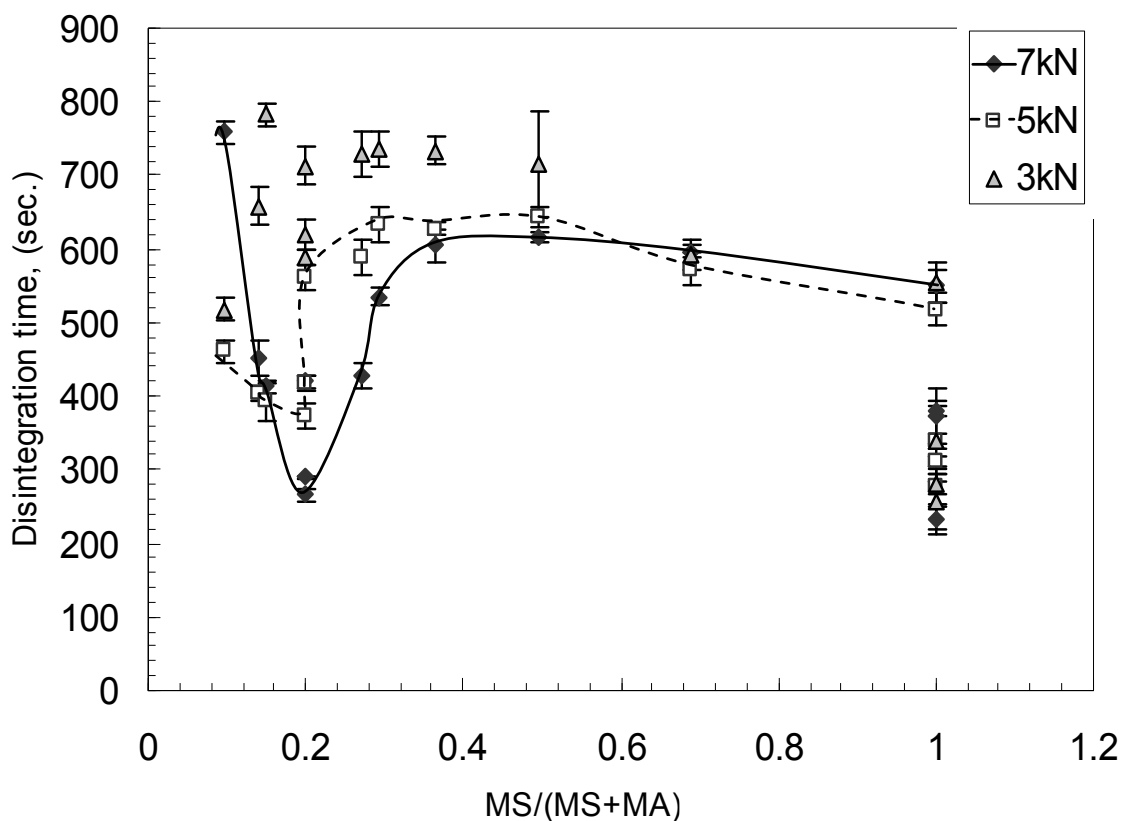


Figure 61. Plot of disintegration time of MA formulations compressed at 7, 5, and 3 kN with respect to renormalized MS concentration.

## 6.6 Critical concentration of MS for MA tablets

The minimum disintegration time of tablets compressed at 7 kN and 5 kN was found for the Tablet O, F and M corresponding respectively to 34.5% v/v, 55.1% v/v and 74.0% v/v of MA was expressed at a renormalized MS concentration;  $MS/(MS+MA) = 0.198$  using only the experimental values (Table 24). In fact, the renormalized MS concentration;  $MS/(MS+MA) = 0.198$  for high dose, i.e. > 20% (w/w) MA tablets corresponds to the critical concentration of MS and represents the percolation threshold of MS. Below and above this percolation threshold of the disintegration time was increasing. The absolute minimum of the disintegration time ( $266 \pm 8$  sec.) was found for MA tablet compressed with the force of 7 kN. This data set exhibits the most distinct percolation event with the sharper minimum of the disintegration time. For this reason this dataset was used for the evaluation of Equation 15.

In Figure 62, the critical concentration of MS was calculated using the spline function with the dataNESIA software. It was leading to a slightly different minimum at 0.206, which was very close to 0.198.

Table 24 Holistic investigation of characteristics of MA tablets for renormalized MS concentrations

Composition (% v/v)			MS/ (MS+MA)	7 kN			5 kN			
MA	LA	MS		Porosity (% v/v) (n=6-7)	TS (N/cm <sup>2</sup> ) (n=6-7)	TDis (sec.) (n=3)	Porosity (% v/v) (n=3)	TS (N/cm <sup>2</sup> ) (n=3)	TDis (sec.) (n=3)	
A	0	69.7	30.3	1	20.6 ± 0.32	103 ± 3.20	550 ± 23	25.4 ± 0.22	58.3 ± 0.16	517 ± 22
B	12	61.4	26.6	0.689	18.2 ± 0.21	128 ± 4.64	596 ± 8	24.3 ± 0.28	67.5 ± 2.14	573 ± 23
C	23.5	53.4	23.1	0.497	17.0 ± 0.28	133 ± 3.60	616 ± 6	23.0 ± 0.14	70.1 ± 2.12	644 ± 14
D	34.5	45.7	19.8	0.365	16.6 ± 0.28	132 ± 3.89	604 ± 21	21.6 ± 0.16	80.4 ± 1.77	627 ± 8
E	45.0	38.4	16.6	0.27	16.2 ± 0.20	134 ± 3.35	428 ± 16	21.2 ± 0.07	79.0 ± 1.28	589 ± 25
F	55.1	31.3	13.6	0.198	15.8 ± 0.24	143 ± 7.14	266 ± 8	20.5 ± 0.20	88.4 ± 0.86	418 ± 11
G	64.8	24.6	10.6	0.141	15.5 ± 0.14	142 ± 4.76	453 ± 24	20.5 ± 0.22	84.8 ± 1.36	403 ± 11
H	74.1	18.1	7.8	0.096	16.4 ± 0.37	143 ± 3.52	758 ± 15	20.2 ± 0.05	92.5 ± 0.53	461 ± 15
I	0	84.8	15.2	1	20.6 ± 0.16	97.6 ± 2.71	379 ± 7	24.5 ± 0.36	70.2 ± 1.87	312 ± 7
J	34.5	51.3	14.2	0.292	17.0 ± 0.26	135 ± 2.10	535 ± 12	21.3 ± 0.10	91.5 ± 1.34	633 ± 23
K	74.1	12.9	13.0	0.15	16.3 ± 0.32	129 ± 1.95	413 ± 8	21.2 ± 0.28	83.5 ± 2.70	392 ± 25
L	0	78.8	21.2	1	19.7 ± 0.15	118 ± 1.96	373 ± 36	25.1 ± 0.10	69.9 ± 1.76	339 ± 11
M	74.0	7.7	18.3	0.198	16.2 ± 0.11	131 ± 2.17	290 ± 2	20.9 ± 0.08	87.2 ± 0.70	373 ± 17
N	0	90.9	9.1	1	20.4 ± 0.47	125 ± 4.07	232 ± 20	23.4 ± 0.48	87.4 ± 1.83	276 ± 25
O	34.5	57.0	8.5	0.198	17.4 ± 0.29	133 ± 4.58	420 ± 9	21.4 ± 0.09	90.4 ± 1.33	561 ± 17

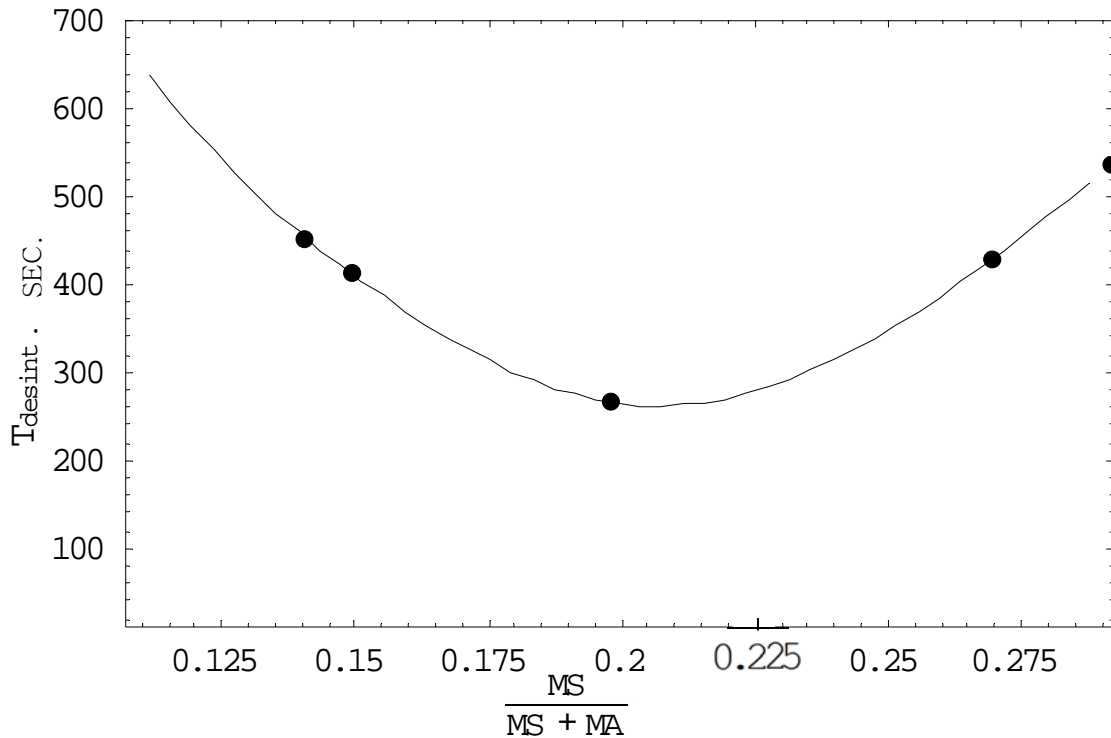


Figure 62. Experimentally obtained results (•) showing critical concentration of MS at 0.198 and spline (dataNESIA/DesignNESIA) approximated data (—) at 0.206 for renormalized MS concentrations regarding to the disintegration time of MA tablets compressed at 7 kN.

### 6.7 Critical volume fraction of MS for MA tablets

The percolation threshold of MS described by renormalized MS concentration; MS/(MS+MA) applying the renormalization technique was always equal 0.198 for 34.5 (% v/v), 55.1 (% v/v) and 74.1 (% v/v) MA tablet compressed at 7 kN and 5 kN. The critical volume fraction of MS ( $\phi_{c,MS}$ ) for 34.5 (% v/v), 55.1 (% v/v) and 74.1 (% v/v) MA tablets compressed at 7 kN and 5 kN was within the range of 0.156-0.167 (v/v). It was calculated by Equation 30 from the basis of Equation 8 and compiled in Table 25 and 26.

$$\phi_{c,MS} = 0.198 \times \{1 - (\text{Porosity of MA tablet})\} \quad \text{Equation (30)}$$

In fact, Equation 30 corresponds to the case II of Equation 14 described below because the ratio of the radius of MS/MA ( $r/R$ ) is  $3.81 > 0.732$ . According to the percolation theory, a minimum disintegration time corresponds to the formation of a continuous water-conducting cluster through the entire tablet. In case II, porosity and disintegrant represent two independent water diffusion network. There are two possibilities for water to diffuse through the entire MA tablets: through a percolating cluster of pores or through an infinite cluster of

MS. However the dominant network that the water can diffuse for the disintegration of MA tablet is considered through the disintegrant network, not through the porous network according to the results of section 6.4. This situation that the particle size of inactive ingredient is bigger than that of API should be necessary for low water soluble drugs because they are normally milled in order to reduce the particle size and increase the dissolution rate. It is concluded that case II of Equation 14 is available not only for the binary tablets but also for the truly ternary pharmaceutical tablet formulation. Moreover the random close packed (RCP) system is also the best model for the pharmaceutical tablet formulation in case of spherical particles regardless the compressed particles are or powder or granules.

$$X_{dis} = \frac{\phi_{c,dis}}{1-\varepsilon}; \quad \text{if } \frac{r}{R} > \sqrt{3}-1 \quad (\text{Case II}) \quad \text{Equation (14)}$$

where  $X_{dis}$  is the critical concentration of disintegrant in powder mixture (v/v),  $\phi_{c,dis}$  is  $0.16 \pm 0.01$  (v/v) and  $\varepsilon$  is the tablet porosity (v/v).

Regarding to Tablet O, the dominant components in terms of volumetric percentage in the tablet is LA, not MA. The case I of Equation 14 has to be taken into account for calculating the critical concentration of MS because the ratio of the radius of MS/LA ( $r/R$ ) is  $0.635 \leq 0.732$  which means the MS particles might be caged by LA. However the critical concentration of MS can be calculated by the case II of Equation 11. It might be considered that the ratio of the radius of MS/LA ( $r/R$ ) being 0.635 is close to 0.732. The particle size of filler and disintegrant should be close to each other for the robust tablet formulation design.

Table 25 Critical volume fraction of MS ( $\phi_{c,MS}$ ) for MA tablets compressed at 7 kN

	Composition (% v/v)			MS/(MS+MA)	Porosity (% v/v)	Disintegration time (sec.)	$\phi_{c,MS}$ (v/v)
	MA	LA	MS				
F	55.1	31.3	13.6	0.198	15.8	266	0.167
M	74.0	7.7	18.3	0.198	16.2	290	0.166
O	34.5	57.0	8.5	0.198	17.4	420	0.164

Table 26 Critical volume fraction of MS ( $\phi_{c,MS}$ ) for MA tablets compressed at 5 kN

	Composition (% v/v)			MS/(MS+MA)	Porosity (% v/v)	Disintegration time (sec.)	$\phi_{c,MS}$ (v/v)
	MA	LA	MS				
F	55.1	31.3	13.6	0.198	20.5	418	0.157
M	74.0	7.7	18.3	0.198	20.9	373	0.157
O	34.5	57.0	8.5	0.198	21.4	561	0.156

### 6.8 Critical concentration of MS for 0% v/v MA tablets

Tablet A, I, L and N were consisted of LA and MS without MA. Critical concentration of MS in these tablets compressed at 7 kN and 5 kN were calculated respectively in Table 27 and 28 according to the case I of Equation 14 because the radius of MS/LA ( $r/R$ ) is  $0.635 \leq 0.732$ .

$$X_{dis} = \left( \frac{\phi_c}{1 - \varepsilon} \right) - \varepsilon; \quad \text{if } \frac{r}{R} \leq \sqrt{3} - 1 \quad (\text{Case I}) \quad \text{Equation (14)}$$

where  $X_{dis}$  is the critical concentration of disintegrant in powder mixture (v/v),  $\phi_c$  is  $0.16 \pm 0.01$  (v/v) and  $\varepsilon$  is the tablet porosity (v/v).

Calculated critical concentration of MS for Tablet A, I, L and N compressed at 7 kN and 5 kN was about 1% v/v (Table 27) and 0% v/v (Table 28). For this reason, the minimum disintegration time was found in a Tablet N which contained the lowest volume of MS in a tablet. However it is still unclear the effect of porosity of tablet on the critical concentration of MS when the porosity of tablet is more than 16% v/v for case I as this study. It is suggested that the porosity of tablet for case I should be much below 16% v/v from its hardness and robustness point of view because the porosity of tablet can be easily changed by tableting condition for example.

Table 27 Critical concentration of MS in 0% v/v MA tablets compressed at 7 kN

	Composition (% v/v)			Porosity (% v/v)	Disintegration time (sec.)	$X_{dis}$ (% v/v)
	MA	LA	MS			
A	0	69.7	30.3	20.6	550	0% - 0.81%
I	0	84.8	15.2	20.6	379	0% - 0.81%
L	0	78.8	21.2	19.7	373	0% - 1.47%
N	0	90.9	8.5	20.4	232	0% - 0.96%

Table 28 Critical concentration of MS in 0% v/v MA tablets compressed at 5 kN

	Composition (% v/v)			Porosity (% v/v)	Disintegration time (sec.)	$X_{dis}$ (% v/v)
	MA	LA	MS			
A	0	69.7	30.3	25.4	517	0%
I	0	84.8	15.2	24.5	312	0%
L	0	78.8	21.2	25.1	339	0%
N	0	90.9	8.5	23.4	276	0%

## 6.9 Comparison of critical volume fraction for MA tablets and Caffeine tablets

For a close comparison with the results obtained in case of the MA tablets, we take into account so far unpublished results of the thesis of Luginbuehl [10].

Luginbuehl studied in his thesis the binary system of caffeine (anhydrous) - StaRX1500<sup>®</sup> at different size fractions. The binary mixtures were directly compressed by using the universal material tester Zwick 1478 (Zwick GmbH & Co). The exact procedure for the tableting process is described in the reference Luginbuehl and Leuenberger [10], where caffeine (anh.) granulate with an average particle size of 727  $\mu\text{m}$  was compressed with StaRX1500<sup>®</sup> (average particle size of 76  $\mu\text{m}$ ). In this case, a critical concentration of StaRX1500<sup>®</sup> was found and interpreted as a percolation threshold  $p_c = 0.071$  (v/v). On the other hand, the caffeine (anh.) granulate with an average particle size of 47  $\mu\text{m}$  was compressed with StaRX1500<sup>®</sup> (average particle size of 76  $\mu\text{m}$ ). In this case, a critical concentration of StaRX1500<sup>®</sup> was found and interpreted as a percolation threshold  $p_c = 0.194$  (v/v). Critical volume fraction ( $\phi_c$ ) was calculated by Equation 14 and compiled in Table 29. Critical volume fractions ( $\phi_c$ ) for both cases were also within the range of  $0.16 \pm 0.01$  (v/v).

Table 29 Critical volume fraction depending on the case

Average particle size ( $\mu\text{m}$ )		Case (r/R)	Critical concentration of StaRX1500 <sup>®</sup> (v/v)	Porosity (% v/v)	$\phi_c$ (v/v)
StaRX1500 <sup>®</sup>	Caffeine (anh.)				
76	727	I (0.10)	0.071	$12 \pm 0.2$	0.168
76	47	II (1.62)	0.194	$12 \pm 0.2$	0.170

The following data [10] refer to a caffeine (anh.) powder with the average particle size of 47  $\mu\text{m}$  which was compressed together with StaRX1500<sup>®</sup> having the average particle size of 76  $\mu\text{m}$  (case II). The present investigation was done in the range ca. 0.1-0.4 volume of StaRX1500<sup>®</sup> in the vicinity of a percolation threshold. In Figure 63, the critical concentration of StaRX1500<sup>®</sup> was calculated using the spline function with the dataNESIA software. It was leading to very close to 0.195 (v/v). It is important to mention here that the solubility of API does not affect the location of critical concentration of non-fibrous disintegrant.

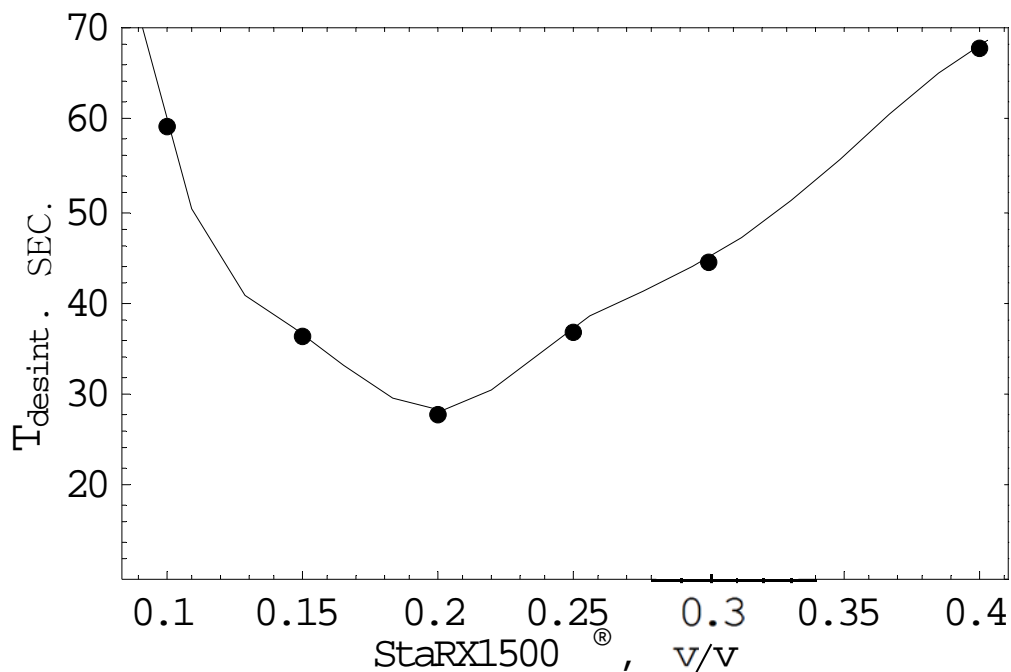


Figure 63. Experimentally obtained results (•) showing critical concentration of StaRX1500<sup>®</sup> at 0.194 (v/v) and spline (dataNESIA/DesignNESIA) approximated data (—) at 0.195 (v/v) regarding to the disintegration time of caffeine tablets for case II.

### 6.10 Critical exponent for disintegration behavior

In this study the percolation thresholds  $p_c$  describe the location of the minimum value of the disintegration time. These  $p_c$ -values were kept constant for the further evaluation of Equation 15. For the determination of the critical exponent  $q$  of Equation 15, a non-linear curve fitting method was applied by using the Levenberg-Marquardt [124] algorithm for both spline approximated and raw datasets of MA tablets compressed at 7 kN (Figure 64) and caffeine tablets (Figure 65) for case II (critical exponent of caffeine tablets for disintegration behavior in case I was reported as  $0.30 \pm 0.05$  [10]). Equation 15 includes the percolation threshold  $p_c$  as an important parameter describing the microstructure and critical concentration of the disintegrant. The second parameter is the critical exponent  $q$  which depends, in general, on the system property related to the probability ( $p$ ) of cluster [71], in other word on nature of the (disintegration) process [97]. Critical exponent for binary (caffeine tablets) and multicomponent tablets (MA tablets) with non-fibrous types of disintegrant (StaRX1500<sup>®</sup> and MS) are 0.30 and 0.28 very close to each other (average values are:  $q = 0.28 \pm 0.06$ , see Table 30).



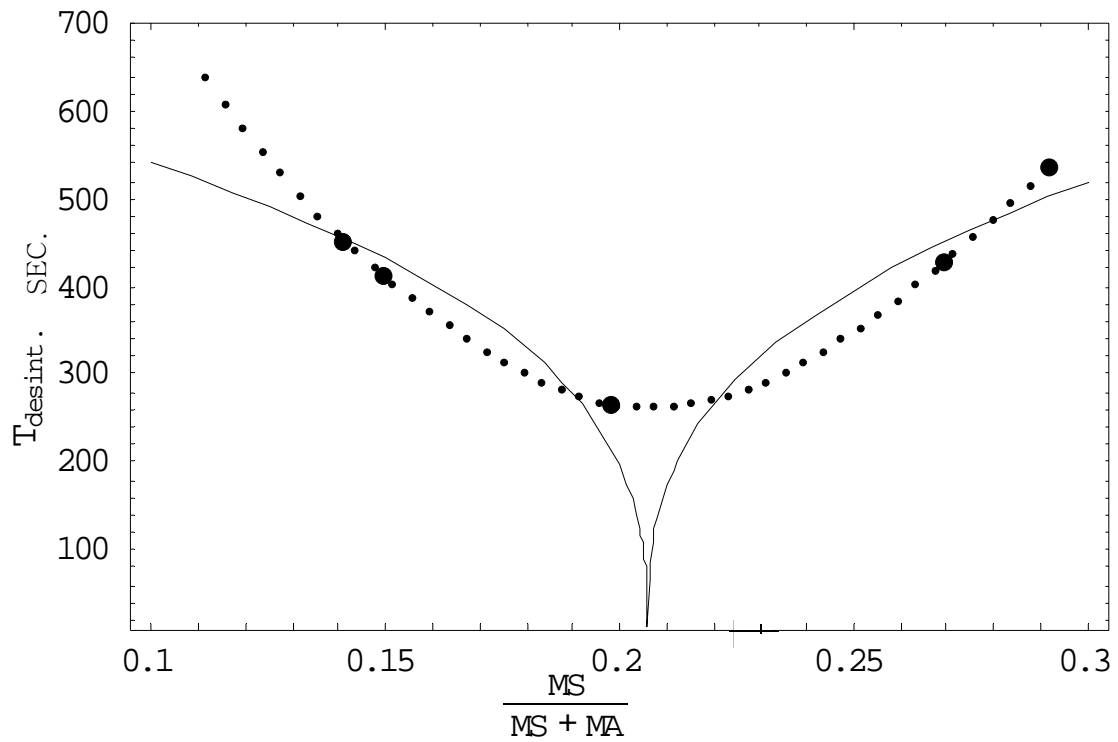


Figure 64. Results of fitting Equation 15 for MA tablets compressed at 7 kN; figure shows fitting (—) with spline approximated data (dotted line) and raw experimental data (•).

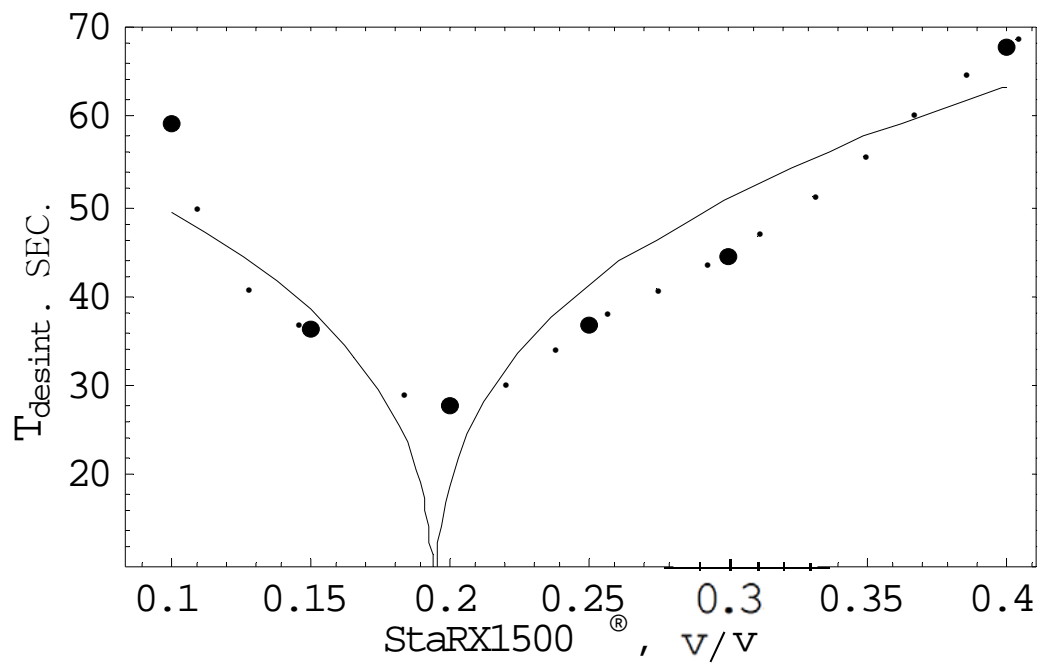


Figure 65. Results of fitting Equation 15 for caffeine tablets for case II, fitting (—) with spline approximated data (dotted line) and raw experimental data (•).

Table 30 Critical exponent and goodness of fit

Data type	q	r <sup>2</sup>
MA 7kN raw data	0.28	0.91
MA 7kN spline approximated data	0.35	0.77
MA 5kN raw data	0.23	0.92
MA 5kN spline approximated data	0.19	0.84
Caffeine raw data	0.30	0.78
Caffeine spline approximated data	0.33	0.79
Average values ± standard deviation	0.28 ± 0.06	0.84

The behavior of the disintegration time in the neighbourhood of the percolation threshold can be mathematically explained with the basic equation of the percolation theory (Equation 15) yielding a critical exponent  $q$  was equal to  $0.28 \pm 0.06$  (The quality of fit:  $r^2 = 0.84$ ). Please note that with one exception, the quality of fit, i.e. the  $r^2$  values are significantly better in case of using the raw data and not the approximated (smoothened) data achieved with the dataNESIA method. The average value in Table 30 is close to 0.3, has the same magnitude as  $\beta$  (see Table 10), but is different from 0.4. In the context of the publication of Luginbuehl and Leuenberger [9] the critical exponent indicates that the presence and the strength of infinite cluster for its concentration above the percolation threshold plays a role. It is suggested that the disintegration behavior is related to the strength of disintegrant cluster [9, 71]. Disintegration time decreases with increasing the disintegrant volumetric percentage (% v/v) of the mixture until percolation threshold. After this percolation threshold of disintegrant, disintegration time increases again with increasing disintegrant volumetric percentage. The excess of disintegrant particles in fact makes disintegration time slower due to the swelling of the excess amount of disintegrant, which slows down the entrance of water by the diffusion process. Thus the critical exponent of disintegration behavior is considered lower than 0.4 [9].

## 6.11 Computing the disintegration time of MA tablet by F-CAD

There are mainly two software to simulate the dissolution profile either F-CAD (algorithm is cellular automata) or DDDPlus™ from Simulation Plus, Inc. (algorithm is mathematical modeling) [125]. DDDPlus™ is commercially available for the pharmaceutical industry. However, so far, there does not exist a specific software to simulate the disintegration time of a solid dosage form as a function of its formulation. In this work, Dissolution simulation (DS) module, which is the one of F-CAD is used to get an estimate of the disintegration time of a MA tablet. It is assumed that the “time elapsed” till water is detected at the geometric center of the virtual tablet is proportional to the disintegration time. The “time elapsed” happens before the disintegration of the tablet is completed. It has to be kept in mind that F-CAD's core module being based on the cellular automata is following a "first principle" approach (see Figure 7) [62, 94, 96, 100].

### 6.11.1 Particle Arrangement and Compaction (PAC) operation

According to Table 11, the mean diameter of MA, LA and MS was 6.57, 39.4, 25.0  $\mu\text{m}$ , respectively. LA and MS particles are six times and four times bigger than MA. Thus the growth function was used for arranging the LA and MS particles into the tablet created by TD module until LA and MS were grown to ca. 550  $\mu\text{m}$  and 350  $\mu\text{m}$  respectively, because the distributed MA particle size was 96.15  $\mu\text{m}$ /cube side. In order to simulate LA granules were arranged into the virtual tablet, LA was once removed and grown again to follow the ‘Swiss cheese’ procedure [100]. Because it is assumed that granulated particle should be grown at limited location in a tablet as competed with direct compressive tablet of powder mixture.

According to the appearance of granules by SEM in Figure 50b, 50c and 50d, it was observed that MA and MS particles were granulated around LA particles. Thus MA and MS particles were removed and distributed again after LA was grown in order to simulate granules observed by SEM.

### 6.11.2 Comparison of experimental and F-CAD computed disintegration time of MA tablets

Comparison of experimental disintegration time of tablets compressed at 7 kN and computed specific time point for water to reach the geometric center of the tablet by F-CAD software has been carried out. Experimental disintegration time and computed specific time point for water to reach the geometric center of the virtual tablet are shown in Table 31 and Figure 66. If all data in Figure 67 (including Tablet K and M) are submitted to a linear regression analysis, no correlation can be found ( $r^2 = 0.0154$ ). However, if the Tablets K and M are not taken into consideration, ca. 66% ( $r^2 = 0.6564$ ) of the data can be explained with a

linear regression, yielding a correlation coefficient of  $r = 0.81$  (Figure 68), however this is much less than expected from the excellent results of F-CAD to simulate the dissolution profile of many different formulations [12, 94, 96, 100]. The reason that it was difficult to compute the disintegration time of Tablet K and M by F-CAD might be related to the fact that the loading volume of MS was higher than that of LA (see Table 31). In other word, MS particles were nice to be grown instead of LA. According to the percolation theory, a minimum disintegration time corresponds to the formation of a continuous water-conducting cluster through the entire tablet. When the MS particle was grown for Tablet M instead of LA, the disintegration time of Tablet M by F-CAD was  $116 \pm 9$  (n=6) sec., which was much closer to the experimental disintegration time. The way of disintegrant particle arrangement in the virtual tablet has to be taken into account in order to compute the disintegration time of tablet by F-CAD if the disintegrant was granulated as a tableting granules as a further investigation.

Table 31 Experimental disintegration time of tablets compressed at 7 kN and computed specific time point for water to reach the geometric center of the tablet by using F-CAD

	Composition (% v/v)			MS/(MS+MA)	Disintegration time (sec.)	
	MA	LA	MS		Experimental data (n=3)	F-CAD data (n=6)
B	12.0	61.4	26.6	0.698	$596 \pm 8$	$338 \pm 10$
C	23.5	53.4	23.1	0.497	$616 \pm 6$	$408 \pm 7$
D	34.5	45.7	19.8	0.365	$604 \pm 21$	$448 \pm 14$
E	45.0	38.4	16.6	0.27	$428 \pm 16$	$395 \pm 14$
F	55.1	31.3	13.6	0.198	$266 \pm 8$	$191 \pm 13$
G	64.8	24.6	10.6	0.141	$453 \pm 24$	$432 \pm 19$
H	74.1	18.1	7.8	0.096	$758 \pm 15$	$785 \pm 24$
J	34.5	51.3	14.2	0.292	$535 \pm 12$	$382 \pm 10$
K	74.1	12.9	13.0	0.15	$413 \pm 8$	$596 \pm 9$
M	74.0	7.7	18.3	0.198	$290 \pm 2$	$897 \pm 8$
O	34.5	57.0	8.5	0.198	$420 \pm 9$	$350 \pm 13$

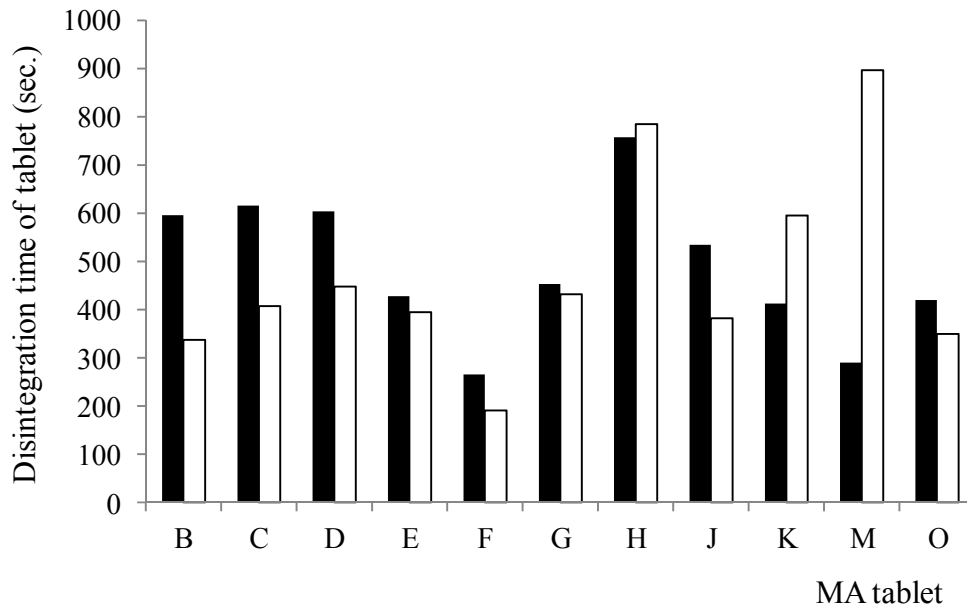


Figure 66. Comparison of experimental disintegration time of tablets compressed at 7 kN (black bar) and computed specific time point for water to reach the geometric center of the tablet by F-CAD (white bar).

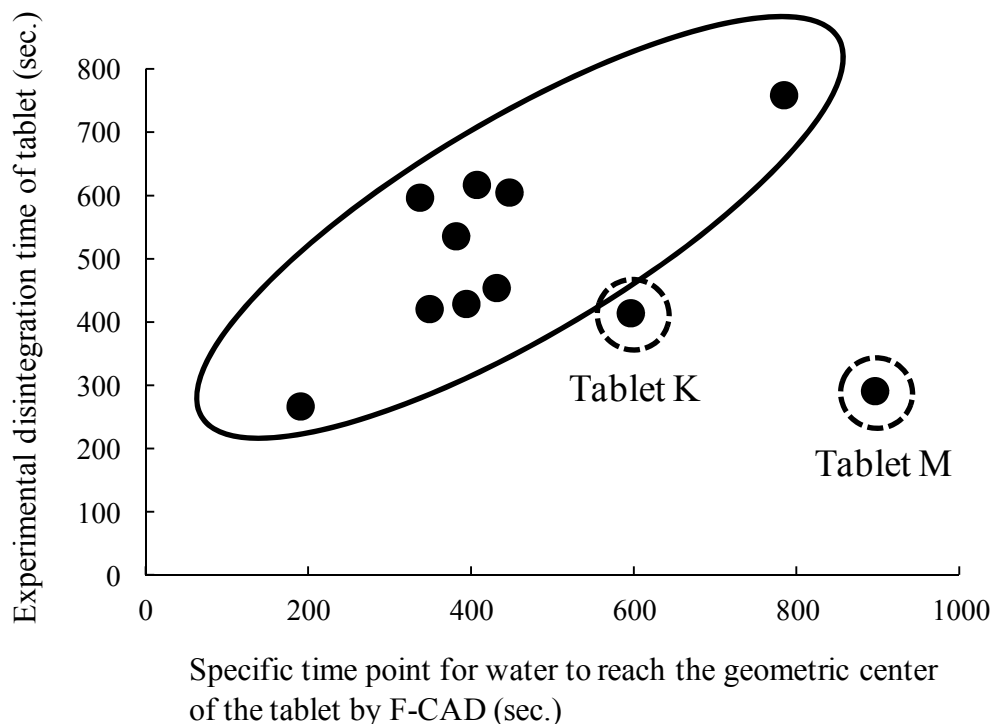


Figure 67. The relationship of the experimental disintegration times and F-CAD computed specific time points for water to reach the geometric center of the virtual tablet. Please note that no significant linear regression can be calculated, if the results of Tablet K and M are included ( $r^2 = 0.0154$ ).

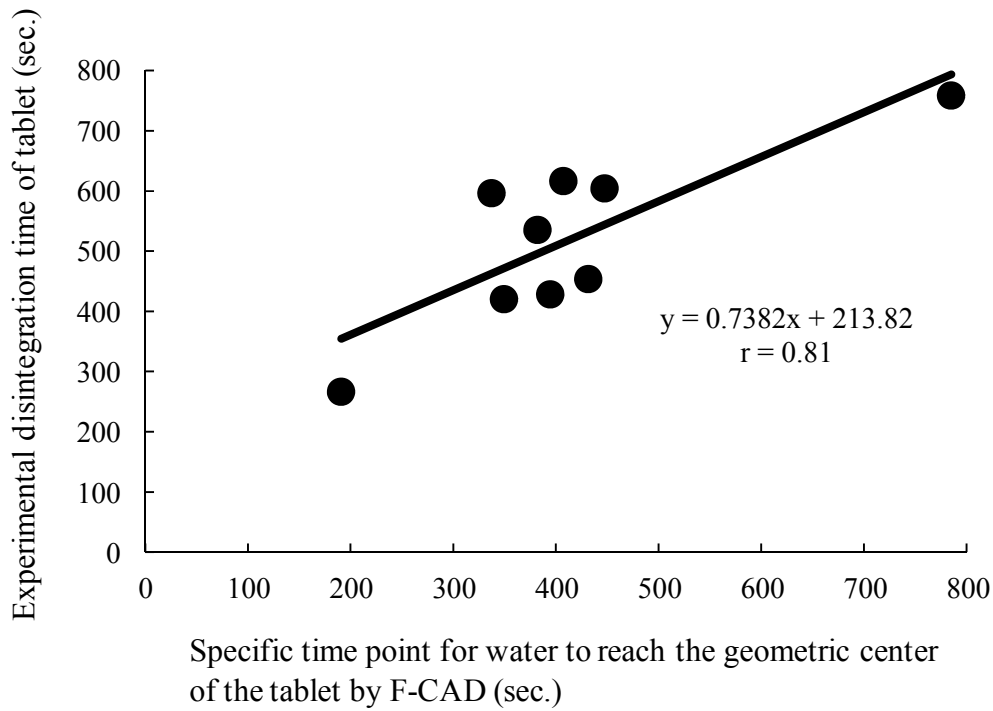


Figure 68. The relationship of the experimental disintegration time and F-CAD computed specific time point for water to reach the geometric center of the virtual tablet in case, that Tablet K and M were excluded ( $r^2 = 0.66$ ,  $r = 0.81$ ).

### 6.11.3 Response surfaces close to the percolation threshold of sensitive tablet properties such as the disintegration time

Figure 69 shows the typical behavior for a percolation effect. The percolation threshold of MS expressed by renormalized MS concentration with respect to the minimum F-CAD disintegration time was observed at 0.198.

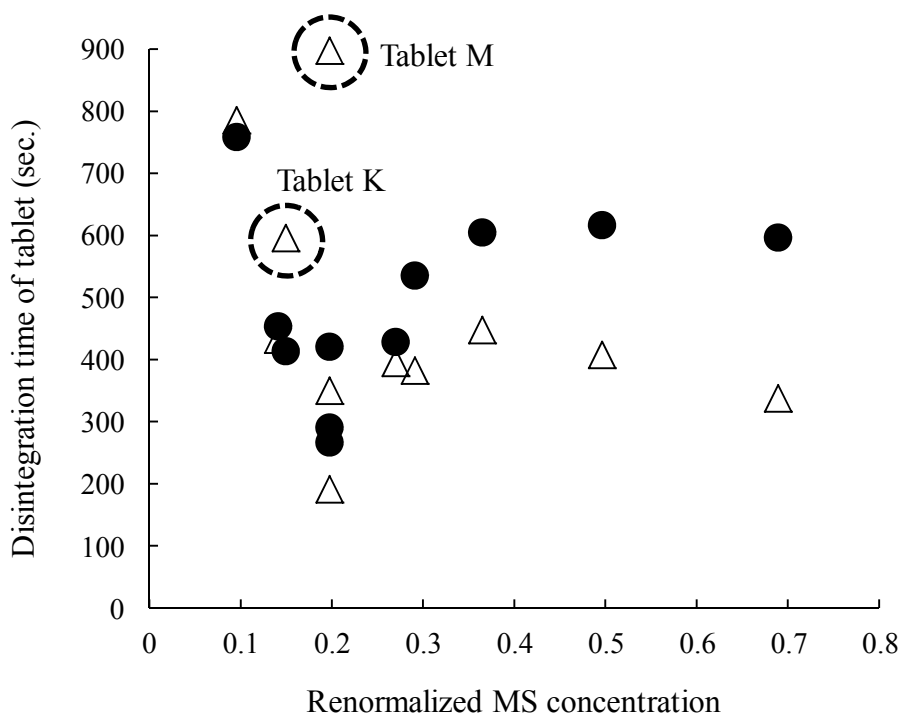


Figure 69. Experimental disintegration time (●) and F-CAD values (△) as a function of the renormalized MS concentration. Please note that the Tablets: E, F, G, J, K, M, and O show close to the percolation threshold of MS, a similar behavior for the values of the experimental disintegration time and for the F-CAD calculated values.

It is important to realize that F-CAD is capable of detecting this percolation threshold (Figure 69). Due to the fact, that F-CAD can be applied without performing any laboratory experiment, it has been decided to explore with F-CAD the behavior of the F-CAD calculated disintegration time in the very close neighborhood of the percolation threshold. Such an exploration is difficult and cost intensive to perform in a laboratory but can be done without major problems in-silico. For this reason, two additional in-silico experiments followed by the central composite design (CCD) with two factors, i.e. MS (% v/v) and the ratio of LA/MA corresponding to the ratio of hydrophilic excipient/hydrophobic drug substance, have been performed, which are described below in Table 32 and 33. The response surfaces (Figure 70

and 71) were described by a software of Design-Expert 7<sup>®</sup>. Interestingly, the percolation effect of disintegration time of tablet computed by F-CAD was clearly observed (Figure 70) near the Trial No. 1 in Table 32 (= Tablet F, see Table 31) which had the absolute minimum disintegration time by experimental results. On the other hand, the percolation effect was not observed near the Trial No. 14 in Table 33 (= Tablet M, see Table 31) where is the high loading volume of MA, more than 64.8% v/v as shown in Figure 71.

Table 32 First additional in-silico experiments (CCD 1) computed the specific time point for water to reach the geometric center of the tablet by using F-CAD

Trial No.	Composition (% v/v)			LA/MA	MS/(MS+MA)	Disintegration time (sec.) F-CAD data (n=4)
	MA	LA	MS			
1	55.1	31.3	13.6	0.568	0.198	199 ± 20
2	45.0	44.4	10.6	0.987	0.191	290 ± 7
3	64.8	24.6	10.6	0.380	0.141	438 ± 10
4	64.8	18.6	16.6	0.287	0.204	1126 ± 14
5	45.0	38.4	16.6	0.853	0.269	395 ± 9
6	45.0	41.4	13.6	0.420	0.232	374 ± 9
7	64.8	21.6	13.6	0.333	0.173	574 ± 24
8	55.1	34.3	10.6	0.623	0.161	422 ± 13
9	55.1	28.3	16.6	0.514	0.232	467 ± 16

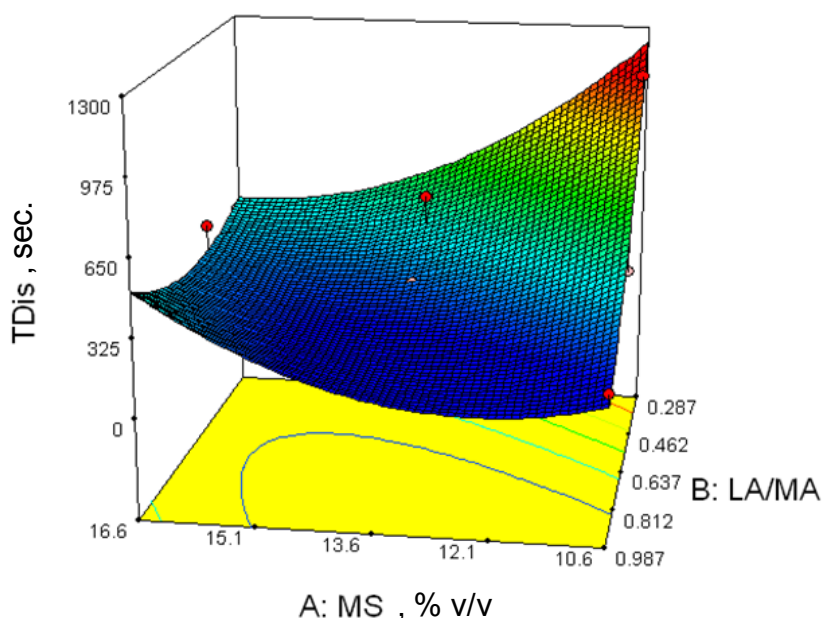


Figure 70. Response surface of the computed F-CAD disintegration time (TDis, sec.) from the first additional in-silico experiments (CCD 1, Table 32).



Table 33 Second additional in-silico experiments (CCD 2) computed the specific time point for water to reach the geometric center of the tablet by using F-CAD

Trial No.	Composition (% v/v)			LA/MA	MS/(MS+MA)	Disintegration time (sec.) F-CAD data (n=4)
	MA	LA	MS			
10	72.4	12.3	15.3	0.170	0.174	668 ± 21
11	79.4	8.3	12.3	0.104	0.134	1070 ± 21
12	70.7	17.0	12.3	0.240	0.148	1103 ± 70
13	65.9	15.8	18.3	0.240	0.217	1232 ± 20
14	74.0	7.7	18.3	0.104	0.198	896 ± 22
15	76.7	8.0	15.3	0.104	0.166	1133 ± 23
16	68.3	16.4	15.3	0.240	0.183	1143 ± 31
17	75.0	12.7	12.3	0.170	0.141	777 ± 16
18	69.8	11.9	18.3	0.170	0.208	1726 ± 46

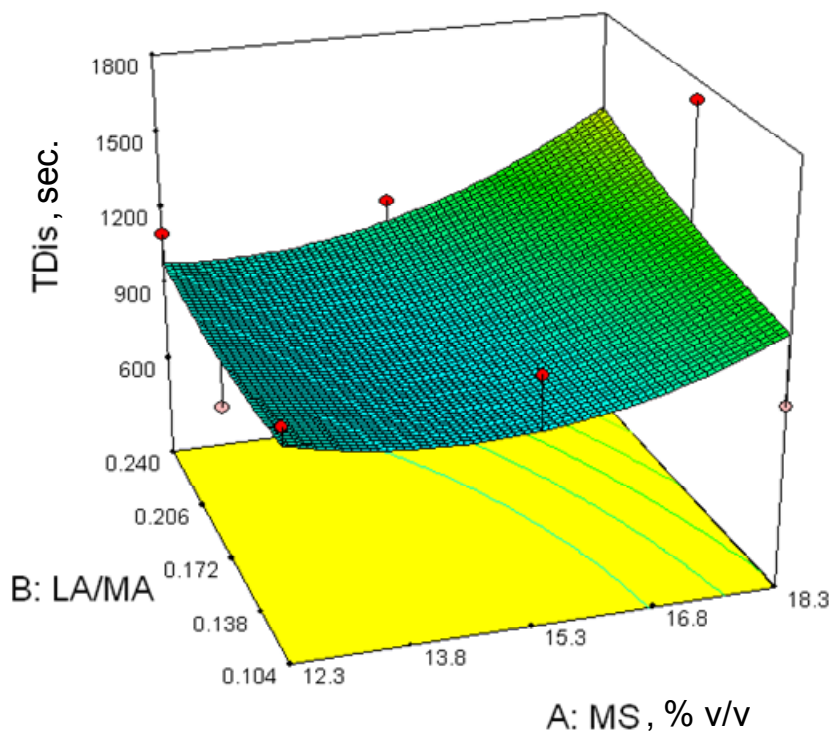


Figure 71. Response surface of the computed F-CAD disintegration time (TDis, sec.) from the second additional in-silico experiments (CCD 2, Table 33).

The need to eliminate Tablet M and Tablet K results show clearly that there is a necessity for further investigations and for an improvement of the method to calculate the F-CAD disintegration time. In fact, it has to be questioned, whether the F-CAD disintegration time is the right surrogate to simulate the experimental disintegration time. The very rigorous PhD study of Luginbuehl [10] with the main scientific findings published in 1994 [9] show as results the behavior of the water uptake constant  $K$ . The disintegration time  $t_{dis}$  and the intrinsic dissolution rate of the active substance close to the percolation threshold. Interestingly, neither the percolation thresholds  $p_{ci}$  nor the corresponding critical exponents  $q_i$  were identical for the three different properties  $i$  of the tablet. However, it can be noted that the parameters  $p_{ci}$  and  $q_i$  are different, but close to each other. It may be possible that the F-CAD disintegration time, which simulates the “time elapsed” till the water molecules reach the center of the tablet, should be better compared with the “water uptake” constant  $K$  as described in the study of Luginbuehl [9]. However, as already stated in the study of Luginbuehl [9] one cannot expect to find identical percolation thresholds and in addition especially not identical critical exponents for different properties of the compact. F-CAD software is the only software so far, which is capable of computing the disintegration time of tablets. The software has a great potential to be further improved and to be not only used for the safe prediction of the dissolution profile of a tablet formulation but also for a safe prediction of the disintegration time. However, it has to be kept in mind that such an application of F-CAD is only possible, if there is the awareness, that for a safe exploration of the design space according to ICH Q8 it is a prerequisite to take into account the effect of percolation theory. This means in practice that the exploration of the design space needs to be done with the appropriate resolution, i.e. the “mesh size” of the lattice points to be investigated in the design space needs to be fine enough. In addition close to the percolation threshold, it is necessary to apply the basic equation of the percolation theory, i.e. the power law, with the parameters  $p_c$  and  $q$ , (percolation threshold and critical exponent). It is not sufficient to use a simple  $2^n$  design or a central composite design as both type of designs yield as a “summarizing equation” by a first or second orders approximation of the reality. Thus, “Dangerous canyon” close to the percolation threshold leading to a high variability of a sensitive tablet property may not be detected by only response surface methodologies. The difference in the resolution of the exploration of the design space becomes visible by comparing Figure 70 and Figure 71. Both response surfaces are the result of a CCD (central composite design) with different a “mesh size” of the lattice points in the design space explored. The minimum in Figure 70 is more prominent than in Figure 71.

It is evident that such a design space exploration with classical laboratory experiments is extremely difficult to realize and would be extremely expensive. In this respect, the

application of F-CAD opens a new research avenue, i.e. a “new kind of science” in the language of Stephan Wolfram (Princeton University) [103].

The results of this thesis show that the application of percolation theory is a must in order to detect percolation thresholds. It is important to know the response surfaces close to the percolation threshold of sensitive tablet properties such as the disintegration time to get information about the robustness of the selected formulation. In this context one has to put the question forward if the application of percolation theory and the use of F-CAD to detect the percolation thresholds should be an integral part of the guidelines of ICH Q8 exploring the formulation design space.

## 7 Conclusions

The present study shows among others that the application of percolation theory is not limited to typical and formal binary tablet formulations. The critical concentration of maize starch (MS) for the truly ternary pharmaceutical mefenamic acid (MA) tablet formulations, has been described by the renormalized MS concentration;  $MS/(MS+MA)$  applying the renormalization technique. The following result is obtained for the critical concentration in terms of the renormalized dimensionless concentration: 0.198.

In case dataNESIA software is applied, there is the advantage that the data of a response surface analysis can be smoothed by interpolation of the measured data with a spline function. It leads to a minimum disintegration time at 0.206, which is very close to 0.198.

According to the percolation theory, a minimum disintegration time corresponds to the formation of a continuous water-conducting cluster through the entire tablet. The critical volume fraction of cluster that water can diffuse through the entire MA tablets are calculated with taking into account the geometrical considerations between MS and MA particles based on random close packed (RCP) spheres system. The critical volume fraction of MS is calculated by the multiplication of critical concentration of MS and the solid fraction of MA tablets; which is within the range of  $0.16 \pm 0.01$  (v/v). It is concluded that the critical volume fraction for three dimensional lattices is equal to  $0.16 \pm 0.01$  (v/v); which is useful for the calculation of the critical concentration of starch based disintegrant in order to design the pharmaceutical tablet formulation based on scientific approach proposed by ICH Q8 guidance.

In addition, the disintegration behavior in the neighborhood of the percolation threshold is explained mathematically by the basic equation of the percolation theory, yielding a critical exponent  $q$  equal to  $0.28 \pm 0.06$  (Quality of fit:  $r^2 = 0.84$ ). This value is close to the critical exponent for three dimensional lattices ( $q = 0.4$ ); which indicates the strength of infinite cluster for its concentration above the percolation threshold.

The comparison of these results between MA tablets and caffeine tablets lead to very similar values for the critical concentration of non-fibrous disintegrant and critical exponent for disintegration behavior. These results can lead to the following conclusions:

1. The solubility of the drug substance does not affect the location of critical concentration of non-fibrous disintegrant and critical exponent for disintegration behavior.
2. The critical exponent  $q$  is close to  $q \approx 0.3$  for the disintegration behavior of pharmaceutical tablets.

From the point of view to choose the best the experimental design to find the critical concentration of the disintegrant, it is highly recommended to take into account the percolation theory. Thus, among others, the experimental range can be narrowed. However it has to be kept in mind that the determination of the percolation threshold and critical exponent does not give an answer about the absolute value of the disintegration time.

Due to the steadily rising costs for developing and finally for registering a new drug substance, the pharmaceutical industry starts to use for a rapid pharmaceutical development more and more software tools. Such an approach is not new and has been successfully introduced in the automotive industry with Toyota as a pioneer using the principle of "Quality by Design" [126]. Today, not only cars but also aircrafts such as the Boeing 777 and the Airbus 380 are first constructed and tested in-silico. Such an approach is considered as best practice. In the present study the software F-CAD (Formulation-Computer Aided design) [95] is used to calculate in-silico the expected time of disintegration. F-CAD has been very successfully applied so far to predict the dissolution profile of a tablet [94, 96, 100] and there is a conjecture, that the "time elapsed" till water molecules reach the center of the tablet, which can be calculated by F-CAD could be a surrogate for the effectively measured disintegration time. Thus, the Dissolution Simulation (DS) module of F-CAD, which is based on cellular automata algorithm has been used to simulate the disintegration time of a MA tablet. In the present study, the experimental disintegration time of tablet is compared with the calculated specific time point for water to reach the geometric center of the tablet. In general, there is not a specific problem to calculate these specific times. However, the Tablet K and M show difficulties to compute the F-CAD disintegration time. Interestingly, if these two Tablets are not taken into account, a correlation between the real disintegration time and the F-CAD estimate a correlation between the two tablet formulation properties could be obtained with a correlation coefficient:  $r = 0.81$ . Compared to the much better achievements of F-CAD by calculating the dissolution profile of a tablet formulation, it become evident that there is a need for further studies and an improvement of F-CAD. It has to be noted, on the other hand, that there is so far no other software available, which is able to predict the disintegration time. The disintegration is the key property, especially for low water soluble drugs. Often the disintegration test can reduce the number of dissolution runs for the design and process development of immediate release tablet formulation at the early stage such as phase I and II before POC study [127].

It is concluded that F-CAD software is one of the tools for the substitution of laboratory experiments for the purpose of the design and development of new pharmaceutical solid dosage forms. The replacement of expensive laboratory experiments by in-silico experiments is an important issue to reduce development costs and to comply with the requirements of ICH Q8 exploring the design space with response surface methodology. The results of this

thesis show in addition, that the application of percolation theory is a must in order to detect percolation thresholds. It is important to know the response surfaces close to the percolation threshold of sensitive tablet properties such as the disintegration time to get information about the robustness of the selected formulation. In this context one has to put the question forward if the application of percolation theory should be an integral part of the guidelines of ICH Q8 exploring the formulation design space.

## 8 Further perspectives

In our laboratory, the critical concentration of fibrous disintegrant was found at about 3% v/v in a binary compact consisting of caffeine or indomethacin and Ac-Di-Sol<sup>®</sup> [12]. Fibrous disintegrant is also used for intra-granular excipient in a pharmaceutical tablet. It is important to know the effect of wet granulation on the critical concentration of fibrous disintegrant. Moreover it is also important to investigate the critical concentration of disintegrant if it is used for extra-granular excipient in order to establish the rule of pharmaceutical tablet formulation design.

## 9 References

- [1] ICH Harmonized Tripartite Guideline: Pharmaceutical Development Q8(R2), Current Step 4 version: [http://www.ich.org/fileadmin/Public\\_Web\\_Site/ICH\\_Products/Guidelines/Quality/Q8\\_R1/Step4/Q8\\_R2\\_Guideline.pdf](http://www.ich.org/fileadmin/Public_Web_Site/ICH_Products/Guidelines/Quality/Q8_R1/Step4/Q8_R2_Guideline.pdf) (accessed December 2011).
- [2] Patel, N.R.; Hopponen, R.E. Mechanism of action of starch as a disintegrating agent in aspirin tablets. *J. Pharm. Sci.* 1966, 55(10), 1065-1068.
- [3] Nogami, H.; Hasegawa, J.; Miyamoto, M. Studies on powdered preparations. XX. Disintegration of the aspirin tablets containing starches as disintegrating agent. *Chem. Pharm. Bull.* 1967, 15(3), 279-289.
- [4] Commons, K.C.; Bergen, A.; Walker, G.C. Influence of starch concentration on the disintegration time of tolbutamide tablets. *J. Pharm. Sci.* 1968, 57(7), 1253-1255.
- [5] Nakai, Y.; Nakajima, S. Relationship between configuration of starch grains in tablet and tablet disintegration. *Yakugaku Zasshi* 1977, 97(11), 1168-1173.
- [6] Yuasa, H.; Kanaya, Y. Studies on internal structure of tablets. II. Effect of the critical disintegrator amount on the internal structure of tablets. *Chem. Pharm. Bull.* 1986, 34(12), 5133-5139.
- [7] Ringard, J.; Guyot-Hermann, A.M. Calculation of disintegrant critical concentration in order to optimize tablets disintegration. *Drug Dev. Ind. Pharm.* 1988, 14(15-17), 2321-2339.
- [8] Leuenberger, H.; Rohera, B.D.; Hass, Ch. Percolation theory-a novel approach to solid dosage form design. *Int. J. Pharm.* 1987, 38, 109-115.
- [9] Luginbuehl, R.; Leuenberger, H. Use of percolation theory to interpret water uptake, disintegration time and intrinsic dissolution rate of tablets consisting of binary mixtures. *Pharm. Acta. Helv.* 1994, 69, 127-134. (*Pharm. Acta. Helv.* is no longer existing, article can however be downloaded from <http://www.ifip.ch/content/de/downloads/articles-download.html>).
- [10] Luginbuehl, R. Anwendung der Perkolationstheorie zur Untersuchung des Zerfallsprozesses, der Wasseraufnahme und der Wirkstofffreisetzung von binären Tablettensystemen. PhD Thesis; University of Basel: Basel, 1994.
- [11] Krausbauer, E.; Puchkov, M.; Leuenberger, H. Rational estimation of the optimum amount of non-fibrous disintegrant applying percolation theory for binary fast disintegrating formulation. *J. Pharm. Sci.* 2008, 97(1), 529-541.
- [12] Krausbauer, E. Contributions to a science based expert system for solid dosage form design. PhD Thesis; University of Basel: Basel, 2009.
- [13] Nakai, Y.; Fukuoka, E., Nakagawa, H. Preferred orientation of crystalline particle within tables II. Effect of shape of aspirin crystals on their orientation within tablets and breaking strength of tablets. *Yakugaku Zasshi* 1978, 98(2), 184-190.
- [14] Nakai, Y.; Fukuoka, E., Nakajima, S., Hasegawa, J. Crystallinity and physical characteristics of microcrystalline cellulose. *Chem. Pharm. Bull.* 1977, 25(1), 96-101.
- [15] Leuenberger, H. The compressibility and compactibility of powder systems. *Int. J. Pharm.* 1982, 12, 41-55.
- [16] Jetzer, W., Leuenberger, H. The compressibility and compactibility of pharmaceutical powders. *Pharm. Technol.* 1983, 7 (4), 33-39.
- [17] Leuenberger, H., Jetzer, W. The compactibility of powder systems. *Power Technol.* 1984, 37, 209-218.
- [18] Roberts, R.J.; Rowe, R.C. Brittle/ductile behaviour in pharmaceutical materials used in tableting. *Int. J. Pharm.* 1987, 36, 205-209.



- [19] Alderborn, G.; Lang, P. O., Sagstroem, A., Kristensen. Compression characteristics of granulated materials. I. Fragmentation propensity and compactibility of some granulations of a high dosage drug. *Int. J. Pharm.* 1987, 37, 155-161.
- [20] Roberts, R.J.; Rowe, R.C. The effect of punch velocity on the compaction of a variety of materials. *J. Pharm. Pharmacol.* 1985, 37, 377-384.
- [21] Alderborn, G.; Pasanen, K.; Nystroem, C. Studies on direct compression of tablets. XI. Characterization of particle fragmentation during compaction by permeametry measurement of tablets. *Int. J. Pharm.* 1985, 23, 79-86.
- [22] Armstrong, N.A.; Palfrey, L.P. The effect of machine speed on the consolidation of four directly compressible tablet diluents. *J. Pharm. Pharmacol.* 1989, 41, 149-151.
- [23] Metropolitan Computing Corporation. [www.mcc-online.com/](http://www.mcc-online.com/) (accessed October 2011).
- [24] EDQM. European Pharmacopoeia (Ph. Eur.) 7<sup>th</sup> edition, 2011.
- [25] FDA/CDER. Waiver of in vivo bioavailability and bioequivalence studies for immediate release solid oral dosage forms based on a biopharmaceutics classification system. Guidance for Industry, August 2000.
- [26] Von Orelli, J.; Leuenberger, H. Search for technological reasons to develop a capsule or a tablet formulation with respect to wettability and dissolution. *Int. J. Pharm.* 2004, 287, 135-145.
- [27] Kawashima, Y.; Imai, H.; Takeuchi, H.; Yamamoto, H.; Kamiya, K. Development of agglomerated crystals of ascorbic acid by the spherical crystallization technique for direct tableting and evaluation of their compactibilities. *KONA* 2002, 20, 251-262.
- [28] Leuenberger, H. Granulation, new techniques. *Pharm. Acta. Helv.* 1982, 57(3), 72-82. (*Pharm. Acta. Helv.* is no longer existing, article can however be downloaded from <http://www.ifip.ch/content/de/downloads/articles-download.html>).
- [29] Leuenberger, H.; Imanidis, G. Monitoring mass transfer processes to control moist agglomeration. *Pharmaceutical Technology* 1986, March, 56-73.
- [30] Newitt, D. M.; Conway-Jones, J.M. A contribution to the theory and practice of granules. *Trans. I. Chem. Eng.* 1958, 36, 422-441.
- [31] York, P. M.; Rowe, R.C. Monitoring granulation size enlargement process using mixer torque rheometry. First International Particle Technology Forum, Denver, USA, 1994.
- [32] Terashita, K.; Watano, S.; Miyunami, K. Determination of end-point by frequency analysis of power consumption in agitation granulation. *Chem. Pharm. Bull.* 1990, 38 (11), 3120-3123.
- [33] Betz, G.; Buergin, S. J.; Leuenberger, H. Power consumption profiles analysis and tensile strength measurement during moist agglomeration. *Int. J. Pharm.* 2003, 252, 11-25.
- [34] 鈴木 祐介. PAT はパラダイムシフトにあらず, “品質は工程で造り込む” の延長上にあり. 第 4 回創薬工業シンポジウム, 2004.
- [35] Watano, S.; Numa, T.; Koizumi, I.; Osaka, Y. Feedback control in high shear granulation of pharmaceutical powders. *Eur. J. Pharma. Biopharma.* 2001, 52(3), 337-345.
- [36] Briens, L.; Daniher, D.; Talleivi, A. Monitoring high-shear granulation using sound and vibration measurements. *Int. J. Pharm.* 2007, 331, 54-60.
- [37] Monney, D. Ein Beitrag zur Prozessueberwachung bei der Wirbelschichtgranulierung. PhD Thesis; University of Basel: Basel, 2000.
- [38] Dussert, A, Chulia, D.; Jeannin, C.; Ozil, P. Parametric study of fluidized-bed granulation of a low density micronized powder. *Drug Dev. Ind. Pharm.* 1995, 21 (12), 1439-1452.

## References

---

- [39] Gao, J. Z. H., Jain, R., Motheram, R.; Gray, D. B., Hussain, M.A. Fluid bed granulation of a poorly water soluble, low density, micronized drug: comparison with high shear granulation. *Int. J. Pharm.* 2002, 237, 1-14.
- [40] Leuenberger, H.; 綿野 哲 訳・監修. How to avoid scale-up problems in manufacturing pharmaceutical granules: The Glatt® Multicell™ Concept. *Pharm Tech Japan* 2001, 17 (10), 67-73.
- [41] Vervaet, C., Remon, J. R. Continuous granulation in the pharmaceutical industry. *Chem. Eng. Sci.* 2005, 60, 3949-3957.
- [42] Sunada, H.; Hasegawa, M.; Makino, T.; Sakamoto, H.; Fujita, K.; Tanino, T.; Kokubo, H.; Kawaguchi, T. Study of standard tablet formulation based on fluidized-bed granulation. *Drug Dev. Ind. Pharm.* 1998, 24 (3), 225-233.
- [43] Adam, A.; Schrimpl, L.; Schmidt, P.C. Factors influencing capping and cracking of mefenamic acid tablets *Drug Dev. Ind. Pharm.* 2000, 26 (5), 489-497.
- [44] Carr, R. L. Evaluating flow properties of solids. *Chem. Eng.* 1965, 18, 163-168.
- [45] Hausner, H. H. Friction conditions in a mass of metal powder. *Int. J. Powder Metall.* 1967, 3, 7-13.
- [46] Guyot-Hermann, A. M. Tablet disintegration and disintegration agents. *S. T. P. Pharma Sciences*, 1992, 2 (6), 445-462.
- [47] Kanig, J. L.; Rudnic, E. M. The mechanisms of disintegrant action. *Pharmaceutical Technology* 1984, April, 50-63.
- [48] Tanino, T.; Aoki, Y.; Furuya, Y.; Sato, K.; Takeda, T.; Mizuta, T. Occurrence of capping due to insufficient air escape during tablet compression and method to prevent it. *Chem. Pharm. Bull.* 1995, 43 (10), 1772-1779.
- [49] Juppo, A.M. Relationship between breaking force and pore structure of lactose, glucose and mannitol tablets. *Int. J. Pharm.* 1996, 127, 95-102.
- [50] Juppo, A.M. Porosity parameters of lactose, glucose and mannitol tablets obtained by mercury porosimetry. *Int. J. Pharm.* 1996, 129, 1-12.
- [51] Juppo, A.M. Change in parameters of lactose, glucose and mannitol granules caused by low compression force. *Int. J. Pharm.* 1996, 130, 149-157.
- [52] FDA. PAT-A framework for innovative pharmaceutical development, manufacturing, and quality assurance. Guidance for Industry, September 2004.
- [53] EDQM. Near-Infrared Spectrophotometry. *European Pharmacopoeia (Ph. Eur.)* 7<sup>th</sup> edition, 2011.
- [54] Maurer, L. Near infrared spectroscopy / imaging and terahertz pulsed spectroscopy / imaging for analysis of solid dosage forms. PhD Thesis; University of Basel: Basel, 2008.
- [55] Terashita, K. Near-infrared chemical imaging and the PAT initiative. *Pharm Tech Japan* 2005, 21 (5), 7-15.
- [56] Li, W.; Woldu, A.; Kelly, R.; McCool, J.; Bruce, R.; Rasmussen, H.; Cunningham, J.; Winstead, D. Measurement of drug agglomeration in powder blending simulation samples by near infrared chemical imaging. *Int. J. Pharm.* 2008, 350, 369-373.
- [57] Sasic, S. Chemical imaging of pharmaceutical granules by Raman global illumination and near-infrared mapping platforms. *Ana. Chim. Acta.* 2008, 611, 73-79.
- [58] Maurer, L.; Leuenberger, H. Terahertz pulsed imaging and near infrared imaging to monitor the coating process of pharmaceutical tablets. *Int. J. Pharm.* 2009, 370, 8-16.
- [59] Shah, R. B.; Tawakkul, M. A.; Khan, M. A. Process analytical technology: Chemometrics analysis of raman and near infra-red spectroscopic data for predicting physical properties of extended release matrix tablets. *J. Pharm Sci.* 2007, 96, 1356-1365.

- [60] Clark, F. Extracting process-related information from pharmaceutical dosage forms using near infrared microscopy. *Vib. Spectrosc.*, 2004, 34, 25-35.
- [61] Leuenberger, H.; Guitard, P. Delivery systems for patient compliance. "Pharmaceutical Medicine-The Future" Lahon, H.; Rondel, R. K.; Krotovchil, C. editors, 3<sup>rd</sup> International Meeting of Pharmaceutical Physicians, Brussels, October 1978, 4-6, 358-372. (Article to be downloaded from <http://www.ifiip.ch/content/de/downloads/articles-download.html>, as the book has not been reprinted.).
- [62] Leuenberger, H.; Lanz, M. Pharmaceutical Powder Technology-from Art to Science: the challenge of FDA's PAT initiative. *Adv. Powder Technol.* 2005, 16, 1-36.
- [63] Leuenberger, H.; Becher, W. A factorial design for compatibility studies in preformulation work. *Pharm. Acta. Helv.* 1975, 50, 88-91. (Pharm. Acta. Helv. is no longer existing, article can however be downloaded from <http://www.ifiip.ch/content/de/downloads/articles-download.html>).
- [64] Leuenberger's lecture at Albi, France in 2007.
- [65] FDA. Challenge and opportunity on the critical path to new medical products. FDA report, March 2004.
- [66] Leuenberger, H. Chapter "Versuchsplanung und Optimierstrategien" in the textbook of Sucker, Fuchs, Speiser, *Pharmazeutische Technologie*, Georg Thieme Verlag, Stuttgart, 1978, 64-80.
- [67] Takayama, K. Formulation design and optimization of solid dosage forms based on a multivariate spline interpolation. *Pharm Tech Japan* 2002, 18 (10), 139-146.
- [68] Kaseda, Ch. Response surface methodology using a spline algorithm. *Geometric modeling and computing*; Lucian, M.L., Neamtu, M., Eds.; Seattle, 2003, 341-352.
- [69] Wahba, G. *Spline models for observational data*. Roy. Stat. Soc. Ser. B; Society for industrial and applied mathematics: Philadelphia, PA, 1990.
- [70] Arai, H.; Suzuki, T.; Kaseda, C.; Ohya, K.; Takayama, K. Bootstrap re-sampling technique to evaluate the optimal formulation of theophylline tablets predicted by non-linear response surface method incorporating multivariate spline interpolation. *Chem. Pharm. Bull.* 2007, 55 (4), 586-593.
- [71] Stauffer, D.; Aharony, A. *Introduction to Percolation Theory*, Revised 2nd edition. Taylor & Francis Group, 1994.
- [72] Stauffer, D.; Aharony, A. 小田垣 孝 訳, パーコレーションの基本理論, 原書第2版・修訂版, 吉岡書店, 2001.
- [73] Niimura H. A role for percolation theory in analysis of gas permeability of magma. *Japanese Magazine of Mineralogical and Petrological Sciences* 2006, 35, 153-165.
- [74] Leuenberger, H. The application of percolation theory in powder technology. *Adv. Powder Technol.* 1999, 10(4), 323-353.
- [75] 小田垣 孝, 九州大学 エクセレント・スチューデント・イン・サイエンス 公開講演会, 2010.
- [76] Scher, H.; Zallen, R. Critical density in percolation processes. *J. Chem. Phys.* 1970, 53, 3759-3761.
- [77] McLachlan, D. S.; Blaszkiewicz, M.; Newnham, R. E. Electrical resistivity of composites. *J. Am. Ceram. Soc.* 1990, 73(8), 2187-2203.
- [78] Powell, M. J. Site percolation in random packed spheres. *Phys. Rev. B.* 1979, 20(10), 4194-4198.
- [79] Sherman, R. D.; Middleman, L. M.; Jacobs, S. M. Electron transport processes in conductor-filled polymers. *Polym. Eng. Sci.* 1983, 23(1), 36-46.
- [80] Fitzpatrick, J. P.; Malt, R. B.; Spaepen, F. Percolation theory and conductivity of random close packed mixture of hard spheres. *Physics letters.* 1974, 47A, 207-208.

## References

---

- [81] Ottavi, H.; Clerc, J. P.; Giraud, G.; Roussenq, J.; Guyon, E.; Mitescu, C. D. Electrical conductivity of conducting and insulating spheres: an application of some percolation concepts. *J. Phys. C: Solid State Phys.* 1978, 11, 1311-1328.
- [82] Lee, S. I.; Song, Y.; Noh, T. W.; Chen, X. D.; Gaines, J. R. Experimental observation of nonuniversal behavior of the conductivity exponent for three-dimensional continuum percolation systems. *Phys. Rev. B.* 1986, 34, 6719-6724.
- [83] Wu, J.; McLachlan, D. S. Percolation exponents and thresholds in two nearly ideal anisotropic continuum systems. *Physica A.* 1997, 241, 360-366.
- [84] Holman, L. E.; Leuenberger, H. The relationship between solid fraction and mechanical properties of compacts - the percolation theory model approach. *Int. J. Pharm.* 1988, 46, 35-44.
- [85] Hernandez-Perni, G.; Leuenberger, H. The characterization of aprotic polar liquids and percolation phenomena in DMSO/water mixture. *Eur. J. Pharma. Biopharma.* 2005, 61, 201-213.
- [86] Caraballo, I. Factors affecting drug release from hydroxypropyl methylcellulose matrix systems in the light of classical and percolation theories. *Expert Opin. Drug Deli.* 2010, 7(11), 1291-1301.
- [87] Caraballo, I.; Fernandez-Arevalo, M.; Millan, M.; Rabasco, A. M.; Leuenberger, H. Study of percolation thresholds in ternary tablets. *Int. J. Pharm.* 1996, 139, 177-186.
- [88] Bunde, A.; Roman, H. E. *Gesetzmaessigkeiten der Unordnung, Physik in unserer Zeit* 1996, 27, 246-256.
- [89] Mandelbrot, B. B. *Die Fraktale Geometrie der Natur*, Birkhaeuser, Basel, 1987.
- [90] Leuenberger, H.; Holman, L.; Usteri, M.; Winzap, S. Percolation theory, fractal geometry, and dosage form design. *Pharm. Acta. Helv.* 1989, 64, 34-39. (Pharm. Acta. Helv. is no longer existing, article can however be downloaded from <http://www.ifiip.ch/content/de/downloads/articles-download.html>).
- [91] Mandelbrot, B. B. *The Fractal Geometry of Nature*, W. H. Freeman and Company, San Francisco, 1982.
- [92] Bonny, J. D.; Leuenberger, H. Determination of fractal dimensions of matrix-type solid dosage forms and their relation with drug dissolution kinetics. *Eur. J. Pharm. Biopharm.* 1993, 39, 31-37.
- [93] Saito, K.; Yamane, S.; Takayama, K.; Nagai, T. Involvement of fractal structure of hydrophilic polymer matrix in drug release behavior. *Yakuzaigaku* 1998, 58(4), 203-212.
- [94] Leuenberger, H.; Leuenberger, M. N.; Puchkov, M. Right First Time: Computer-Aided Scale-up for manufacturing solid dosage forms with a shorter time to market. *SWISS PHARMA* 2010, 32(7-8), 3-13.
- [95] CINCAP GmbH. [www.cincap.ch/](http://www.cincap.ch/) (accessed December 2011).
- [96] Leuenberger, H.; Leuenberger, M. N.; Puchkov, M. Implementing virtual R & D reality in industry: In-silico design and testing of solid dosage forms. *SWISS PHARMA* 2009, 31(7-8), 18-24.
- [97] Leuenberger, H. Pharmaceutical technology: drug delivery, formulation, and process research. *Chimia* 2006, 60, 40-45.
- [98] *Pharma 2020: Virtual R & D - Which path will you take?*, PricewaterhouseCoopers, 2008.
- [99] Puchkov, M.; Leuenberger, H. Improving tablet coating yield and quality via computer-based simulations. *Tablet & Capsule* 2010, 20-23.
- [100] Puchkov, M.; Leuenberger, H. Computer-aided design of pharmaceutical formulations: F-CAD software and a mathematical concept. *Glatt International Times* 2011, 31, 2-6.
- [101] Bourquin, J.; Schmidli, H.; Van Hoogevest, P.; Leuenberger, H. Basic concepts of artificial neural networks (ANN) modeling in the application to pharmaceutical development. *Pharm. Dev. Technol.* 1997, 2(2), 95-109.

- [102] Bourquin, J.; Schmidli, H.; Van Hoogevest, P. Leuenberger, H. Application of artificial neural networks (ANN) in the development of solid dosage forms. *Pharm. Dev. Technol.* 1997, 2(2), 111-121.
- [103] Wolfram, S. *A New Kind of Science*, Wolfram Media Inc., 2002.
- [104] Kita, E.; Toyoda, T. Structural design using cellular automata. *Struct. Multidisc. Optim.* 2000, 19, 64-73.
- [105] Zygourakis, K.; Markenscoff, P. A. Computer-aided design of bioerodible devices with optimal release characteristics: a cellular automata approach. *Biomaterials* 1996, 17, 125-135.
- [106] Barat, A.; Ruskin, H. J.; Crane, M. Probabilistic models for drug dissolution. Part 1. Review of Monte Carlo and stochastic cellular automata approaches. *Simul. Model. Pract. Theory* 2006, 14, 843-856.
- [107] Laaksonen, T.; Laaksonen, H.; Hirvonen, J.; Murtomaekj, L. Cellular automata model for drug release from binary matrix and reservoir polymeric devices. *Biomaterials* 2009, 30, 1978-1987.
- [108] Laaksonen, H.; Hirvonen, J.; Laaksonen, T. Cellular automata model for swelling-controlled drug release. *Int. J. Pharm.* 2009, 380, 25-32.
- [109] Kier, L. B.; Cheng, C.-K.; Testa, B. A cellular automata model of the percolation process. *J. Chem. Inf. Comput. Sci.* 1999, 39, 326-332.
- [110] Brunauer, S.; Emmett, P.H.; Teller, E. Adsorption of gases in multimolecular layers. *J. Am. Chem. Soc.* 1938, 60, 309-319.
- [111] Micromeritics Corporate. *PoreSizer 9320 Operator's Manual*, March 2001, Appendix J: Automatic data reduction.
- [112] Juppo, A.M.; Yliruusi, J. Effect of amount of granulation liquid on total pore volume and pore size distribution of lactose, glucose and mannitol granules. *Eur. J. Pharm. Biopharm.* 1994, 40(5), 299-309.
- [113] Fell, J.T.; Newton, J.M. The tensile strength of lactose tablets. *J. Pharm. Pharmacol.* 1968, 20, 657-658.
- [114] Dees, P.J.; Polderman, J. Mercury porosimetry in pharmaceutical technology. *Powder Technol.* 1981, 29, 187-197.
- [115] Kamba, M.; Seta, Y.; Takeda, N.; Kusai, A.; Nakane, H.; Nishimura, K. Measurement of agitation force in dissolution test and mechanical destructive force in disintegration test. *Int. J. Pharm.* 2003, 250(1), 99-109.
- [116] Amidon, G.L.; Lennernaes, H.; Shah, V.P.; Crison, J.R. A theoretical basis for a biopharmaceutic drug classification: The correlation of in vitro drug product dissolution and in vivo bioavailability. *Pharm. Res.* 1995, 12 (3), 413-420.
- [117] Tokumura, T. A screening system of solubility for drug design and discovery. *Pharm Tech Japan* 2000, 16(13), 19-27.
- [118] Yazdaniyan, M.; Briggs, K.; Jankovsky, C.; Hawi, A. The "high solubility" definition of the current FDA guidance on biopharmaceutical classification system may be too strict for acidic drugs. *Pharm. Res.* 2004, 21 (2), 293-299.
- [119] Adam, A.; Schrimpl, L.; Schmidt, P.C. Some physicochemical properties of mefenamic acid. *Drug Dev. Ind. Pharm.* 2000, 26(5), 477-487.
- [120] Wikberg, M.; Alderborn, G. Compression characteristics of granulated materials. IV. The effect of granule porosity on the fragmentation propensity and the compactibility of some granulations. *Int. J. Pharm.* 1991, 69, 239-253.
- [121] Zuurman, K.; Bolhuis, G.K.; Vromans, H. Effect of binder on the relationship between bulk density and compactibility of lactose granulations. *Int. J. Pharm.* 1995, 119, 65-69.

## References

---

- [122] Kimura, G.; Betz, G.; Leuenberger, H. Influence loading volume of mefenamic acid on granules and tablet characteristics using a compaction simulator. *Pharm. Dev. Technol.* 2007, 12, 627-635.
- [123] Kimura, G.; Puchkov, M.; Betz, G.; Leuenberger, H. Percolation Theory and the Role of Maize Starch as a Disintegrant for a Low Water-Soluble Drug. *Pharm. Dev. Technol.* 2007, 12, 11-19.
- [124] Marquardt, D. W. An algorithm for least-squares estimation of non-linear parameters. *J. Soc. Ind. Appl. Math.* 1963, 11, 431-441.
- [125] Simulations Plus, Inc. [www.simulations-plus.com/](http://www.simulations-plus.com/) (accessed December 2011).
- [126] Morgan, J. M.; Liker, J. K. *The Toyota product development system: Integrating people, process and technology*, Kindle edition, Productivity Press Inc., 2006.
- [127] Sally Grieb, S. Opportunities for the Application of Quality by Design to Dissolution Strategy in Commercial Formulation Development. PASG 2010 Spring Conference.

**Curriculum vitae**

Name Go Kimura  
Date of Birth 18<sup>th</sup> March, 1975  
Nationality Japan

**Education:**

Since Feb, 2004 PhD study under the supervision of Prof. Dr. H. Leuenberger at the Institute of Pharmaceutical Technology, University of Basel, Switzerland

Sep, 2003 Visiting scientist from Shionogi & Co., Ltd. under the supervision of Prof. Dr. H. Leuenberger at the Institute of Pharmaceutical Technology, University of Basel, Switzerland

Mar. 1999 Master of Science in Pharmacy from Kyoto Pharmaceutical University  
Master thesis is "Sustained release technology by delivering drugs in the colon" under the direction of Prof. K.Takada

May 1997 Registered Pharmacist in Japan

Mar. 1997 Bachelor of Science in Pharmacy from Kyoto Pharmaceutical University

**Career:**

Since Apr. 1999 Shionogi & Co., Ltd.  
Engaged in;

- Solid dosage form design and process development for NCEs, OTC products and life cycle management.
- Site change and CAPA of deviation for existing products of Shionogi Japan, Shionogi Taiwan and Shionogi Inc.





---

## Achievements

### Publications (in English)

- [1] Go Kimura, Maxim Puchkov, Hans Leuenberger. : An attempt to calculate in-silico disintegration time of tablets containing mefenamic acid, a low water soluble drug. In preparation, 2012.
- [2] Go Kimura, Maxim Puchkov, Gabriele Betz, Hans Leuenberger. : Percolation Theory and the Role of Maize Starch as a Disintegrant for a Low Water-Soluble Drug. *Pharm. Dev. Technol.*, 12, 11-19, 2007.
- [3] Go Kimura, Gabriele Betz, and Hans Leuenberger. : Influence of Loading Volume of Mefenamic Acid on Granules and Tablet Characteristics Using a Compaction Simulator. *Pharm. Dev. Technol.*, 12, 627-635, 2007.
- [4] Nobuhito Shibata, Tatsuharu Shimokawa, Zhi-Qiang Jiang, Young-Il Jeong, Tomoya Ohno, Go Kimura, Yukako Yoshikawa, Kenji Koga, Masahiro Murakami, Kanji Takada. : Characteristics of intestinal absorption and disposition of glycyrrhizin in mice. *Biopharmaceutics & Drug Disposition*, 21 (3), 95–101, 2000.
- [5] Zhaopeng Hu, Shunsuke Mawatari, Tatsuharu Shimokawa, Go Kimura, Yukako Yoshikawa, Nobuhito Shibata and Kanji Takada. : Colon delivery efficiencies of intestinal pressure-controlled colon delivery capsules prepared by a coating machine in human subjects. *J. Pharm. Pharmacol.*, 52, 1187-1193, 2000.
- [6] Yukako Yoshikawa, Zhaopeng Hu, Go Kimura, Masahiro Murakami, Hiroshi Yoshikawa and Kanji Takada. : A dissolution test for a pressure-controlled colon delivery capsule: Rotating beads method. *J. Pharm. Pharmacol.*, 51, 979-989, 1999.
- [7] Zhaopeng Hu, Tatsuharu Shimokawa, Tomoya Ohno, Go Kimura, Shun-suke Mawatari, Megumi Kamitsuna, Yukako Yoshikawa, Shigeki Masuda and Kanji Takada. : Characterization of norfloxacin release from tablet coated with a new pH-sensitive polymer, P-4135F. *J. Drug Target*, 7, 223-232, 1999.
- [8] Zhaopeng Hu, Go Kimura, Yoshiaki Ito, Mawatari Syunsuke, Tatsuharu Shimokawa, Hiroshi Yoshikawa, Yukako Yoshikawa and Kanji Takada. : Technology to obtain sustained-release characteristics of drugs after delivered to the colon. *J. Drug Target*, 6, 439-448, 1999.
- [9] Zhaopeng Hu, Go Kimura, Shun-suke Mawatari, Tatsuharu Shimokawa, Yukako Yoshikawa and Kanji Takada. : New preparation method of intestinal pressure-controlled colon delivery capsules by coating machine and evaluation in beagle dogs. *J. Controlled Release*, 56, 293- 302, 1998.
- [10] Tomohiro Takaya, Kiyoshi Niwa, Motoki Muraoka, Ikuo Ogita, Noriko Nagai, Ryo-ichi Yano, Go Kimura, Yukako Yoshikawa, Hiroshi Yoshikawa and Kanji Takada. : Importance of dissolution process on systemic availability of drugs delivered by colon delivery system. *J. Controlled Release*, 50, 111-122, 1998.

### Oral presentations (in English)

- [1] Influence of loading amount of mefenamic acid on granulation and tablet characteristic using a compaction simulator. Go Kimura, Gabriele Betz, Hans Leuenberger. 8<sup>th</sup> International Symposium on Agglomeration, Bangkok, Thailand, March 16-18 2005.
- [2] Influence of loading amount of mefenamic acid on granulation and tablet characteristic using a compaction simulator. Go Kimura, Gabriele Betz, Hans Leuenberger. Continuing Education Course of the Center of Pharmaceutical Sciences Basel-Zurich, 2004.

### Posters (in English)

- [1] Percolation theory and the role of maize starch as a disintegrant for a low water soluble drug formulation. Go Kimura, Maxim Puchkov, Gabriele Betz, Hans Leuenberger. 2<sup>nd</sup> International Technical Forum Inspiring Powder Technology, Makuhari, Japan, Nov. 9 2006.
- [2] Understanding the factors influencing tablet qualities by NIR chemical imaging. Go Kimura, Takashi Hayashi, Ryuichi Kume, Tsuyoshi Furukawa, Shukichi Ochiai. 125<sup>th</sup> Annual Meeting of the Pharmaceutical Society of Japan, Sendai, Japan, March 28-30 2006.
- [3] Influence of amount of maize starch on the disintegration time of mefenamic acid containing tablet using a compaction simulator. Go Kimura, Maxim Puchkov, Gabriele Betz, Hans Leuenberger. Pharmaceutical Sciences Fair, Nice, France, June 12-17 2005.
- [4] Influence of compression force on the disintegration time of mefenamic acid containing tablet using a compaction simulator. Go Kimura, Gabriele Betz, Hans Leuenberger. 3<sup>rd</sup> World Conference on Drug Absorption, Transport and Delivery, Barcelona, Spain, April 18-20 2005.
- [5] Influence of loading amount of mefenamic acid on granule characteristic and compression behavior using a compaction simulator. Go Kimura, Gabriele Betz, Hans Leuenberger. 12<sup>th</sup> International Pharmaceutical Technology Symposium, Istanbul, Turkey, Sep. 12-15 2004.
- [6] Preparation and evaluation of sustained-release colon delivery capsule containing 5-aminosalicylic acid in beagle dogs. Go Kimura, Zhaopeng Hu, Yumi Goto, Wataru Hagihara, Yukako Yoshikawa, Kanji Takada. 9<sup>th</sup> Japanese-American Conference on Pharmacokinetics and Biopharmaceutics, Nagoya, Japan, Sep. 1998.
- [7] New preparation method of intestinal pressure-controlled colon delivery capsules by coating machine and evaluation in beagle dogs. Zhaopeng Hu, Go Kimura, Motoki Muraoka, Shun-suke Mawatari, Tatuharu Shimokawa, Yukako Yoshikawa and Kanji Takada. 9<sup>th</sup> Japanese-American Conference on Pharmacokinetics and Biopharmaceutics, Nagoya, Japan, Sep. 1998.
- [8] Design and evaluation of intestinal pressure-controlled colon delivery capsules (PCDC) in beagle dogs and human subjects. Motoki Muraoka, Zhaopeng Hu, Go Kimura, Tomohiro Takaya and Kanji Takada. CRS-CPS Joint Workshop on Recent Advances in Drug Delivery Science and Technology, Beijing, China, Sep. 1997.

### Publications (in Japanese)

- [1] 木村 豪, 胡 兆鵬, 馬渡 俊輔, 下川 達張, 高田 寛治: 大腸ターゲッティング徐放性製剤技術. *Drug Delivery System*, 1999, 14, 191-196.
- [2] 胡 兆鵬, 木村 豪, 馬渡 俊輔, 萩原 由紀, 高田 寛治, 荒川 彰, 吉田 佳一. 生体磁気計測装置による磁気化大腸デリバリーカプセルのヒトにおける大腸送達性の評価: γ-シンチグラフィに代わる非侵襲的手法の試み. *臨床薬理*, 1999, 30(1), 253-254.
- [3] 胡 兆鵬, 木村 豪, 馬渡 俊輔, 下川 達張, 高田 寛治. 大腸内圧崩壊型大腸デリバリーカプセル intestinal luminal pressure-controlled colon delivery capsule (PCDC) のコーティング機による量産法の確立とその大腸送達性評価. *Drug Delivery System*, 1999, 14, 123-127.
- [4] 村岡 元樹, 木村 豪, 胡 兆鵬, 高田 寛治. 炎症性大腸疾患. *日本臨牀*, 1998, 56 (3), 788-794.
- [5] 胡 兆鵬, 木村 豪, 吉川 由佳子, 高田 寛治. 蛋白分解酵素阻害薬を利用した薬物吸収改善法. *日本臨牀*, 1998, 56 (3), 595-600.
- [6] 村岡 元樹, 木村 豪, 胡 兆鵬, 高田 寛治. 大腸特異的疾患の経口療法. *総合臨床*, 1997, 46, 2326-2331.

### Oral presentations (in Japanese)

- [1] 木村 豪, 胡 兆鵬, 馬渡 俊輔, 下川 達張, 吉川 由佳子, 高田 寛治. 大腸ターゲティング後の徐放性付与に関する研究～大腸デリバリー剤の応用研究～第 14 回日本 DDS 学会 (横浜), 1998, 7.
- [2] 木村 豪, 胡 兆鵬, 村岡 元樹, 馬渡 俊輔, 下川 達張, 高田 寛治. O-157 腸管出血性大腸菌感染症治療薬への大腸デリバリー技術の適用 第 3 回腸管出血性大腸菌感染症シンポジウム (東京), 1998, 7.
- [3] 木村 豪, 胡 兆鵬, 伊東 良晃, 馬渡 俊輔, 吉川 由佳子, 高田 寛治. 潰瘍性大腸炎治療薬 5-aminosalicylic acid (5-ASA) の大腸ターゲティング徐放性剤の設計と評価 日本薬学会第 118 年会 (京都), 1998, 3.

### Posters (in Japanese)

- [1] 吉川 由佳子, 村岡 元樹, 木村 豪, 胡 兆鵬, 伊東 良晃, 大谷 仁恵, 熊野 栄治, 浜田 圭子, 小川 典子, 壽山 晴香, 高田 寛治. 大腸デリバリーカプセルからの薬物溶出試験法の検討: in vitro 評価法の確立と in vivo との相関 日本薬剤学会第 13 年会 (山梨), 1998, 2.
- [2] 山田 秀徳, 福澄 正規, 木村 豪, 杉山 真紀, 藤田 卓也, 山本 昌, 村西 昌三. 消化管粘膜からの有機アニオン分泌機構に関する検討. 日本薬学会第 117 年会 (東京), 1997 3.
- [3] 山田 秀徳, 福澄 正規, 木村 豪, 杉山 真紀, 続 正芳, 西岡 純子, 藤田 卓也, 山本 昌, 村西 昌三. 消化管粘膜からの有機アニオン排出機構に関する研究 第 11 回日本薬物動態学会年会 (金沢), 1996 10.

### Patents

- [1] Satoshi Sakuma, Takuo Sugita, Go Kimura. TABLET CONTAINING VANCOMYCIN HYDROCHLORIDE. PCT disclosed on Oct. 22, 2006 (WO/2009/128489), PCT applied on Apr. 16, 2009 (PCT/JP2009/057632), 特許出願 2008-107608
- [2] 木村 豪, 谷口 陽一, 塚田 隆之. ビタミン B1 誘導体組成物. 特許 4573542 号 (特許公開 2005-247693, 特許出願 2004-055752)
- [3] 谷口 陽一, 塚田 隆之, 木村 豪. 混合顆粒剤の製造方法. 特許 4462476 号 (特許公開 2005-060276, 特許出願 2003-290503)

END